



**HAL**  
open science

**High intensity focused ultrasound in ophthalmology :  
part one, transscleral drug delivery : part two, infrared  
thermography for scalable acoustic characterization, an  
application in the manufacture of a glaucoma treatment  
device**

Arash Razavi Mashoof

► **To cite this version:**

Arash Razavi Mashoof. High intensity focused ultrasound in ophthalmology : part one, transscleral drug delivery : part two, infrared thermography for scalable acoustic characterization, an application in the manufacture of a glaucoma treatment device. Human health and pathology. Université Claude Bernard - Lyon I, 2014. English. NNT : 2014LYO10066 . tel-00996286

**HAL Id: tel-00996286**

**<https://theses.hal.science/tel-00996286>**

Submitted on 26 May 2014

**HAL** is a multi-disciplinary open access archive for the deposit and dissemination of scientific research documents, whether they are published or not. The documents may come from teaching and research institutions in France or abroad, or from public or private research centers.

L'archive ouverte pluridisciplinaire **HAL**, est destinée au dépôt et à la diffusion de documents scientifiques de niveau recherche, publiés ou non, émanant des établissements d'enseignement et de recherche français ou étrangers, des laboratoires publics ou privés.

*To my family*

*To freedom*

## THESE DE L'UNIVERSITE DE LYON

Délivrée par

L'UNIVERSITÉ CLAUDE BERNARD - LYON 1  
L'ECOLE DOCTORALE INTERDISCIPLINAIRE SCIENCES-SANTE

### DIPLOME DE DOCTORAT

SPÉCIALITÉ ACOUSTIQUE-MEDICALE  
(Arrêté du 7 août 2006)

soutenue publiquement le 14 Avril 2014

Par

Arash RAZAVI MASHOOF

**High intensity focused ultrasound in ophthalmology**  
**Part one: Transscleral drug delivery;**  
**Part two: Infrared thermography for scalable acoustic characterization-**  
**An application in the manufacture of a glaucoma treatment device**

Directeur de thèse: M. Jean-Yves CHAPELON  
Co-directeur de thèse: M. Cyril LAFON  
Tuteur Entreprise: Mme. Aurélie BEGLE

### Jury

Mme. BEGLE Aurélie  
M. CACHARD Christian  
M. CHAPELON Jean-Yves  
M. LAFON Cyril  
M. MARI Jean-Martial (Rapporteur)  
M. PATAT Frédéric (Rapporteur)  
M. TRANQUART François (Rapporteur)

## UNIVERSITE CLAUDE BERNARD - LYON 1

### Président de l'Université

Vice-président du Conseil d'Administration

Vice-président du Conseil des Etudes et de la Vie Universitaire

Vice-président du Conseil Scientifique

Directeur Général des Services

**M. François-Noël GILLY**

M. le Professeur Hamda BEN HADID

M. le Professeur Philippe LALLE

M. le Professeur Germain GILLET

M. Alain HELLEU

### *COMPOSANTES SANTE*

Faculté de Médecine Lyon Est – Claude Bernard

Directeur : M. le Professeur J. ETIENNE

Faculté de Médecine et de Maïeutique Lyon Sud – Charles Mérieux

Directeur : Mme la Professeure C. BURILLON

Faculté d'Odontologie

Directeur : M. le Professeur D. BOURGEOIS

Institut des Sciences Pharmaceutiques et Biologiques

Directeur : Mme la Professeure C. VINCIGUERRA

Institut des Sciences et Techniques de la Réadaptation

Directeur : M. le Professeur Y. MATILLON

Département de formation et Centre de Recherche en Biologie Humaine

Directeur : M. le Professeur P. FARGE

### *COMPOSANTES ET DEPARTEMENTS DE SCIENCES ET TECHNOLOGIE*

Faculté des Sciences et Technologies

Directeur : M. le Professeur F. DE MARCHI

Département Biologie

Directeur : M. le Professeur F. FLEURY

Département Chimie Biochimie

Directeur : Mme le Professeur H. PARROT

Département GEP

Directeur : M. N. SIAUVE

Département Informatique

Directeur : M. le Professeur S. AKKOUCHE

Département Mathématiques

Directeur : M. le Professeur A. GOLDMAN

Département Mécanique

Directeur : M. le Professeur H. BEN HADID

Département Physique

Directeur : Mme S. FLECK

Département Sciences de la Terre

Directeur : Mme la Professeure I. DANIEL

UFR Sciences et Techniques des Activités Physiques et Sportives

Directeur : M. C. COLLIGNON

Observatoire des Sciences de l'Univers de Lyon

Directeur : M. B. GUIDERDONI

Polytech Lyon

Directeur : M. P. FOURNIER

Ecole Supérieure de Chimie Physique Electronique

Directeur : M. G. PIGNAULT

Institut Universitaire de Technologie de Lyon 1

Directeur : M. C. VITON

Institut Universitaire de Formation des Maîtres

Directeur : M. A. MOUGNIOTTE

Institut de Science Financière et d'Assurances

Administrateur provisoire : M. N. LEBOISNE



## **Acknowledgements**

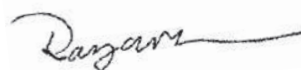
I would like to express my appreciation and thanks to my principal advisors at INSERM Mr. Jean-Yves CHAPELON and Mr. Cyril LAFON. I'm proud of being educated in one of the major renowned laboratories in the field of medical ultrasound, labTAU, with its impressive scientific achievements. It was a great experience working with you during the past three years. The foreign researchers in your home- lab are welcomed and supported considerably, and for that matter here is my sincere appreciations; without your support both scientifically and personally, this thesis would not be possible. Mr. Lafon, I have benefited greatly from your dedicated guidance and scientific directions. It was a pleasure working with you. I would like also to express my gratitude to Mrs. Françoise CHAVIER, Mr. Jean-Luis MESTAS, and Mr. Alain BIRER. You are dedicated, generous scientists and above all amazing people. I would also like to thank my committee members, Mr. Jean-Martial MARI, Mr. Christian CACHARD, Mr. Frédéric PATAT, Mr. François TRANQUART for letting my defense be an enjoyable moment, and for your brilliant comments and suggestions. I also appreciate much the scientific contributions of my fellow lab-mates during the past three years.

Hereby, I specially want to thank Mrs. Aurélie BEGLE my supervisor at Eyetechnicare. Your scientific contribution and trust had a defining role in this endeavor. Having you as an advisor essentially helped me to put the hardships behind and always move forward; working and living in a new country and culture could be far more challenging for me without your continuous and generous support. My deep appreciation also goes to the co-founders of Eyetechnicare Mr. Fabrice ROMANO, Mr. Philippe CHAPUIS, and Mr. Laurent FARCY. Thank you for starting-up such a unique company which highly values innovation and hosts remarkable people; moreover, thank you for making this study possible. Dear Mr. Thomas CHARREL, Mr. David CLEMENT, and Mrs. Laure BAFFI, merci for your direct contribution in this work; it is such a pleasure working with you and I have learned a lot in different aspects from each of you. In addition, lots of thanks to my fellow workmates at Eyetechnicare for their support and cheerfulness. We spend a great portion of our days together throughout hardships and happiness. Each single day however, it is a pleasure to see you again which makes me deeply glad to be a member of this unique society.

My sincere thanks also go to Mrs. Sima Asvadi my former mentor at Philips research. I feel lucky to know you; it is an honor which I treasure. My dear scientist-artist friends Michael Canney, Azziz Lumiere, and Andrew Fowler, thank you for your direct contribution to this work. It was such a pleasure to work with you guys and then to pass pleasant happy-hour moments after work.

Above all, I am grateful to my beloved family. Words are not functional as they should be in such contexts; therefore, I just name you here as a gesture that you are present on my mind every single moment of my life away from you: Nader, Ani, Rose, Iran, Mercedes, Patrik, Kevin, and Hamed. May one day all these nonsense causes of family members being apart disappear from our society. This dissertation is dedicated to you.

Lyon, May 2014

A handwritten signature in black ink, appearing to read "Razvan", with a long horizontal flourish extending to the right.

---

**RESUME en français**

Les ultrasons (US) thérapeutiques sont devenus un sujet d'intérêt croissant en ophtalmologie. Les ultrasons focalisés de haute intensité (HIFU) pour le traitement du glaucome et pour la délivrance de médicaments dans l'œil sont les deux principaux domaines de recherche dans ce domaine. Cette thèse traite des deux sujets en deux parties distinctes : l'administration de médicaments ou drug delivery par d'ultrasons (USDD) à travers la sclère et la caractérisation par rayonnement infrarouge (IR) d'un dispositif HIFU ophtalmique pour le traitement du glaucome. Bien que plus perméable que la cornée, l'administration de médicaments efficace à travers la sclère reste un réel challenge. Dans ce travail, nous avons évalué l'effet d'une propagation d'us en mode pulsé sur l'administration de médicaments à travers la sclère. Parmi les mécanismes sous-jacents, la cavitation semble être un contributeur à une USDD renforcée. L'activité maximale de cavitation sous-jacente à une émission d'ultrasons en mode pulsé peut donc être une méthodologie viable pour l'amélioration de l'administration de médicaments à travers l'œil. Dans la deuxième partie de la thèse, une nouvelle méthode de caractérisation ultrasonore de terrain a été développée pour un dispositif HIFU multi-éléments. Ce dispositif médical développé par Eyetechcare est destiné au traitement du glaucome réfractaire (Rillieux-la-pape, France). Une alternative basée sur la thermographie par infra-rouge a été développée pour une évaluation rapide et qualitative de la distribution d'intensité émise spécifiquement par ce dispositif à haute fréquence (19-21 mhz) constitué de multiéléments à focalisation en ligne. Cette méthodologie permettra de caractériser les sondes de thérapie à l'échelle industrielle.

---

**TITRE en anglais**

High intensity focused ultrasound in ophthalmology. Part one: Transscleral drug delivery;  
Part two: Infrared thermography for scalable acoustic characterization-an application in the manufacture of a glaucoma treatment device.

---

**RESUME en anglais**

Therapeutic ultrasound has become a topic of growing interest in ophthalmology. High intensity focused ultrasound (HIFU) for the treatment of glaucoma and ultrasound (US) drug delivery are the two main areas of research in this field. This work addresses these domains in two separate parts: transscleral ultrasound drug delivery (USDD), and infrared (IR) field characterization of an ophthalmic HIFU device for glaucoma treatment. The sclera is a promising pathway for ocular drug delivery, since transscleral administration can address both the anterior and posterior segments of the eye. Due to the low permeability however, efficient drug delivery is challenging. In this study, HIFU was investigated as a potential modality for an enhanced transscleral drug delivery (in vitro). Among US effects, cavitation was shown to be the major contributor to an enhanced USDD. A pulsed US protocol designed to maximum cavitation activity may therefore be a viable method for enhancing ocular drug delivery. In the second part, a new method of ultrasonic field characterization was developed for a multi-element HIFU device. This system is designed and produced for glaucoma treatment by Eyetechcare Company (Rillieux-la-Pape, France). The traditional hydrophone method for field characterization was prohibitively slow on an industrial scale. An alternative modality for rapid qualitative assessment of the intensity distribution based on infra-red (IR) thermography was developed specific to this high frequency (19-21 MHz) device with line-focus US radiators. The second part of the study was aimed to expand the application of a R&D technique for ultrasonic field characterization to an industrial scale.

---

**DISCIPLINE**

Acoustique Médical

---

**MOTS-CLES**

Ultrasound, Ophthalmology, Drug Delivery, Transscleral, Cavitation, Glaucoma, Miniaturized devices, High Frequency, Infrared Thermography

---

**INTITULE ET ADRESSE DE L'U.F.R OU DU LABORATOIRE:**

INSERM U1032 , LabTAU, 151 cours Albert Thomas, 69424 Lyon Cedex 03  
EyeTechCare, 2871 Avenue Europe, 69140 Rillieux-la-Pape

## Outline:

<b>Chapter I, Introduction</b> .....	1
<b>1.1 Motivation</b> .....	1
1.1.1 Part I: Ultrasound enhanced transscleral drug delivery .....	1
1.1.2 Part II: Infrared thermography and ultrasonic field characterization .....	2
<b>1.2 Hypothesis and Specific Aims</b> .....	3
1.2.1 Part I: Ultrasound enhanced transscleral drug delivery .....	3
1.2.2 Part II: Infrared thermography and ultrasonic field characterization .....	4
<b>1.3 Organization of the Dissertation</b> .....	4
1.3.1 Part I: Ultrasound enhanced transscleral drug delivery .....	4
1.3.2 Part II: Infrared thermography and ultrasonic field characterization .....	5
<b>Chapter 2 (P.I), Ocular drug delivery</b> .....	7
<b>2.1 Introduction</b> .....	7
<b>2.2 EYE structure</b> .....	9
<b>2.3 Ocular drug delivery</b> .....	12
2.3.1 Ocular barriers .....	13
2.3.2 Drug administration .....	15
2.3.3 Alternative modalities .....	18
2.3.4 Controlled release .....	18
2.3.5 Iontophoresis: .....	22
2.3.6 Ocular ultrasound-mediated drug delivery: .....	23

<b>Chapter 3 (P.I), Ultrasound mediated ocular drug delivery</b> -----	24
<b>3.1 Introduction</b> -----	24
<b>3.2 Therapeutic ultrasound</b> -----	24
<b>3.3 Ultrasound mechanisms in drug delivery</b> -----	26
3.3.1 Ultrasound effects-----	26
3.3.2 Cavitation and drug delivery-----	30
<b>3.4 Ultrasound mediated drug delivery systems</b> -----	31
3.4.1 Targeted delivery-----	32
3.4.2 Sonoporation-----	33
3.4.3 Blood-brain barrier opening-----	34
3.4.4 Transdermal sonophoresis-----	35
3.4.5 Ocular sonophoresis-----	38
<b>Chapter 4 (P.I), Transscleral drug delivery: in vitro studies</b> -----	43
<b>4.1 Introduction</b> -----	43
<b>4.2 Material and methods</b> -----	44
4.2.1 Preparation of samples-----	44
4.2.2 Ultrasonic setup-----	45
4.2.3 Ultrasound exposure parameters-----	48
4.2.4 Measurements of permeability-----	48
4.2.5 Preliminary studies of cavitation contribution-----	50
<b>4.3 Results</b> -----	52
4.3.1 Permeability measurements-----	52

4.3.2	Inertial cavitation validation	52
<b>4.4</b>	<b>Discussion</b>	<b>53</b>
<b>4.5</b>	<b>Conclusion</b>	<b>55</b>
<b>Chapter 5 (P.I), Action mechanisms: cavitation contribution</b>		<b>56</b>
<b>5.1</b>	<b>Introduction</b>	<b>56</b>
<b>5.2</b>	<b>Material and methods</b>	<b>58</b>
5.2.1	Preparation of samples and diffusion cell	58
5.2.2	Ultrasonic setup	59
5.2.3	US parameters	61
5.2.4	Measurements of permeability	61
5.2.5	Assessment of damage induced by ultrasound on scleral tissue	62
<b>5.3</b>	<b>Results</b>	<b>64</b>
5.3.1	Evaluation of cavitation activity and scleral permeability enhancement	64
5.3.2	Assessment of scleral damage induced by ultrasound	68
<b>5.4</b>	<b>Discussion</b>	<b>72</b>
<b>5.5</b>	<b>Conclusion</b>	<b>79</b>
<b>Chapter 6 (P.II), IR thermography</b>		<b>81</b>
<b>6.1</b>	<b>Introduction</b>	<b>81</b>
<b>6.2</b>	<b>HIFU characterization</b>	<b>84</b>
<b>6.3</b>	<b>Eyeop1<sup>®</sup> therapy probes quality control, current methods</b>	<b>86</b>
<b>6.4</b>	<b>IR thermography</b>	<b>88</b>
6.4.1	IR thermography and Ultrasonic field visualization-state of the art	89

<b>Chapter 7 (P.II), Ultrasonic field characterization via IR thermography: A feasibility study</b>	<b>94</b>
<b>7.1 Introduction</b>	<b>94</b>
<b>7.2 Materials and methods</b>	<b>95</b>
7.2.1 Acoustic set-up	95
7.2.2 IR systems	97
7.2.3 Data analysis	101
7.2.4 Overview of feasibility studies	103
<b>7.3 Results</b>	<b>108</b>
7.3.1 IR thermography: an inspection tool (I)	108
7.3.2 IR thermography/ pressure hydrophone measurement (I)	109
7.3.3 US parameters adjustment for IR inspection method	110
7.3.4 IR thermography/ pressure hydrophone measurement (II)	113
7.3.5 IR thermography: an inspection tool (II)	114
7.3.6 IR thermography: a statistical reliability survey of current set-up	116
<b>7.4 Discussion</b>	<b>118</b>
<b>7.5 General discussions and Conclusion</b>	<b>123</b>
<b>List of figures</b>	<b>126</b>
<b>List of tables</b>	<b>129</b>
<b>Bibliography</b>	<b>130</b>





# ***Chapter I, Introduction***

## ***1.1 Motivation***

Therapeutic ultrasound has become a topic of growing interest in ophthalmology. Up to recent days, high intensity focused ultrasound (HIFU) for ocular drug delivery and treatment of glaucoma are the two main areas of research and clinical applications in this field (Aptel and Lafon 2012). This work is dedicated to these applications in two separate parts.

### ***1.1.1 Part I: Ultrasound enhanced transscleral drug delivery***

The outer layers of the eye function as a highly effective barrier against penetration from the outside environment. Anatomical barriers such as cornea and sclera, as well as physiological barriers such as tear washing and nasolacrimal drainage all contribute to form a non-permeable organ i.e. Eye globe. In other words, these barriers prevent the permeation of externals; non-selectively however to harmful and therapeutic agents. In case of ophthalmic drugs, this characteristic significantly reduces the bioavailability of therapeutic agents that could be used to treat various diseases such as glaucoma. This issue has been addressed in many studies by application of various modalities. As been explained later in the text, the majority of these methods are invasive with low efficiency. With these concerns, the investigation of alternative methods for a non-invasive yet efficient drug delivery into the eye is of significant clinical interest.

Therapeutic ultrasound is an emerging modality in ocular drug delivery due to its minimally invasive nature. Although preliminary studies were promising, they were mostly performed on the cornea as the delivery route. On the other hand the sclera offers some advantages over the cornea; for example, contrary to cornea, it can address a wide range of ocular segments and diseases.

Therefore, stands to reason to develop an ultrasound drug delivery system which applies scleral routes where there is therapeutic values.

### ***1.1.2 Part II: Infrared thermography and ultrasonic field characterization of a HIFU device for glaucoma treatment***

Regarding the fact that current ocular drug delivery methods such as topical administration are not efficient, surgical operations are needed for treating the glaucoma in severe cases. By an innovative procedure, the destructive side of the therapeutic ultrasound could be applied for glaucoma treatment and still benefit from the non-invasive side of the HIFU therapy. Glaucoma is a progressive degeneration of the optic nerve cells up to vision loss due to the increase of intraocular pressure (IOP). By application of recent advancements in HIFU technology, it is possible to damage the responsible tissue for this increase of IOP i.e. ciliary body. A newly developed device, Eyeop1<sup>®</sup> (Eyetechnicare, Rillieux-la-Pape, France) could perform destructive HIFU treatments in a controlled manner. By applying multi-elements miniaturized transducers, it is possible to confine the damage within the ciliary body, sparing the tissue around. This device is in the post-marketing stage. In the production line of Eyeop1<sup>®</sup>, hydrophone scanning and phantom gels are used for quality control tests. However, both of these methods have prohibitively high cost in terms of time and resources. An alternative modality for rapid qualitative assessment of the intensity distribution of a HIFU device is based on infra-red (IR) thermography. This modality has been used by other groups for characterizing specific spherical and phased array HIFU systems that operate in the frequency range of 1-5 MHz (Shaw and Nunn 2011, Bobkova et al. 2012, Khokhlova et al. 2013). Therefore, given the specific features of our device e.g. high frequency (21 MHz) and the manufacturing requirements, it stands to reason to assess the industrial values of this method by a feasibility study.

## ***1.2 Hypothesis and Specific Aims***

### ***1.2.1 Part I: Ultrasound enhanced transscleral drug delivery***

Our hypothesis was that ***'ultrasound can provide enhancement of drug delivery into and through the sclera with minimal induced damage. Among the ultrasound effects, the major contributor to this enhancement is cavitation phenomenon.'***

The work described in the first part of this dissertation is divided into 3 specific aims:

**Specific aim 1:** *Evaluate the ability of ultrasound to enhance drug delivery through the rabbit sclera, in vitro.*

The application of 1.1 MHz focused ultrasound (Pulsed regime 2-5% duty-cycle, acoustic power 0.5-5.4 W, peak pressure 6.8-12.8 MPa, and exposure durations of 2-10 min) was investigated for enhancement of scleral permeability to a drug mimicking compound (fluorescein). The experiments were performed using a diffusion cell built in house specifically to the requirements of this study.

**Specific aim 2:** *Investigate ultrasound effects on the scleral structures.*

A microscopic study was performed by transmission electron microscopy (TEM) to evaluate the US induced damage in cellular (fibroblast) and intercellular network (collagenic bundles) levels.

**Specific aim 3:** *Investigate the contribution of cavitation in an enhanced scleral drug delivery.*

By application of a passive-cavitation-detection (PCD) method the level of inertial cavitation activity was measured; its correlation with permeabilization was then studied. For this matter the exposure conditions were designed in a way that cavitation effect could be studied in an isolated matter with regards to the rest of US effects.

## ***1.2.2 Part II: Infrared thermography and ultrasonic field characterization of a HIFU device for glaucoma treatment***

***Our hypothesis was that 'IR thermography can provide a qualitative characterization method for quality control of a high frequency (19-21 MHz) lined-focus HIFU system (Eyeop1®). This control tool is fast and reliable to be applied on an industrial scale'.***

The work described in the second part of this dissertation is divided into 2 specific aims:

***Specific aim 1: Evaluate the capability of IR thermography for field characterization of the device as a potential quality control modality.***

The current control methods are hydrophone measurements and phantom gel lesion methods. An IR inspection method has been developed to provide qualitatively close estimations to hydrophone and phantom gel methods considering the specifics of the HIFU device (Eyeop1).

***Specific aim 2: Investigate the reliability of the method in terms of repeatability and reproducibility.***

A statistical survey was performed to investigate the influence of environment temperature and experimental set-up conditions on repeatability and reproducibility of the IR inspection tool.

## ***1.3 Organization of the Dissertation***

### ***1.3.1 Part I: Ultrasound enhanced transscleral drug delivery***

Starting from chapter 2 (P.I), it provides background information of ocular anatomy and physiology. It introduces the current ocular drug delivery systems. Following that, it explains the general challenges of ocular drug delivery in terms of ocular barriers and then describes the pros and cons of each system with these regards. In this way it shows why developing a non-invasive method such as ultrasound mediated could be of a great clinical value.

Chapter 3 (P.I) provides background information of therapeutic ultrasound in drug delivery and explains the main involved mechanisms. It introduces two main fields of the ongoing research on

ocular ultrasound-enhanced drug delivery: corneal and scleral drug delivery. It then explains why the scleral pathway for drug delivery is of a major value. It also explains why the previous studies formed the hypothesis that inertial cavitation effect is the major contributor in an ocular drug delivery system. Generally speaking, it provides back up explanations of first, why a scleral drug delivery system was chosen here to perform feasibility studies; and secondly, why the experimental protocols and ultrasound exposure conditions were designed as such.

Chapter 4 (P.I) describes the preliminary results of the feasibility studies and experiments (*in vitro*). It demonstrates that short pulses of ultrasound at 1.1MHz can increase the permeability of the sclera tissue.

Chapter 5 (P.I) delves more into the action mechanisms of ultrasound-enhanced drug delivery; with the aim that a good understanding of involving ultrasound effects could eventually help to a safer and better system design. It validates the hypothesis of inertial cavitation participation in a scleral enhanced-ultrasound drug delivery by application of a modified diffusion system. It tries to demonstrate the characteristic of inertial cavitation contribution and provides the results of a microscopic study for the assessment of ultrasound induced damage.

### ***1.3.2 Part II: Infrared thermography and ultrasonic field characterization of a HIFU device for glaucoma treatment***

Starting from the chapter 6 (P.II), it introduces the Eyeop1<sup>®</sup>, a HIFU therapy device made for glaucoma treatment. It explains why ultrasonic field characterization of such devices is problematic on an industrial scale with refer to traditional methods e.g. hydrophone measurements and phantom gel lesion method. It then introduces the IR thermography and shows why it can be considered as a substitute for quality control inspections.

Chapter 7 (P.II) provides the results of the feasibility studies. It demonstrates the application of two different set-ups and tells the evolution story of the final system. It shows that the developed IR inspection system is fast and reliable and potentially can be used in the place of traditional quality inspection methods.

## ***Chapter 2(P.I), Ocular drug delivery***

### ***2.1 Introduction***

Generally speaking, drug delivery systems are defined in several ways based on their application. However these definitions share conceptual similarities which are well described by Medical Reference: “(these are) systems for the delivery of drugs to target sites of pharmacological actions. Technologies employed include those concerning drug preparation, route of administration, site targeting, metabolism, and toxicity”<sup>1</sup>.

For targeting one tissue/organ of interest, there might be several routes of drug delivery (DD). In a general classification, the common delivery routes are per-oral, topical, per injections (e.g. Intravenous, subcutaneous, intramuscular), sublingual, rectal, vaginal, transdermal, and ophthalmic. The choice of delivery route and administration method addresses the therapeutic site by overcoming the physioanatomical barriers along the pathway. This in turn defines the bioavailability kinetics i.e. drug bio-distribution and elimination, and thus the efficiency of a system; in other words, an efficient transport to the target tissue/organ, while attaining the therapeutic concentration well-below the toxicity threshold in a clinically relevant administration time and application frequency (Saltzman 2001, Chari 2008). For instance, the application of non-invasive systems and routes such as topical or per-oral seems to be advantageous due to the high patient compliance; however, in addition to a limited bioavailability, they are not satisfying all range of compounds and disease. For some such as peptides, vaccines, and gene based drugs more invasive methods such as injection are currently practiced. On the other hand, the invasive methods increase the risk of infection. Furthermore, this mode of administration produces substantial change in drug concentration and can easily result in systematic toxicity (Saltzman 2001). Therefore, for many target tissues/organs the efficiency of such systems is limited.

---

1- <http://www.reference.md/files/D016/mD016503.html>

In order to tackle these challenges, drug delivery systems might employ technologies such as iontophoresis and ultrasound (US). In case of transdermal drug delivery for instance, the efficiency of such employments has been improved greatly endorsed with approved clinical results (Bommannan et al. 1992, Mitragotri et al. 1995 and 1996). In some other fields such as ophthalmology however, integrating such technologies is still under development to achieve clinical acceptance. This delay in the ophthalmic applications is mainly due to the specific physioanatomical barrier properties of ocular tissues. Although, the adaptation of such technologies is far more challenging when compared to other applications e.g. dermatology, the needs and demands for multi-disciplinary drug delivery systems in the ophthalmology field is growing day by day.

As mentioned *in the introductory chapter*, first part of the present dissertation is dedicated to ultrasound mediated scleral drug delivery. Before getting there however it stands to reason to have a general overview on ocular drug delivery, ultrasound mediated drug delivery (USDD), and ocular USDD. In this chapter an overview on ocular drug delivery systems is provided. It starts by an introductory description of the eye anatomy and physiology as far as it serves to the cause of this essay. It then proceeds by exploring the ocular barrier properties and how each drug delivery system addresses them applying alternative delivery routes. These systems might be based on different technologies with specific pros and cons. By the end of the chapter, the focus will be more on corneal and scleral drug delivery systems and the state of the art.



## 2.2 EYE structure

Eye is a conscious sense organ that detects and collects light from the environment. After regulation of the received light intensity via its diaphragm and focusing through its lens, sets of electro-chemical signals are transmitted through optic nerves to the visual cortex of the brain where the images are constructed and perceived. Anatomically, the eye globe is in the form of a sphere which is slightly asymmetrical. For average human, both sagittal and transverse diameter of the eyeball is 23-24 mm. The contents of the eye are covered by supportive multifunctional layers known as cornea and sclera (Fig. 1).

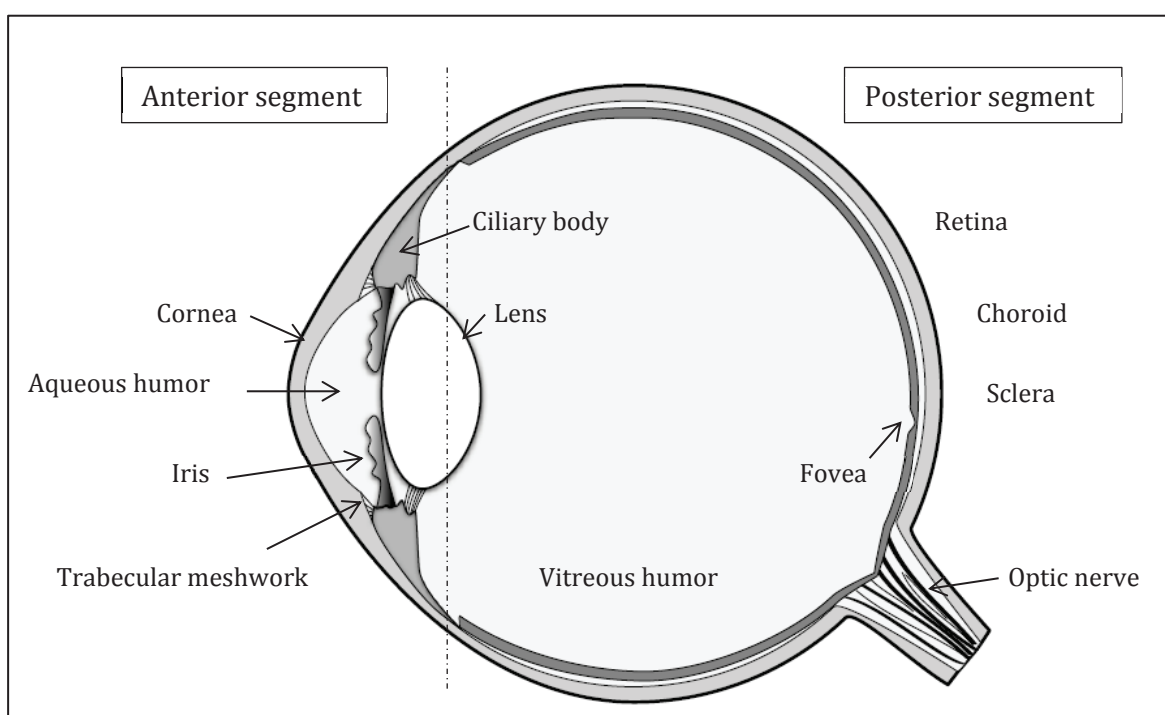
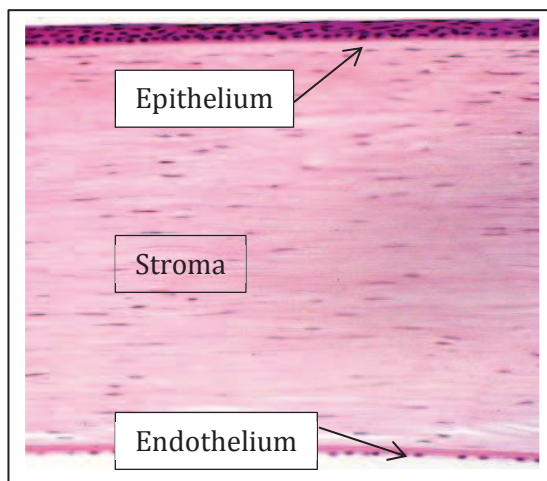


Figure 1- Schematic diagram of human eye.

The inside of the eye consists of two anterior and posterior segments (Fig.1). The anterior segment occupies the front third of the total inner space and is covered by cornea exteriorly. The cornea is the transparent front part of the eye. It protrudes anteriorly from the eyeball. As a powerful lens, it shares the two thirds of the total ocular optical power. Its avascular structure is 0.5 mm thick and consists of three main layers: epithelium, stroma, and endothelium. The outermost layer of the cornea, epithelium, is 50 $\mu$ m thick and consists of 5-7 layers of epithelial cell layers. The apical cell layers form tight intercellular junctions. The needed moisture, nutrients, and dissolved

oxygen for epithelium are provided by the lacrimal fluid. The stroma with a thickness of 450  $\mu\text{m}$  lies under this layer. The collagenic structure with parallel fibers of the stroma gives the cornea its strength, transparency, and the curved shape. It is hydrophilic and more porous compare to epithelium. Endothelium with a one layer cell thick forms the inner lining of the cornea (Fig. 2).



**Figure 2- Histologic section of human cornea**  
(Ocular pathology, [www.missionforvisionusa.org](http://www.missionforvisionusa.org)).

Behind the cornea, the anterior segment is divided itself into two anterior and posterior chambers. These two chambers are filled with aqueous humour. This fluid provides cornea and lens with nourishments and removes out the breakdown products. These two chambers are separated by the iris, the colored tissue which is visible through the cornea. The opening right in the middle of it is the pupil which regulates the amount of light intakes. Behind the iris ciliary body is located which is responsible of producing the aqueous humour. The aqueous humour drainage out of the eye is possible through a fibrillar structure around the base of the cornea known as trabecular meshwork (Fig. 1). This structure is channeled to several veins out of the eye by so called Schlemm's canal and lies in the intersection of the iris and cornea where is called angle (Fig. 3). The posterior chamber of the anterior segment is the space between the iris and the crystalline lens. The crystalline lens is attached to the anterior part of ciliary body by ligaments called zonular fibers. The contraction and dilation of this structure is translated to the shape changes of the flexible crystalline lens. In this way the focus power of the lens can be shifted back and forth according to the relative objects distance.

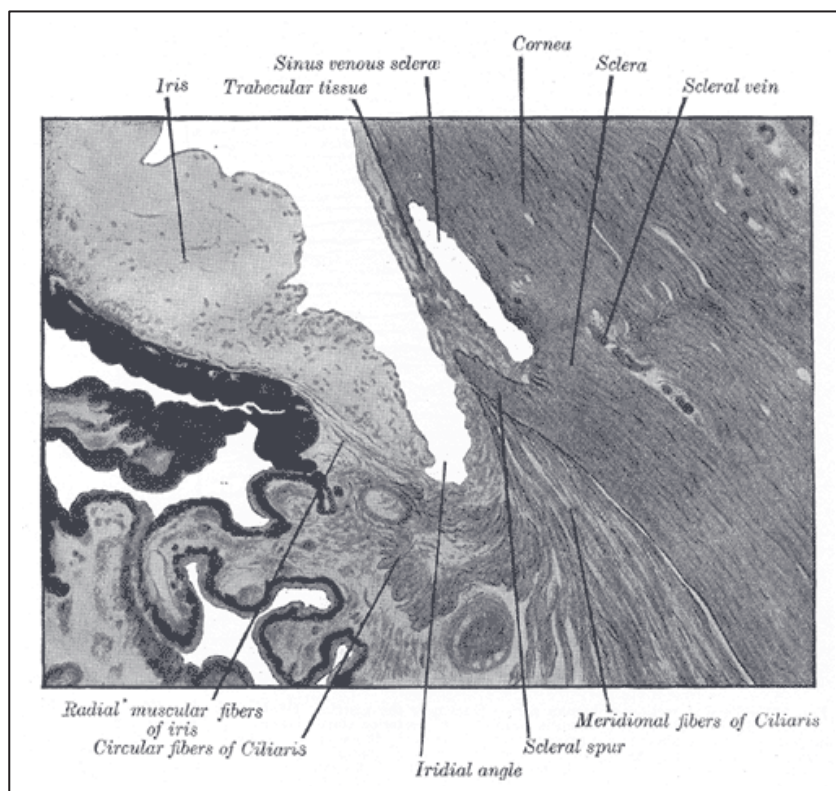


**Figure 3- Histologic section of human corneascleral junction and iridial angle** (Grey's anatomy, bartleby.com).

The posterior segment, the rest of the eye, consists of the vitreous humour, the retina, the choroid and posterior sclera. The vitreous humour is the gel-like structure behind the lens and in front of the retina. The retina which is lining the inner surface of the segment consists of nerves and vascular tissue. Between retina and the sclera lies the choroid which is vascular layer and provides the retina with nourishment (Fig. 4). The sclera is the white outer-layer of the eye external to the choroid and retina. It forms the posterior five sixths of the outer wall of the eyeball. It is made of connective tissue, composed of flattened fibroblasts, bundles of collagen, and elastic fibrils (Watson and Young 2004). The main role of sclera is believed to be as a guard shield for protection of the eye against external trauma and to provide the global mechanical strength necessary to cope with the intra-ocular pressure. The collagens and elastic fibrils are synthesized by fibroblasts. The packs of parallel collagen fibrils form bundles. Contrary to the cornea, the scleral collagen bundles are irregular in size and structural arrangement (Meek and Fullwood 2001). The thickness of the sclera

varies from 0.9 mm at the posterior pole to 0.4 at the peripapillary scleral flange (Vurgese et al. 2012).

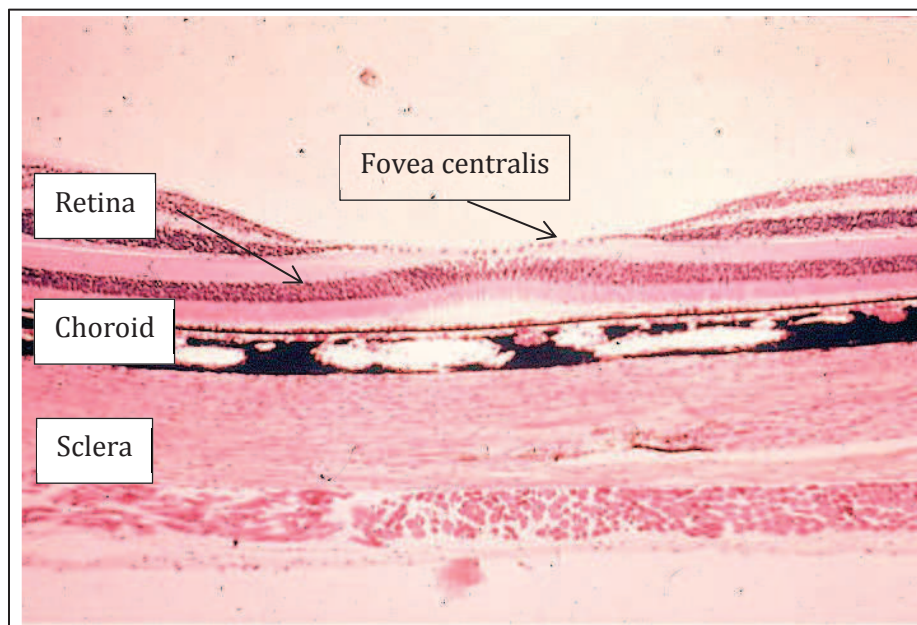


Figure 4- Histologic section of human sclera, choroid, and retina (www.udel.edu).

### ***2.3 Ocular drug delivery***

The outer layers of the eye function as a highly effective barrier against penetration from the outside environment. Anatomical barriers such as the conjunctiva, cornea, sclera, retina and blood, as well as physiological barriers such as choroidal blood flow, tear washing, and nasolacrimal drainage all contribute to form this barrier. While these barriers protect the eye from various harmful external agents, they pose a major limitation to the bioavailability of therapeutic agents that could be used to treat various diseases. Attempts to overcome these barriers have been catalogued in numerous studies (Patton and Francoeur 1978, Urtti 1994, Park et al. 2012). These attempts cover both invasive and non-invasive methods. The majority of the invasive methods that have been investigated for ocular drug delivery involve direct injections into different regions of the eye. Such injections, whether periorbital or intravitreal, present numerous risks and side-effects such as severe infections, cataract formation and retinal detachment (Kuo et al. 2005; Short 2008; Kuruvilla et al. 2012; Khan et al. 2013). On the other hand, the efficacy of non-invasive methods such as systemic or

topical administration of drugs is severely limited by the bioavailability due to the blood-eye barrier and the low tissue permeability to drug compounds (Aptel and Lafon 2012). For these reasons, the investigation of alternative methods for efficient, non-invasive drug delivery in the eye is of significant clinical interest.

### ***2.3.1 Ocular barriers***

In a general classification, the ocular barriers can be classified in three levels: drug loss from the ocular surface, lacrimal fluid-eye barriers (e.g. cornea), and blood-ocular barriers (Urtti 2006). All the existing ocular drug delivery methods endeavor to overcome these barriers one way or another. The most practiced systems are topical administration and per-oral methods. As mentioned, the efficacy of these non-invasive methods is severely limited due to the mentioned barriers. After topical administration, the surface of the eye removes effectively a great portion of the compounds by flow of lacrimal fluid. A portion of the instilled drug is also removed by systematic absorption either directly by the blood capillaries within the conjunctival sac or from the nasal cavity. Another limitation of the drug absorption from lacrimal fluid is posed by the corneal epithelium.

The corneal routes are the main (so far utilized) pathways for the drug delivery from the lacrimal fluid to the aqueous humour (Urtti 2006). The transcorneal drug delivery can address the anterior segment disorders such as iritis (the inflammation of the iris and anterior chamber). However, the efficacy of this route is also severely limited due to the very low permeability of the cornea and its small surface area (Davies 2000). In general, the cornea favors the lipophilic drugs to hydrophilic ones. While the lipophilic drugs can permeate the cell lipid membrane in intracellular routes, the tight junctions of epithelial cells are an impediment in the paracellular pathways for the hydrophilic drugs (Prausnitz and Noonan 1998). That said, the most non-invasive methods of delivery i.e. topical and per oral are the less efficient ones. The bioavailability of these methods estimated to be less than 5%.

Occupying the two third of the eye surface, the sclera is an attractive route for ocular drug delivery, as drugs delivered by this pathway can target both anterior and posterior segments of the eye (Schoenwald et al. 1997, Maurice 2002, Thrimawithana et al. 2011). When comparing scleral and corneal permeability, the sclera presents the additional advantage of being permeable to macromolecules (Pescina et al. 2011). Furthermore, the sclera can provide a shorter diffusional path length for targeting the choroid (Onami et al. 2013) and retina (Praustnitz et al. 1998, Duvvuri et al. 2003).

The work of Schoenwald et al. (1997) could demonstrate the advantage of scleral routes over corneal posterior chamber drug delivery. It was reported that in the case of certain antiglaucoma agents, such as methazolamide, after transcorneal penetration of drug, the chances of diffusion through the pupil and reaching the posterior chamber and ciliary body was significantly low, thus resulting in a minimal improvement in therapeutic efficacy. In the same study however, transscleral delivery provided a direct pathway for the agents to reach ciliary body for the better treatment of glaucoma.

The blood-retina barrier (BRB) and blood-aqueous barrier (BAB) protect the eye from the xenobiotics in the blood stream, including chemicals and drugs. The endothelial cells of the choroids and ciliary body forms the anterior segment of the blood-ocular barrier. This segment limits the permeation of the hydrophilic drugs from plasma into the aqueous humor. The retinal pigment capillaries, on the other hand, pose a posterior segment barrier. The ocular blood flow is not sufficient to overcome these barriers since it is a minor fraction of the total body's blood flow. Consequently systematic drug delivery exhibits a low inefficiency (Uttri et al. 1993, Uttri 2006). Due to the low efficiency of these non-invasive methods, direct drug injection is considered as a remedy for addressing the posterior chamber / segment and to improve the drugs bioavailability; however, as an invasive method with considerable side effects the application of invasive methods are limited to more severe ocular diseases.

## 2.3.2 Drug administration

As been said, each administration method addresses specific delivery routes, barrier properties, and ocular disease. In the following classification, these are summarized along with the pros and cons of each administration methods in bullet points. The main references for this summary are Delamo and Uttri (2008), Gaudana et al. (2010), and Ahn et al. (2013).

### 2.3.2.1 Topical administration

The ocular barriers severely limit the efficiency of topical administration method such as eye drops. The frequent administration of drug is needed in order to reach the therapeutic concentration within the anterior segment. In case of posterior segment drug delivery, even frequent administrations would not be effective. Figure 5 demonstrates a schematic of ocular routes which after a topical administration pose a barrier for the drug to reach posterior segment (Hughes et al. 2005).

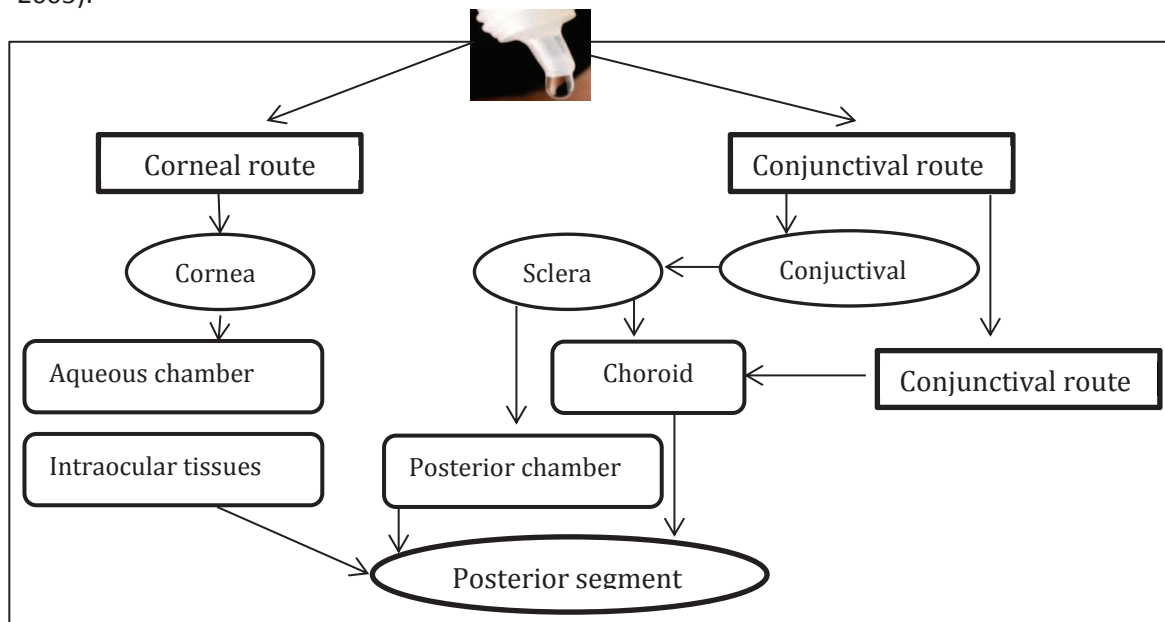


Figure 5- Topical administration and ocular barriers against drug delivery to the posterior segment.

- *Advantages:* non-invasive and self-administrable
- *Disadvantages:* low bioavailability (< 5%), short action duration, and low patient compliance in frequent administration
- *Barriers:* conjunctiva, cornea, sclera, and lacrimal fluid



- *Application examples:* Keratitis, uveitis, conjunctivitis, scleritis, episcleritis, and blepharitis

### 2.3.2.2 Systematic administration (per-oral):

- *Advantages:* non-invasive and self-administrable, more effective to treat diseases of the posterior segment when compared to eye-drop
- *Disadvantages:* low bioavailability (< 2%) and systematic toxicity risk
- *Barriers:* BRB and BAB
- *Application examples:* Scleritis, episcleritis, cytomegalovirus retinitis, and posterior uveitis

### 2.3.2.3 Invasive administration by injections:

There are several methods of injection in terms of delivery routes. In this subsection they are introduced briefly.

#### ***Intravitreal injections (direct injection to the posterior segment, Fig. 6):***

- *Advantages:* sustained delivery and surpassing the BRB by direct delivery to vitreous and retina
- *Disadvantages:* invasive, requires repeated administration, patient incomppliance, risk of retinal detachment, hemorrhage, cataract, and endophthalmitis
- *Application examples:* age-related macular degeneration, posterior uveitis, branched and central retinal vein occlusion, diabetic, cystoid and uveitic macular edema, and cytomegalovirus, implants and nonoparticles

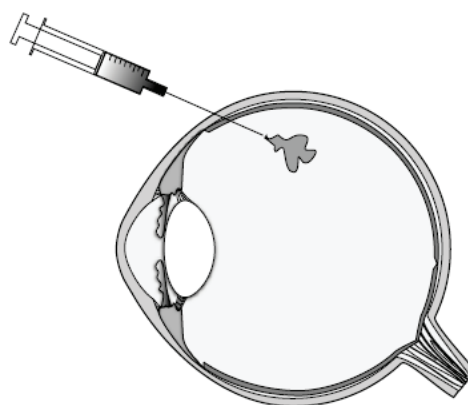


**Figure 6- Intravitreal injection.**

#### ***Intracameral injections (direct injection to the anterior chamber):***

- *Advantages:* sustained delivery, surpassing lacrimal-corneal, cornea, and BAB barrier by direct delivery to the anterior chamber
- *Disadvantages:* invasive, requires repeated administration, toxic endothelial cell and anterior segment syndrome



- *Application examples:* Anesthesia, prevention of endophthalmitis, inflammation and pupil dilation

***Subtenon (periocular) injections*** (Fig. 7):

- *Advantages:* medium invasive, and relatively high bioavailability
- *Disadvantages:* requires repeated administration, chemosis and subconjunctival hemorrhage
- *Application examples:* diabetic macular edema, age-related macular degeneration, retinal vein occlusion, and uveitis

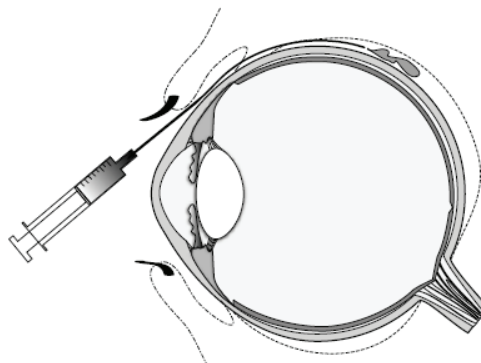


**Figure 7- Subtenon injection.**

***Subconjunctival (periocular) injection*** (Fig. 8):

- *Advantages:* medium invasive, delivery to both anterior and posterior segments
- *Disadvantages:* requires repeated administration
- *Barriers:* conjunctival and choroidal circulation
- *Application examples:* glaucoma, cytomegalovirus retinitis, age-related macular degeneration, and posterior uveitis

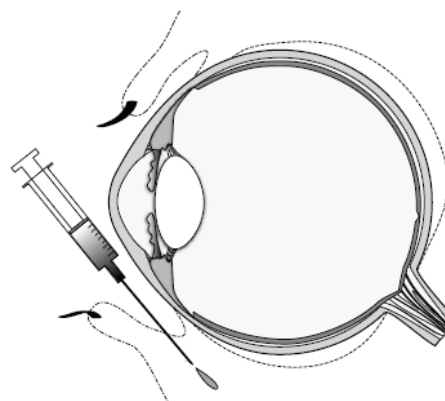
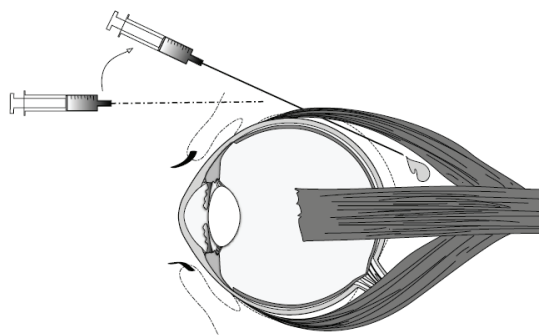


**Figure 8- Subconjunctival injection.**

***Retrobulbar (periocular) injections*** (Fig. 9):

- *Advantages:* more effective than peribulbar for anesthetics administration with minimal influence on IOP
- *Disadvantages:* retrobulbar hemorrhage, globe perforation, respiratory arrest, requires repeated administration



- *Application examples: anesthesia*

Figure 9- Retrobulbar injection in two steps.

### **2.3.3 Alternative modalities**

In the previous section, we have explained the limitations of the topical, systematic, and injection methods. These limitations give rise to the need of alternative modalities with more efficiency. For this matter, a range of different ocular drug delivery systems has been developed incorporating different technologies. For instance, implants are engineered to modify the drug release profile in a more controlled manner than the injections yet to provide a greater bioavailability when compared to topical or systematic administration. Some other modalities aim to modify the ocular barrier properties to make the tissue more permeable to the drug compounds e.g. iontophoresis and ocular sonophoresis. A general classification of these modalities could be found below with a short description of each system (Del amo and Uttri 2008, Gaudana et al. 2010, Achouri et al. 2013).

### **2.3.4 Controlled release**

The drug delivery systems which are based on controlled release try to address the drug delivery challenges by first, improving the bioavailability of the compounds; secondly, sustaining the drug release as required; and finally, minimizing the possible ocular complications (Thrimawithana et al. 2011). Some modalities that function based on these strategies are implants and colloidal systems.

#### **2.3.4.1 Implants**

In general, implants are designed to prolonged action duration of the drugs with a controlled release. By minor surgery or injection, they are placed intravitreally posterior to the lens and anterior to the retina.

**Biodegradable implants:** after the insertion, the biodegradable implants release the drug in two sequences; a burst release immediately after the insertion and a following slow release. Implants are made from polymers either industrial or natural (e.g. collagen). Milani et al (1993) showed

that the collagen-shield implants impregnated with anti-viral drugs, antibiotics, and anti-inflammatory drugs could be regarded as an alternative therapy to subconjunctival injections after intraocular surgery.

A wide range of biodegradable, thermoplastic polymers are also used to make this type of implants such as polyglycolide, polylactide, poly-lactic-glycolic-acid (PLGA), and polyglactin 910 (Vicryl). After insertion, these implants undergo very fast erosion which leads to a drug release burst consequently. Similar to the natural polymers, a relatively slower release occurs after this stage; however, the final degradation phase of the unnatural polymers leads to an additional final burst. The drug release from this burst is uncontrollable. An example of unnatural biodegradable implants is Surodex (Oculex Pharmaceuticals, Inc, Sunnyvale, CA, USA) which is commercially available. This implant contains 60 µg of dexamethasone incorporated into the polymer matrix (PLGA) and can be applied for post-cataract surgery inflammation treatment. Clinical studies (Lee et al. 2006) showed the higher effectiveness of the system when compared to topical eye drop administration.

- *Advantages:* no removal need, drug stabilization, bypassing BRB, increase drug action duration, and avoid the associated risks of repeated administration compared to injections
- *Disadvantages:* invasive device insertion, risk of retinal detachment, hemorrhage, and uncontrollable burst in drug release profile
- *Application examples:* CMV retinitis, postoperative inflammation, and macular edema

**Non-biodegradable implants:** these systems provide more controlled drug release when compared to biodegradable implants. However, they introduce more surgical risk due to the removal procedure. The ethylene vinyl acetate (EVA) and polyvinyl alcohol (PVA) are kind of polymers that the non-biodegradable implants can be made of from. The EVA membranes have been utilized to make episcleral implants for the treatment of the retinal and choroidal diseases. This type of degradable implants is showed to be a promising delivery system for sustained drug

release in a period of three months (Kato et al. 2004). An example of PVA implant is the Retisert (Bausch & Lomb, Rochester, NY, USA), which is a commercially available system. As for most of the degradable implants, the application of PVA is in treatment of chronic non-infectious uveitis of the posterior segment. The structural combination of this polymer and silicon laminate provides the possibility of corticosteroid for a duration of three years. However, there are some associated side effects have been reported in clinical trials (Del Amo and Urtti 2008).

- *Advantages:* more controllable delivery profile and longer drug release compared to biodegradable implants
- *Disadvantages:* invasive device insertion, risk of retinal detachment, hemorrhage, more risk of complication due to the device harvest
- *Application examples:* chronic non-infectious uveitis of the posterior segment.

**Cell encapsulation:** the so called encapsulated cell technology (ETC, Neurotech pharmaceuticals, Cumberland, IR, USA) is the basis of such implants. The ETC implants consist of a hollow capsule cultured with engineered cells and wrapped with a semi-permeable polysulfone. After the injection within the site, these cells continuously produce therapeutic proteins. The semi-permeability of the capsule provides a dual advantage: an entrance for the nutrients and an exit for the recombinant biotherapeutic. The capsule itself functions as a barrier to the host cellular immune system.

- *Advantages:* elongated drug action duration, limited toxicity
- *Disadvantages:* invasive, risks associated with surgery and implants
- *Application examples:* retinitis pigmentosa, potential application in neuroprotection in glaucoma, anti-angiogenesis in choroidal neovascularization, anti-inflammatory factors for uveitis

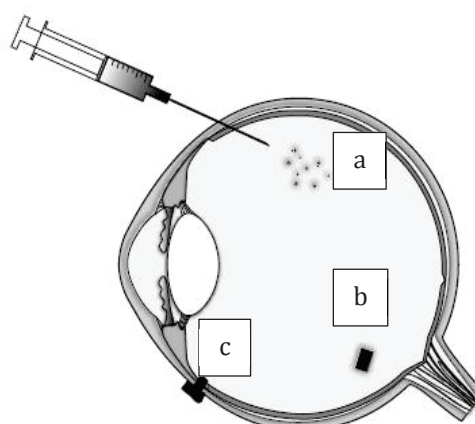


**Figure 10-** Schematic presentation of intravitreal injection of (a) micro- and nanoparticles and liposomes, (b) surgically introduced biodegradable or non-biodegradable implants, and (c) scleral sutured implants (Achouri et al. 2013).

### 2.3.4.2 Colloidal systems

These systems can target the delivery site with intravitreal injections of drug carriers. Concerning the fact that they prolong the drug action time, the frequency of injections can be reduced significantly (Fig. 10). Furthermore, the carriers can protect the therapeutic agents against enzyme inactivation (Achouri et al. 2013). Various models have been developed so far such as nanoparticles, liposomes, niosomes, cubosomes, and micro- and nano-emulsions. Most of them are at the very early stages of developments. Herein, we explore a couple of them that are in the pre-clinical stage

**Micro- and nanoparticles:** a sustained release also can be achieved by encapsulating the drug in the microparticles (1-1000  $\mu\text{m}$ ) and nanoparticles (1-1000 nm). This encapsulation protects the therapeutic agents from degradation. Similar to implants, these particles are made from biocompatible materials such as biodegradable polymers e.g. PLGA; when compared to implants however, the drug action period is typically shorter i.e. from weeks to months. The targeted delivery is also possible by engineering the encapsulation process. Furthermore, the prolonged release time of these systems reduces the complications associated with the more frequent injections. Although even with less frequent injections, the vitreal clouding is possible as a drawback of this method.

- *Advantages:* drug stabilization, less risk of toxicity compared to implants, localize delivery, reduce number of injections
- *Disadvantages:* invasive, vitreous clouding, risks associated with injections
- *Application examples:* choroidal neovascularization, intracellular delivery

**Liposomes:** liposomes are made from natural lipids vesicles ranging about 25 – 10,000 nm in diameter. The lipophilic drugs can be encapsulated to the natural lipid walls of the vesicles and the hydrophilic drugs within the interior aqueous of them. The natural structure of these carriers

opens up various potential applications. Intracellular delivery, for instance, is achievable since liposomes can be taken up by the phagocytic cells within the therapy site. Preferential binding is also possible by modifying the surface of vesicles. These systems are delivered by intravitreal injections, and as colloidal systems, they share similar characteristics with micro- and nanoparticles.

### **2.3.5 Iontophoresis:**

This delivery system applies low electrical current for transferring ionized drugs through transcorneal and transscleral routes. Several studies have shown that transcorneal iontophoresis could effectively increase the corneal permeability to certain compounds. For instance, the permeability increase of fivefold was achieved *in vitro* by Vaka et al. (2008) for the ciprofloxacin hydrochloride (anti-infection drug). The *in vivo* (rabbit model) tolerability studies and cytotoxicity studies in cultured corneal tissue, provided promising results. The studies on oligonucleotides delivery by transcorneal iontophoresis also showed encouraging results for ocular gene therapy (Voigt et al. 2002).

In comparison however, the transscleral iontophoresis has received more interests. The electro resistivity of sclera is relatively lower; it has a larger surface area with higher hydration degree; moreover, it can address the posterior segment of the eye and is more permeable to larger molecules when compared to the cornea. Studies have shown that application of this system increased the permeability of various drug compounds such as fluorescein, steroids, antibiotics, and antivirals (Thrimawithana et al. 2011). Although by this system delivery of macromolecules has not been fully achieved yet. Some *in vivo* studies on rabbit model reported no significant permeability increase of macromolecules such as Galbumin (Molokhia et al. 2009).

It has been also reported that application of iontophoresis could cause a decrease in endothelial cells and inflammatory infiltration. Even some choroidal and retinal damage were associated to higher current densities and longer iontophoresis (Parkinson et al. 2003). It is recently that some

newly developed systems considered safer with better tolerability when compared to previous models (Halhal et al. 2004, Del amo and Uttri 2008, Thrimawithana et al. 2011). Some of these systems are commercially available such as Ocuphor1 (Iomed Inc., Salt Lake City, UT, USA), Eyegate II Delivery System (EyeGate Pharma, Waltham, MA, USA), and Visulex1 (Aciont Inc., Salt Lake City, UT, USA). The following characteristics have been attributed to the recent models; however, more studies are still needed to further explore the efficiency and the adverse effects of this delivery system.

- *Advantages:* non-invasive, less risk of toxicity, addresses both anterior and posterior segments
- *Disadvantages:* requires repeated administration, low patient compliance due to the frequent administration, and specific drug formulation
- *Barriers:* Conjunctiva, cornea and sclera

### ***2.3.6 Ocular ultrasound-mediated drug delivery:***

There is a growing interest in application of US in ocular drug delivery. This topic is covered with details in the next chapter.

## ***Chapter 3(P.I),***

### ***Ultrasound mediated ocular drug delivery***

#### ***3.1 Introduction***

Application of ultrasound due to its non-invasive nature is shown to be a promising modality in ocular drug delivery. There are various routes which can be addressed by this system. Therapeutic ultrasound can be utilized to increase the permeability of drugs when they are applied exterior to the cornea or sclera i.e. topical administration (Zderic et al. 2004, Cheung et al. 2010). It also can be applied for transient blood-retinal opening and targeted ocular drug delivery (Park et al. 2012, Wang et al. 2012). Following the increase of therapeutic US application in the field of drug delivery, the interests in ocular DD has increased accordingly. The recent progress of this technology in terms of irradiators manufacturing and controlling physical parameters and effects has provided the opportunity to address the most challenging fields such as ocular drug delivery. The following chapter is focused on the ocular ultrasound drug delivery systems state of the art and principles.

In the previous chapter the concept of ocular drug delivery was discussed and the most practiced modalities were introduced. In this chapter, general aspects of ultrasound (bio-) effects and ultrasound drug delivery systems (USDD) are explained. More specifically, we will explore the ocular USDD and the state of the art. This background information is the basis of our studies in scleral USDD which are going to be presented in the next chapter of this essay.

#### ***3.2 Therapeutic ultrasound***

The ultrasound (US) energy can pass through the body without being fully absorbed at relevant power ranges. In other words it can see through the body. It is this non-invasive quality of the US which makes it one of the main modalities among the most practiced imaging technologies. This sort of energy is also found to be capable of creating therapeutic effects without damaging the non-targeted tissues and organs. With this regard, the ultrasound therapy has been explored, developed and practiced extensively in different applications. The clinical applications of ultrasound therapy



could be categorized to high intensity focused ultrasound (HIFU) cancer therapy, shockwave lithotripsy, and drug delivery (Bailey et al. 2003).

By focusing the US beams, it is possible to deliver high intensity US within the focal area while the prefocal regions remain rather untouched. This has given rise to application of HIFU systems to treat the inner tissues/organs in a non-invasive manner. The general aim of such therapy is to generate coagulative necrosis within the target tissue (Sanghvi and Hawes 1994). A wide range of cancerous organs have been already examined for HIFU therapy such as brain (Hynynen and Jolesz 1998), liver (Leslie et al. 2012), prostate (Blana et al. 2004), uterine (Keshavarzi et al. 2002), and ocular ciliary body (Aptel et al. 2011).

The application of HIFU in ophthalmology also has been long practiced. This aspect of HIFU application is explored in more details in part II of this manuscript.

The shockwave lithotripsy modality relies on the power of US generated shockwaves to destroy kidney and gall stones (Delius et al. 1994). The shockwave can be formed in an US focal field where the non-linear effects are sufficiently strong. As described by non-linear acoustic theory (Hamilton 1986), a distortion of wave propagation occurs due to the non-constant propagation speed where higher-pressure portions of the US wave travel faster than lower-pressure portions. As this distortion increases significantly within the focal zone, shock fronts are formed (Canney et al. 2010). In the case of lithotripsy, this shockwave formation causes the break of kidney stones within the US focal field.

In addition to the ablative properties of HIFU, ultrasound-mediated drug delivery is an approach that also holds promise. The possibility of enhancing the efficacy of non-invasive drug administration while avoiding the risks of invasive methods is an enticing goal indeed. In the following sections this application of therapeutic US will be discussed in more details starting with a short description of US mechanisms.

### ***3.3 Ultrasound mechanisms in drug delivery***

Depends on the application, some therapeutic effects of US energy may or may not be desirable. For instance, in the field of USDD, a system might benefit from the cavitation phenomenon for modifying the barrier properties of the target but not the hyperthermia which might lead to target damage. With this concern, understanding the mechanisms is crucial to achieving the intended therapeutic effects (Bailey et al. 2003). Some contributing mechanisms in USDD are reviewed in this section.

#### ***3.3.1 Ultrasound effects***

Generally speaking, by application of ultrasound it is possible to induce a wide range of biological effects. Numerous studies and clinical data have shown that application of ultrasound enhances the permeability of drugs into the region of interests (Pitt et al. 2004). This permeability increase generally is attributed to the target's barrier modification where the ultrasound effects make the target more receptive.

In the literature the ultrasound effects have been categorized broadly to thermal and non-thermal effects (Kitchen and Partridge 1990, Bommanna et al. 1997, Baker et al. 2001, ter Haar 2007). As US propagates through the biological tissue some of its energy is absorbed and converted to heat due to scattering, relaxation, and viscous absorption processes (Fry 1952). The consequent temperature rise and thermal effect induce different biological reactions within the target tissue. The magnitude of this temperature rise depends on the intrinsic acoustic properties of the tissue. Some of these properties are frequency dependent e.g. the tissue absorption increases almost linearly with US frequency. The heating rate can be controlled to some extent by adjusting the exposure duration, US intensity, and duty cycle (on/off ratio). Therefore, in designing a delivery system where tissue necrosis is not an intended effect e.g. scleral USDD system, the US needs to be applied in lower frequency ranges in pulse regime with lower duty cycles.

Generally in drug delivery systems however, a mild thermal effect enhances the drug permeability by heat-induced physiological modification. It increases the kinetic energy of drug molecules as well as membrane structure. It may also dilate the membrane pores and increase the circulation to the delivery target (Byl 1995). Based on the heat induced viscosity alteration, the diffusivity is also enhanced according to the Stokes-Einstein equation (Saltzman 2001):

Eq. 1

$$\frac{D_2}{D_1} = \frac{T_2 \times \mu_1}{T_1 \times \mu_2}$$

where  $D$  is diffusion coefficient ( $\text{cm}^2/\text{s}$ ),  $T$  is the absolute temperature (K), and  $\mu$  is the dynamic viscosity of the medium (Pa.s). Based on this equation, if application of US leads to temperature increase of one degree Celsius from the room temperature (from  $T_1 = 20^\circ$  to  $T_2 = 21^\circ$  C), the diffusivity will be enhanced by 2.7%. In this way, the temperature rise as a result of ultrasound energy absorption, actively contributes to the enhancement of drug permeability to some extent.

The non-thermal effects of ultrasound exposure are generally associated with mechanical effects such as radiation force, bulk streaming, cavitation and cavitation induced effects. Along with thermal effects, these also potentially contribute to drug delivery enhancement. For instance, bulk streaming occurs as ultrasound propagates within a liquid medium. This effect leads to the movement of the liquid along the direction of the beam which is believed to be one of the involving effects in transdermal USDD systems – sonophoresis (Mitragotri 2005 A). Interestingly, this bulk streaming reduces the US induced temperature rise at the interface of the medium and the tissue (Wu et al. 1994). Tachibana (2001) showed that this effect increases the drug permeation into the thrombus.

Among all mechanical effects, cavitation phenomenon is thought to be the major contributor effect in US enhanced drug delivery. Bommannan et al. (1992) showed that a significant transdermal USDD enhancement could be achieved due to the presence of cavitation activity in their system. In the intra-cellular level, studies showed that reversible modification of viable cell membrane was

induced by cavitation which eventually increased the uptake of drugs, genes, and various macromolecules (Liu et al. 1998, Guzman et al. 2001).

Cavitation can be defined as the formation of cavities and/or micron-sized bubbles due to an acoustic pressure gradient within the acoustic medium. If the pulsation of cavitation bubbles continues over many pressure cycles without bubble collapse, it is considered stable cavitation. In this case the bubbles follow the pressure gradient of the sound field almost linearly. However, the sequence of dramatic growth of the bubbles and the transmitted inertia of the surroundings in turn, results in a fierce collapse within just a few pressure cycles. The collapsed bubbles fragment into much smaller bubbles and may serve as the nuclei for the next cycle of growth and collapse. This cycle is referred to as inertial cavitation.

The formation of initial nuclei for cavitation activity depends on pressure gradient, energy absorption, and US frequency. In order to participate in cavitation activity, bubbles need to reach the resonant size within the pressure field. This resonant bubble radius is frequency dependent and approximately estimated to be  $3/f \mu\text{m}$  where  $f$  is frequency in MHz (Young 1989). This estimation is valid when the acoustic medium is water; in tissue however, this expression leads to an underestimation of the bubble size since they are stiffer under the tissue constraints and resonant radius is almost larger of an order of magnitude (Bailey et al. 2003).

There are several phenomena associated to cavitation as its secondary effects. For example the stable vibrating bubbles induce a localized liquid flow around them which results in a form of acoustic streaming called microstreaming (Fig. 11, Elder 1959, ter Haar 2007). This effect is mechanically far more powerful than bulk streaming (Duck 1998). The occurrence of this phenomenon near the cell induces shear stress on the membrane and eventually leads to disruption. Therefore, bulk and micro-streaming are considered as two different US effects; while bulk streaming facilitates the drug diffusion through a membrane, microstreaming is capable of rupturing the surface of the membrane.

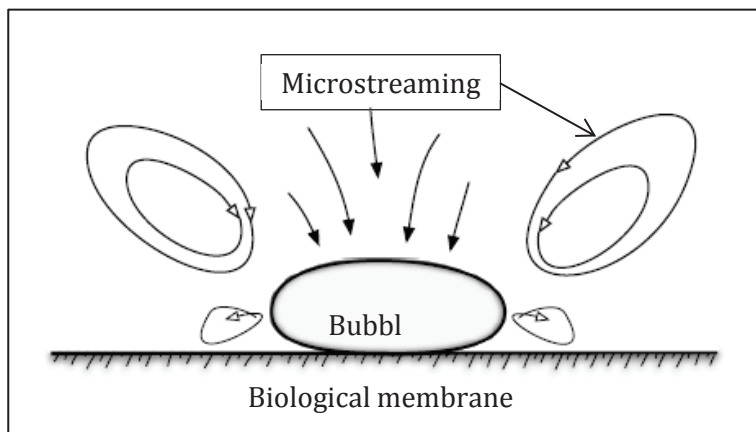


Figure 11- Fluid microstreaming around oscillating bubble (Elder 1959).

The inertial cavitation also induces some secondary local phenomena. Very high local pressure (above 10 MPa) and local temperature increase (up to 10,000 K) are two major cavitation induced effects which can be expected within the acoustic medium. Consequently, this high local (in the vicinity of a cavitating bubble) temperature increase generates free radicals in the cavitation site (this phenomenon can serve as chemical detector of the inertial cavitation, See 3.2.5). Formation of microjets is another effect of bubble collapse near a solid surface (Leighton 1994). These high speed liquid jets can induce pits in the tissue in the vicinity of bubble collapse (Fig. 12). It has been demonstrated that almost every stage of inertial cavitation i.e. bubble expansion, collapse, induced shock waves, and microjets may contribute to an enhanced drug delivery and membrane permeabilization (Sundaram et al. 2003).

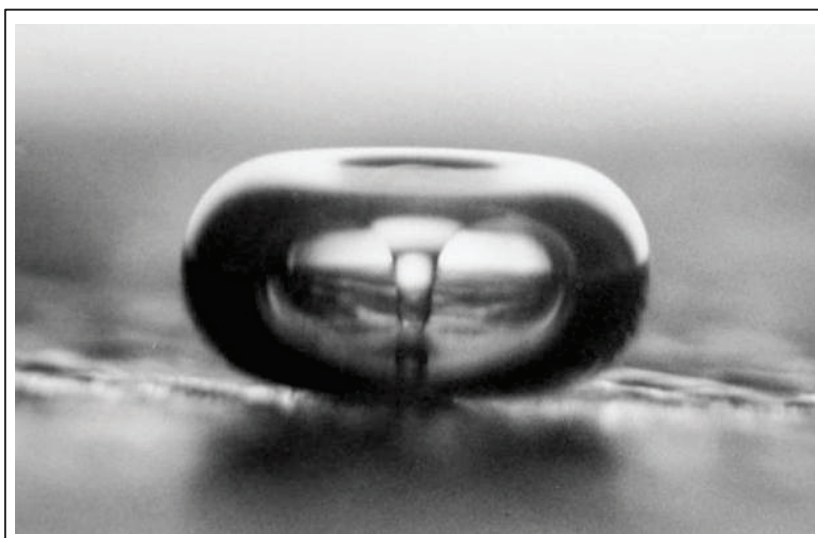


Figure 12- Formation of microjet during inertial cavitation (courtesy of Dr. Crum).

The bubble activity also leads to more heat production. Bailey et al. (2003) associated this phenomenon to several mechanisms. The cavitation heat production is the result of energy conversion of bubbles to heat due to the fact that the viscosity inside and in the vicinity of the bubbles damps their oscillation. In addition, the nonlinear scattering of the bubbles distributes the energy on higher harmonics hence more ready to be absorbed by the surrounding tissues. These all contribute to more mechanical energy to be converted to heat and result in secondary thermal effects. As been mentioned earlier, the combination of these effects candidates the cavitation phenomenon as a major contributor in an enhanced drug delivery. In the following sub-section, these contributions are explored further.

### ***3.3.2 Cavitation and drug delivery***

The contribution of cavitation in USDD can be classified into three major modes of action: drug transport, disruption of the drug carrier, and target barrier modification.

The streaming and convection effects of US, contribute directly in drug transport augmentation and hence diffusivity increase. As an US beam propagates through a partially absorptive medium, some of its momentum is transferred to the medium which in turn, results in a convective oscillatory motion within the medium. This effect is believed that contributes in overall drug transport enhancement (Starritt et al. 1989). This mechanism becomes dramatically pronounced in the presence of cavitation. The microstreaming effect of stable cavitation conducts a high velocity drug transport in the vicinity of the oscillating bubbles and the target site (Pitt et al. 2004).

A range of drug carriers and vesicles was introduced in the previous chapter. Despite of their structural difference, they are all denser than the suspending liquid around them. With this regard, as the stable cavitation generates microstreaming, the carriers get drawn into the shear field around the oscillating bubble. Consequently, the imposed shear stress ruptures the wall of the vesicles and the imprisoned drug will be released. The same mechanism of shear stress and vesicles rupture can happen in the presence of inertial cavitation. The shockwave from the bubble collapse generate a

dense fluid front over the surface of the vesicles in the vicinity. If the induced shear stress exceeds the critical point, the vesicle ruptures consequently. In the same manner, the cells or target membrane that are in the vicinity of cavitation bubbles, undergo a high shear stress to some extent that ruptures and openings can be created on their surface (Fig. 13). As the result, the membranes become more permeable and the passage of drug compounds significantly improves for intra- and intercellular delivery.

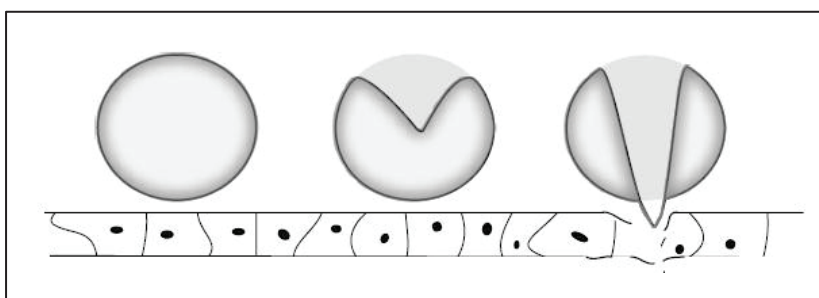


**Figure 13- Asymmetric bubble collapse near the membrane produces a jet of liquid toward the surface that ruptures the lining.**

Many USDD systems aim to benefit from these mechanisms such as sonoporation and sonophoresis. As been explained, through a design process, it is possible to increase the likelihood of some desired US mechanisms for a specific drug delivery system. In the following section, several systems will be introduced with this consideration.

### ***3.4 Ultrasound mediated drug delivery systems***

The advantages of ultrasound mediated drug delivery systems have expanded its application in various drug delivery fields of study; it is non-invasive; it facilitates the drug transportation; it modifies the barrier properties of the target; its energy itself improves the treatment absorption rate. In case of targeted delivery, the possibility of precise drug targeting is a great advantage of US application where it lowers the systematic drug toxicity significantly. The principles of US mediated blood-brain barrier (BBB) or blood-retina barrier (BRB) opening lie also upon these advantages. In recent years encouraging results have been achieved in intra-cellular drug delivery of genes and rather large molecules, a technique known as sonoporation. The inter-cellular drug delivery,

sonophoresis (or phonophoresis), is also an emerging alternative drug delivery system for topical administration.

### **3.4.1 Targeted delivery**

As been explained before, the low bio availability and side effects for non-targeted organs in terms of toxicity are some of the main challenges of common drug delivery systems. With this regard, the concept of local drug activation has been investigated substantially in the past decades especially for some therapies such as cancer therapy (Feril and Tachibana 2012). Some targeted drug delivery systems try to deal with the above challenges through drug design process. As described in previous chapter, one example could be encapsulating the drug compounds within the long-circulating liposomes. By application of this system in cancer therapy, it is possible to maintain the drug stability and achieve more efficient systematic transport while avoiding large dosing and toxicity (Allen 1994). In spite of this advantage, colloidal methods alone are not efficient enough due to the poor drug unloading and very low bio-availability of the compounds at the cancer site. With this regard, application of some multidisciplinary technologies has provided the possibility of overcoming these complex challenges e.g. by applying UV, visible light, US, mild heating and hyperthermia. These modalities can facilitate the drug unloading within the target site. Expectedly among them, application of ultrasound technology is shown to be distinctively efficient. This efficiency is mainly due to the fact that the US energy can be focused into the region of interest with shielding the non-targeted tissues from side effects (Oude Blenke et al. 2013).

As been mentioned, the *in vitro* studies showed the presence of cavitation activity enhances the targeted drug delivery process. Within the tissue (*in vivo*) however, cavitation is less likely to happen when applied with rather lower and safer US parameters. Therefore, the need of an enhancer to introduce the cavitation locally *in vivo*, led to application of ultrasound contrast agents (UCA) which was preliminary designed for the ultrasound imaging (Blomley et al. 2001). Application of UCA on lowers the threshold of cavitation as an enhancer. In addition, they can be used as cavitation nuclei



themselves. The UCA are micron-sized bubbles with a stabilized shell. They can be customized in different sizes i.e. different resonance frequencies to be applied with different US frequencies. At a desired site *in vivo*, exposing the microbubbles to the US energy highly increases the occurrence of cavitation which in turn, it increases the local release of the therapeutic agents.

### **3.4.2 Sonoporation**

Application of ultrasound with certain exposure conditions can increase the porosity of the cell membrane. This phenomenon can serve in intra-cellular drug delivery and non-viral gene transfection. The openings of the membrane provide opportunity for up taking genes, macromolecules, and drug compounds within a cell. By definition, this opening process should be a transient effect and drug transfection is limited to the exposed cells. There are numerous studies been carried out and results shown to be promising (Escoffre et al. 2013). By application of ultrasound at 24 KHz, Liu et al. (1998) demonstrated that the membrane permeabilization of porcine red blood cells was achievable and increased in accordance with the increase of acoustic pressure in a range of 0.1 to 0.9 MPa. In this work, release of hemoglobin was taken as the degree of membrane permeabilization and was determined as a function of ultrasound parameters.

In cancer treatment, application of HIFU is instrumental to induce hyperthermia. By the aid of thermal effects of HIFU, it has been demonstrated that drug and antibody accumulation in the ablated regions is increasing. By the aid of mechanical effects of HIFU on the other hand, the drug penetration also increases. In the studies of Wang et al. (2012), this enhancement was traced back by fluorescently labeled drugs and efficacy of the treatment was determined by monitoring the tumor size. Their results showed a significant penetration of antibodies by application of HIFU in pulsed regime at 1 MHz (average intensity of 2 KW/cm<sup>2</sup>).

The ultrasound mechanical effects are shown to be the major contributors in permeabilization of different types of cells. In the *in vitro* studies of Bazan-Peregrino et al. (2012), the role of inertial cavitation was found to be central in sonoporation of breast cancerous cells. Based on the effects of

inertial cavitation, sonoporation is also found to be highly potential system for selective tumor treatment (Umemura et al. 1997). This has been partially attributed to cavitation induced local shockwaves which might modify the cell membrane and enhance the drug uptake (Unger et al. 2002).

With this regard, the application of microbubbles is of an advantage in sonoporation in order to facilitate the cavitation activities. In case of targeted sonoporation, sorts of lipid-coated microbubbles have been developed which can bind to cell-specific receptors or antigens by incorporation of ligands into the cell membrane. In addition, the microbubbles can be loaded by drugs and be delivered to precise locations in the body. As ultrasound can be focused tightly to defined delivery sites within the body, the microbubbles can be unloaded in the regions of interest for precise treatment of the tissue (Unger et al. 2004).

### ***3.4.3 Blood-brain barrier opening***

Another promising application of ultrasound is in drug and gene delivery to the central nervous system (CNS) which is one of the most challenging fields of drug delivery. The vessels in the CNS are lined by endothelium which consists of an inter-cellular tight junction and forms blood–brain barrier (BBB). Over 95% of therapeutically potential molecule drugs cannot penetrate from the barrier between blood and cells in the CNS (Hynynen 2008).

The preliminary studies in 90s showed that this barrier could be disrupted at certain US parameters to facilitate the passage of drug mimicking compounds. However, some unwanted damage was found in different brain regions. In addition, the opening was also not consistent and reproducible (Vykhodtseva et al. 2008). Later on, by coupling the microbubbles with focused ultrasound, these problems were tackled effectively. As microbubbles decrease the cavitation threshold, much less intensities were needed for BBB disruption. Hynynen et al. (2001) examined this combination on the rabbit brain at 1.63 MHz pulsed focused ultrasound (0.7 -1 MPa). Repeatable BBB disruption was possible at targeted locations by introduction of microbubbles into the delivery

system at much lower pressure levels compared to previous studies. In addition, the transient openings got closed within 48 hours after sonication, shown by contrast enhanced MR imaging. The histological studies also reported a minimal damage. In the following studies, focused US with lower frequencies e.g. 260 KHz was applied (Hynynen et al. 2006). In this way, it was possible to increase the focal volume and also reduce the energy absorption of the skull along the beam pathway.

The exact mechanism which leads to the BBB disruption is not fully understood yet. The transient disruption is thought to be a contribution of mechanical US effects i.e. cavitation activity and acoustic radiation forces. For that matter, the bubbles must be in contact/near-contact with the endothelium in order to deal with tight junctions of endothelial cells. Acoustic radiation forces can push the bubbles towards the vessel walls along the US beam direction. The generated pressure thus may be involved in the opening process by activating the stretch-sensitive ion channels in the vascular endothelium. The microstreaming effect of stable cavitation can also play a role in lower applied pressure. Inertial cavitation however, would likely to be the most significant effect, due to induced microjets disruptive power (Vykhodtseva et al. 2008).

#### ***3.4.4 Transdermal sonophoresis***

Generally speaking, the delivery routes in transdermal drug delivery systems are the inter-cellular channels. Through these channels the delivery target can be addressed either systematically e.g. for kinetosis (motion sickness) treatment by delivery of scopolamine, or locally in case of cortisone application. In most cases though, transcutaneous drugs are aimed to pass through the skin and enter the vascular system for systematic drug interactions. It has been shown that topical administration has advantageous over intravenous drug delivery; beside the great advantage of being non-invasive, it provides better drug control release with less chances of under dose delivery or toxicity (Byl 1995). However, the efficiency of topical administration is severely limited by the outermost layer of skin, stratum corneum, where it poses a major barrier to the drug penetration.

Recent studies in dermal drug design have been resulted in achieving more permeable drugs (Cevec et al. 1995). Even with rather new formulated drugs still, the efficiency of topical administration is not yet considerable. On the other hand, it has been shown that application of enhancers such as electric current i.e. iontophoresis and ultrasound energy i.e. sonophoresis, can increase the DD efficiency. These enhancers could be applied prior to, during, or after the topical administration (Byl 1995). By application of ultrasound after the administration, it was possible to enhance the delivery of transcutaneous drugs or some large molecules such as proteins (Mitrgorti et al. 1995 B).

The first sonophoresis study is dated back to 1954 (Fellinger and Schmid). Since then, numerous studies, including pre-clinical trials, have shown the safety and efficacy of US application. Although the exact involved mechanisms in the enhancement process are yet not clear. Fellinger and Schmid (1954) concluded that the alteration to the skin is the preliminary effect of US enhancement by showing its efficacy with prior application of the US to the drug administration. Later on, similar experiments and microscopic studies validated this alteration in terms of opening of the inter-cellular channels (Bommannan et al. 1992).

Similar studies by other groups demonstrated the influence of the US frequency on the permeability. Mitragotri et al. (1996) showed that for both lipo- and hydrophilic drugs, the penetration could be enhanced greatly by application of 20 KHz US. In their studies, the molecular weight played no significant role in permeation enhancement. For example for two different hydrophilic drugs, Aldosterone (360 D) and Butanol (74 D), the enhancement was 1400 and 29 fold respectively. Prior to this achievement, they also showed that at 1-3 MHz relatively fewer enhancements could be obtained. They hypothesized that stable cavitation could induced disorders in the stratum corneum lipid bilayers which facilitated the drug transportation (1995). On the other hand, Bommannan et al. (1992) achieved a significant increase of 4 and 2.5 fold for salicylic acid at 10 and 16 MHz respectively. In the same study but at a lower frequency, contrary to the latter study,

there was no significant enhancement achieved at 2 MHz when compared to passive diffusion. At 10-16 MHz the cavitation activity is less probable since the required resonant bubble size is dramatically small (See 2.3.1). The thermal effect of US on the other hand, could explain this outcome since at higher frequencies the energy absorption increases significantly (ter Haar 2007).

The fact that bubble activities play a central role in sonophoresis has been hypothesized by many research groups. However, there are very a few studies which provided evidences and back up for this hypothesis. One from this short list is the studies of Tang et al. (2002). In their studies the application of an *in vitro* high-pressure-sonophoresis cell provided the opportunity to promote or suppress the cavitation activities selectively. According to the results, presence of cavitation was directly related to the permeability enhancement of the tissue. While at the same exposure conditions but without cavitation (by applying high-viscosity coupling medium) no significant result was achieved (Although several shortcomings could be pointed out in this study, See 4.4). Later on, by theoretical prediction and some back up experiments, Tezel and Mitragotri (2003) demonstrated that at low range frequencies, the interaction of inertial cavitation and induced microjets with the stratum corneum played a major role in their studies. This interaction could result in disruption of the lipid layer and more facilitated drug transportation.

### **3.4.5 Ocular sonophoresis**

The ocular sonophoresis is one of the most challenging fields in the USDD. Several reasons contribute to this fact. Contrary to the transdermal sonophoresis, the accessibility to the ocular tissue is very limited. In addition, the specific barrier properties of ocular tissues have made this organ almost non-permeable. In spite of these facts, several studies provided encouraging results to pursue the development of this modality. The preliminary studies are carried out in former Russia, Soviet Union (Cherkasov et al. 1974, Marmur et al. 1979, Filippenko and Tretiak 1989, Iakimenko et al. 1989)<sup>1</sup>. Among them one of the first studies on general ocular permeability could be found, done by Tsok et al. (1990). The purpose of their *ex vivo* study was to investigate the influence of different ultrasound frequencies (127 KHz - 2.75 MHz) on the ocular tissues permeability. The ultrasound was applied in continuous regime at 0.2-0.3 W/cm<sup>2</sup>. The permeability measurements were done using radionuclides such as mTc and pertechnetate. After each experiment their accumulation were measured in the aqueous humor, vitreous body, cornea, iris, sclera, crystalline lens, choroid and retina. The results showed a dependence of permeability modification on frequency variations. The maximum increase was found at the frequency level of 660 KHz. Except this work, most of the ocular sonophoresis studies focused on one single delivery route, either the cornea or the sclera.

#### **3.4.5.1 Corneal USDD**

The first documented studies are dated back to the late 1960's by Tsok. In his studies the anterior segment of the eye was addressed by the corneal pathway. In 1971, he developed the first ocular USDD device and ten years later, the device was applied in a clinical study on 251 children aged 2-14 years old. It was reported that the system was well tolerated by children as opposed to invasive methods such as injection. Their results showed a significant recovery of spasms of accommodation, local injuries, amblyopia, and increase in visual acuity by application of 880 kHz US in continuous regime at 0.2-0.3 W/cm<sup>2</sup> (Tsok et al. 1983).

---

1- Most of these preliminary studies are not available except in Russian language. For the purpose of this study, we translated some of their major works that are discussed in this section.

In a try to understand the mechanism of ultrasound induced permeability enhancement, Nuritdinov (1981) found that sonication in aerated medium induces damage to the cornea. The damage was limited to the epithelium layer in form of visible small pits (at 880 KHz, 0.2 W/cm<sup>2</sup>). In degassed solution on the other hand, no damage was noticed and the permeability of the drug was less than aerated medium. The studies were carried out both *ex vivo* on rabbit eyes and *in vivo* on human. In case of *in vivo* studies the induced damage disappeared within six hours. The separate sonication and drug exposure still showed penetration enhancement.

In these studies, the first hypothesis was that the cavitation-induced epithelial damage was the main reason for corneal permeability increase. The hypothesis of cavitation contribution was tested further by modifying the viscosity of the acoustic medium. By adding Fibrinolysin, the viscosity and thus cavitation resistance of the medium was expected to be increased. The permeability experiments also demonstrated that less permeability enhancement could be achieved when compared to unmodified medium set-up. With regard to these outcomes, the permeability enhancement was associated with cavitation phenomenon. One of the major limitations of this study however, was that no acoustic measurement was performed. In addition, changing the viscosity of the medium would change some other US effects as well e.g. streaming effect; therefore, the level of their participation in the permeability process could be altered as well. Moreover, the increase of viscosity decreases the drug absorption consequently (Levy and Jusko 1965).

In more recent studies, the permeability of several  $\beta$ -blockers (glaucoma drugs) was also shown to be modifiable *in vitro* by application of pulsed ultrasound with duty cycle of 15% at 20 kHz and 2 W/cm<sup>2</sup> (Zderic et al. 2002). The authors believed that convection and cavitation were the major contributors in inducing corneal disorganization which ultimately led to permeability enhancement. To further explore this hypothesis, separate exposure of US and drug performed; there was no significant enhancement was achieved. By this, they concluded that the immediate US effects, convection and cavitation, played the major role in permeability enhancement.

Later on, their microscopic studies provided some evidence of corneal disorganization by application of US at 880 KHz, 0.19-0.56 W/cm<sup>2</sup> (Zderic et al. 2004). The US induced damage was found to be limited to the epithelium. This damage was believed to be a player in the permeability enhancement process since the tight intracellular junctions of the epithelium represent a major barrier in corneal drug delivery. In the same study it was shown that corneal permeability increased by increasing the US intensity. In a free acoustic field set-up it was also shown that with the applied US parameters cavitation could be induced accordingly to the ultrasound intensity. Based on this, the permeability increase was associated to the cavitation effect. However, some shortcomings of this study keep this association more speculative.

This investigation was limited by the fact that direct cavitation studies were performed in free acoustic fields with different experimental setups of permeability studies. Given the sensitivity of cavitation events to aberrations at interfaces, the amount and more importantly the type of bubble activity can differ distinctively between these two set-ups. Additionally, the permeability increase was associated to the cavitation increase which was in fact induced by applied power increase. In this way the contribution of cavitation to the permeability increase with respect to the other acoustic phenomena cannot be determined. Moreover, it needs to be considered that these studies were performed in the continuous regime, thus the contribution of thermal effect is significant and whether the cavitation effect plays a major role or not, is even more difficult to determine.

In the following studies of same research group, the permeability modification was investigated at 400, 600, 800, and 1000 kHz applying the same experimental protocol (Nabili et al. 2013). The efficiency of the USDD was found to be more dependent on the applied drug (sodium fluorescein, dexamethasone, and tobramycin) rather than frequency. For instance, significant increase in permeability of fluorescein was achieved for all applied frequency with no significant order. In case of dexamethasone, the same results were achieved except at 1 MHz. In case of tobramycin, no significant enhancement was observed at all frequencies. In terms of enhancement, the effects were



attributed to streaming, cavitation, and thermal effects. A semi-quantitative damage measurement was also performed by histology. Similar to previous studies, signs of epithelial damage were found and considered as the barrier openings for the drug diffusion.

The cornea is found to be a promising route for gene delivery with the advantage of noninvasive monitoring by microscopic observation (Bennett and Maguire 2000). In an *in vitro* study, Sonoda et al. (2006) showed that no gene transfer occurred when cultured epithelial cells were exposed to DNA but not ultrasound. By application of US at 1 MHz gene transfer was enhanced limitedly. By use of microbubbles however, a significant increase of gene transfer was achieved. In the follow up *in vivo* studies the combination of US and microbubbles again increased significantly the gene transfection compared to DNA injection. The *in vivo* US exposure parameters were chosen based on the *in vitro* parameters by which an efficient gene transfer with low cellular damage was achieved (pulsed regime with 50% DC at 1-2 W/cm<sup>2</sup>).

#### **3.4.5.2 Transscleral USDD**

With regards to the anatomical approach to treatment, most studies for ocular USDD have focused on transcorneal delivery (Zderic et al. 2002 and 2004, Sonoda et al. 2006, and Nabili et al. 2013) but the number of studies which have investigated the use of USDD for transscleral drug delivery is limited. Given the stark difference between scleral and corneal tissue within the eye, it stands to reason that a unique approach must be developed and validated with regards to physical parameters and permeability kinetics. With this consideration that the scleral route innate some advantages over corneal delivery route (See 1.3.1).

The work of Cheung et al. (2010), to the knowledge of author, is the only published study so far that has explored the scleral USDD. In their rabbit *ex vivo* studies, they aimed to measure the penetration of the proteins through the sclera applying 1 MHz and acoustic intensity of 0.05 W/cm<sup>2</sup>. They demonstrated that application of 30s US increased the intracellular penetration of protein by 1.6 folds when compared to sham treatments. The histological studies showed no significant damage

to the retina. In a try to understand the mechanism of this enhancement, temperature and acoustic noise measurement were performed; the temperature rise was limited to less than 0.5° C; acoustic measurements showed that the applied power could promote stable cavitation activity. On the other hand, increasing the frequency to 3 MHz resulted in no significant enhancement at the same power and US exposure time as 1 MHz. Considering the fact that at 3MHz stable cavitation was less possible and the thermal effect should not be significant (treatment T increase <0.5° C), the hypothesis of cavitation contribution as a major player was formed. The studies however, have not progressed any further to explore this speculation. Considering the advantages of sclera as a drug delivery pathway, more investigations are needed to shed light on the mechanisms of US enhanced scleral drug delivery.

## **Chapter 4(P.I),**

### ***Transscleral drug delivery: in vitro studies***

#### **4.1 Introduction**

As mentioned before, despite the fact that sclera is an attractive pathway for ocular drug delivery, limited work has been done so far to study US mediated transscleral drug delivery. Herein, the aim of present studies is first, to investigate the feasibility of US application in transscleral drug delivery enhancement; secondly, to investigate the involving mechanisms in scleral permeabilization by a mechanistic study. The endeavor of feasibility study, *in vitro*, is presented in this chapter.

With regards to study design, the *in vitro* model presents numerous advantages for the scope and goals of the USDD studies presented here (Feril et al. 2012). The choice of an *in vitro* model allowed a large sample size, and for many parameters to be investigated, as well as allowing the isolation of the sclera from other anatomical structures in the eye. The tissue samples were placed within a diffusion cell built in-house (Fig. 14) with an integrated 1.1 MHz US apparatus. A range of US exposure conditions have been studied and the permeability of the compound drug, sodium fluorescein, was measured for further investigations.

Concerning the choice of model drug compound, the physicochemical properties of sodium fluorescein (376 Da, 0.5 nm) are comparable in terms of molecular weight and size to a range of drugs which are used in current ophthalmic practice (Wen et al. 2010) e.g. Atenolol (266 Da, 0.47 nm), Metoprolol (267 Da, 0.47 nm), Fluconazole (306 Da, 0.50 nm), and [3H] dexamethasone (392 Da, 0.54 nm).

As previous studies suggested, among US effects, cavitation phenomenon can enhance the drug permeability predominantly compared to other effects. A preliminary study has been also been performed to explore this hypothesis in this phase of the study.

## 4.2 Material and methods

### 4.2.1 Preparation of samples

Permeability experiments were carried out on rabbit eyes, which are a well-characterized model in ophthalmic research (Tsok 1990; Zderic et al. 2004; Wu et al. 2013). The use of in vitro animal samples was approved by the local animal ethics committee.

Immediately after euthanasia, the eyes of adult New Zealand white rabbits were excised, immersed in a storage medium (Dulbecco's phosphate-buffered saline, DPBS, D6650, Sigma), and stored at a temperature of 4°C. Tissue samples were used within 8 hours of excision. The samples were transferred to a phosphate buffered saline PH 7.4 solution (PBS, P5368, Sigma) at 20° C approximately 30 minutes before experiments. A few minutes before being placed in the diffusion cell for treatment, each eye was covered with saline buffer and dissected with a scalpel to obtain full-thickness incisions. A cotton tip applicator was used to remove adherent tissue associated with other ocular structures and to isolate the bare sclera (Lee 2004).

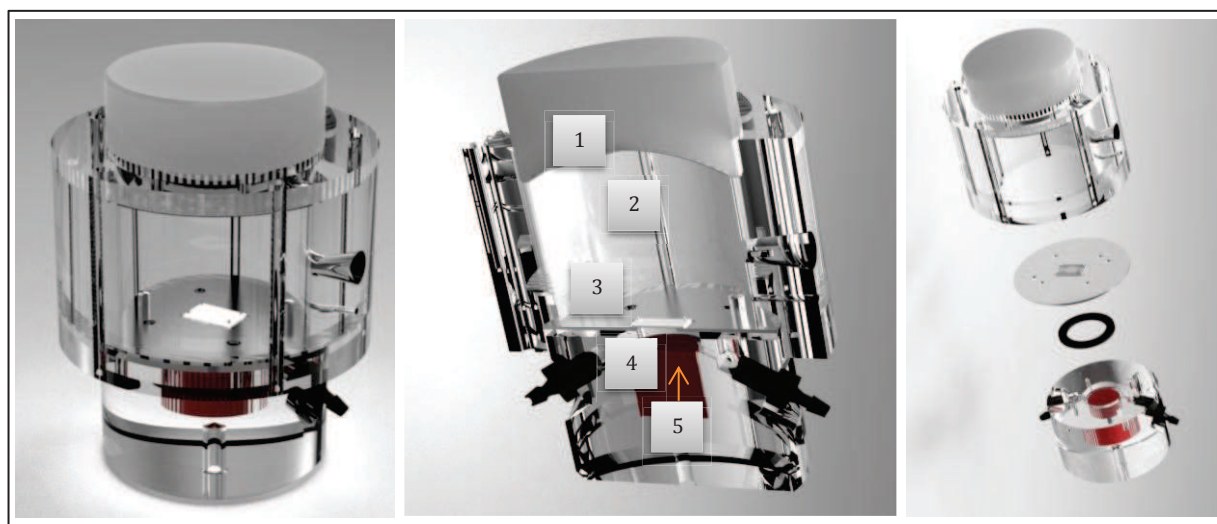


Figure 14- Custom diffusion cell. (1) US transducer; (2) donor chamber; (3) tissue membrane; (4) receiver chamber; (5) ultrasonic absorber.

A custom diffusion cell was designed and built for the purpose of this study (Fig. 14). It consisted of 2 chambers, donor and receiver, with two plates for holding the sample in between the chambers.

Thus, the transscleral route was the only passage between the two chambers of the cell. Dissected samples of sclera were mounted between the two plates (with an orifice of  $9 \times 6 \text{ mm}^2$ ). The plates were then attached to a receiver chamber to be filled with solution. Once attached, the chamber was filled with phosphate buffered saline (10 ml) to such an extent that the tissue retained some of its curved shape in the natural outward direction that is observed in vivo (Fig. 15).



**Figure 15- Placement of sclera sample while maintaining the natural outward curvature.**

After filling the receiver chamber, the donor chamber was attached to the apparatus and filled with 80 ml of diluted sodium Fluorescein solution (0.03 mg/ml, Fluorescéine faure 0.5%, Novartis, RM, France). The ultrasound transducer was mounted on the side of the donor chamber. The ultrasonic beam was normally incident to the tissue sample which was placed at the focal plane. The whole cell was then placed horizontally to eliminate gravitational diffusion. Additionally, by placing the cell in a horizontal position, the presence of bubbles on the transducer and membrane surface was less prevalent than when placed in a vertical position.

#### **4.2.2 Ultrasonic setup**

A focused piezoceramic ultrasound transducer (PZ26, Ferroperm Piezoceramics, Kvistgaard, Denmark), 50 mm in diameter and focal length, operating at a frequency of 1.1 MHz was used in this study. The transducer was electrically matched at  $50 \Omega$ . Tone bursts were generated by an arbitrary function generator (NI PXI- 5412, National instruments, Austin, TX USA), and amplified by an RF Power Amplifier (400 W, 55 dB; 1040L, Electronics and Innovation Ltd., Rochester, NY, USA). The total time-averaged electrical power of the transducer was measured by a wattmeter (Power Reflection Meter NAP and Power Head 1950 W, Rhode and Schwarz, Munich, Germany).

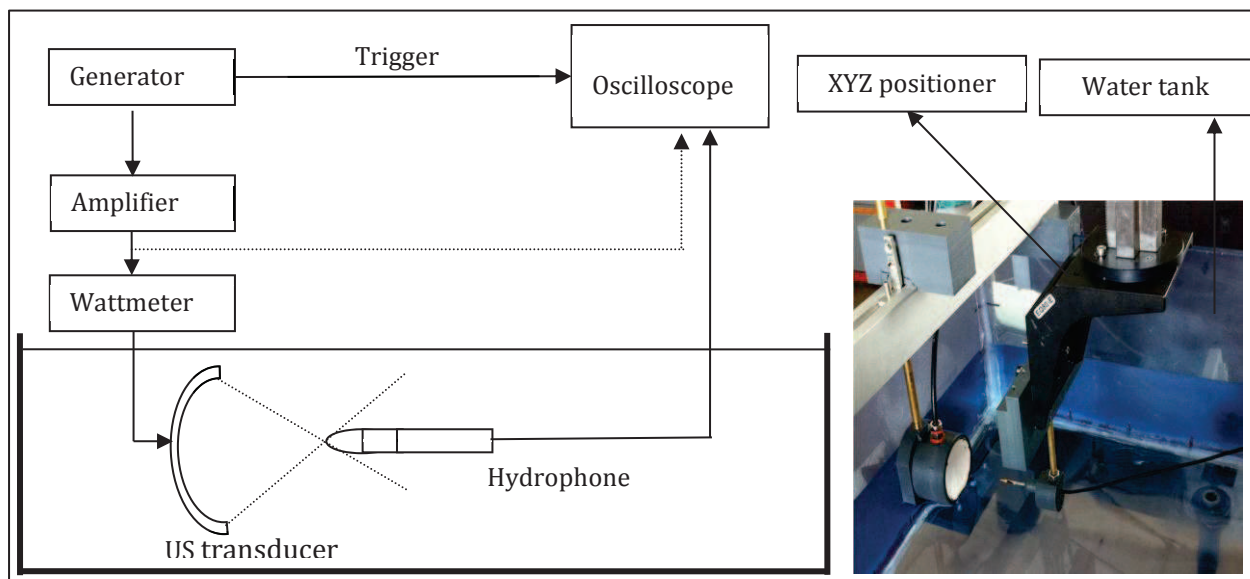


Figure 16- US field characterization set-up.

Acoustic calibration of the transducer was performed using the force balance method (Davidson 1991). By this method the average efficiency of the transducer estimated to be 65%. Acoustic field maps were performed at low pressures using a Müller-Platte needle probe hydrophone (Müller Ingenieurtechnik, Bensheim, Germany) when the transducer was operated using a low amplitude driving signal and acoustic propagation in the focal region was strictly linear (Fig. 16). By acquiring the 2D pressure field maps of the transducer at the focal plane ( $xy$ ) and also along the acoustic axis ( $z$ ), the focal volume was measured to be  $2 \times 2 \times 14$  mm at the full width at half maximum of the acoustic pressure (FWHM, Fig. 17).

In the higher amplitude regime of operation used herein, in which there was significant nonlinear acoustic propagation observed in the focal region, measurements of focal waveforms were performed using a fiber optic hydrophone (FOPH 2000, RP Acoustics, Leutenbach, Germany, Fig. 18).

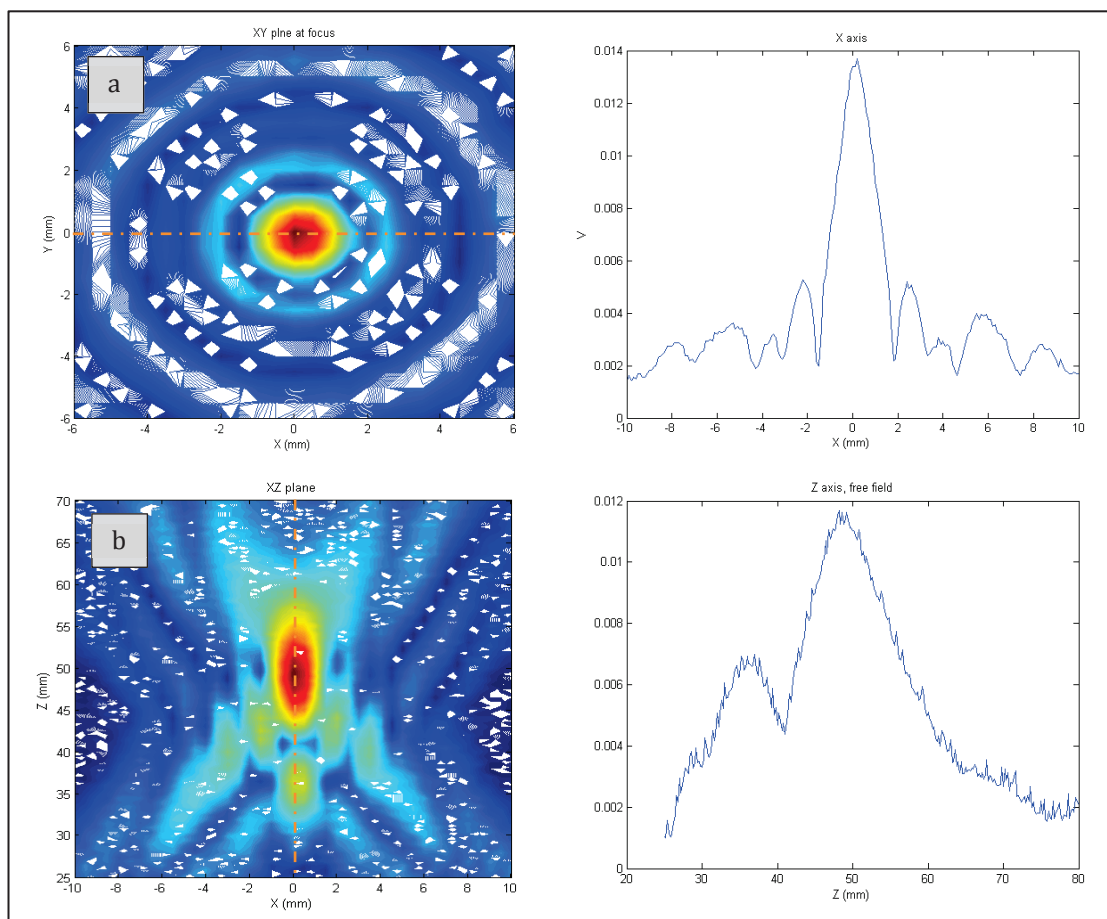


Figure 17- Pressure field maps (a) of the focal plane at the focal distance of 50mm, and (b) along the acoustic axis.

Evolution of positive and negative peak pressure values (optic fiber measurements) in accordance with input voltage increase could be observed in figure 18. The measurements showed that within a defined input voltage range (234 – 431 Vpp) the peak positive pressure had a maximum 52% increase versus 28% of magnitude in case of peak negative pressure.

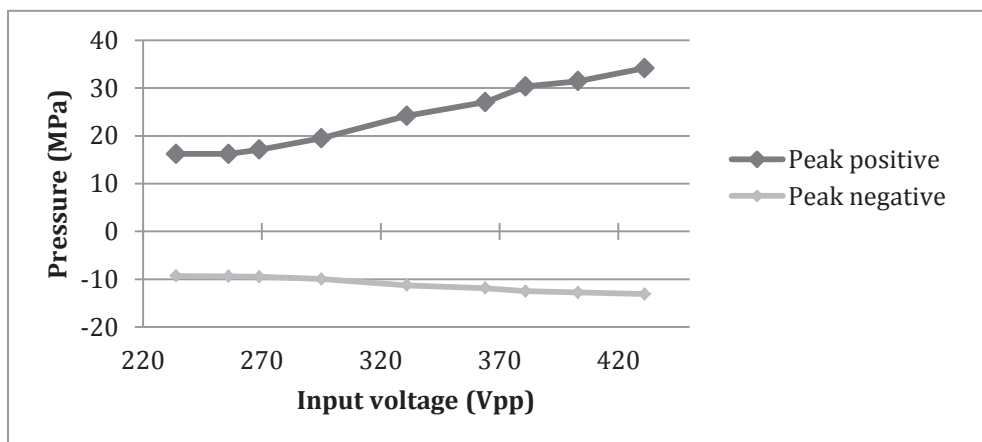


Figure 18- Peak pressure value corresponding the input voltage.

### 4.2.3 Ultrasound exposure parameters

Ultrasound energy was applied in a pulsed regime with duty cycles (DC) of 2.5 and 5% at a PRF of 300 Hz (table 1). Relatively low duty cycles were chosen in this study to reduce the significance of thermal effects (ter Haar 1987) and possible hyperthermia effects. The applied US parameters could be considered in two groups of input pressure levels of 11.2 and 12.7 MPa (peak negative) in a range of 3.2-14.2 acoustic watts.

Peak negative pressure (MPa)	Duty cycle %	Electrical power (W)	Acoustic power (W)
11.2	2.5	4.9	3.2
11.2	5	12	7.7
12.7	2.5	8	5.2
12.7	5	22	14.2

Table 1- US parameters applied in feasibility study.

### 4.2.4 Measurements of permeability

After each treatment, a 10 ml aliquot was drawn from the receiver chamber and the absorbance of the compound in the sample was measured by a spectrophotometer (Scientific-grade Spectrometer QE65000, ocean optics, Delray Beach, FL, USA). Absorbance measurements were performed at a wavelength of 515 nm, the maximum absorbance for fluorescein. A standard curve was made for the concentration-dependent absorbance of fluorescein at this wavelength (Fig. 19).

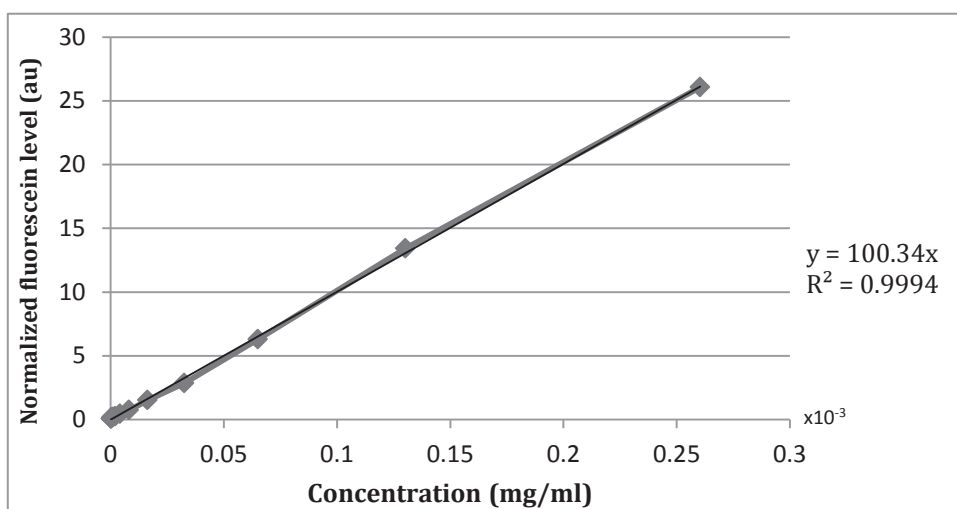


Figure 19- Example of calibration curve for estimating the concentration of diffused compound to the receiver chamber.



All measurements were averaged over 5 acquisitions, after which the concentration of fluorescein in the sample was calculated from the standard curve. By applying Fick's law of diffusion, it is possible to correlate the permeability of the sclera samples with the concentration of fluorescein in the receiver chamber after each experiment. Using this law, an average rate of scleral permeability,  $P$  in cm/s, was calculated using the following equation (Zderic et al. 2004):

Eq. 2

$$P = \frac{V \cdot Cr_t}{A \cdot \Delta t \cdot Cd}$$

where  $V$  is the volume of the receiver chamber ( $\text{cm}^3$ ),  $Cr_t$  is the concentration of fluorescein in the receiver chamber after treatment (mg/ml),  $A$  is the cross-sectional area of the tissue sample ( $\text{cm}^2$ ),  $\Delta t$  is the duration of fluorescein exposure (s), and  $Cd$  is the concentration of fluorescein in the donor chamber (mg/ml). This expression is valid if the cumulative total amount of compound transferred to the receiver cell is less than 5% of the total amount present in the donor cell (Ahmed et al. 1987a). In our study, the stock solution was prepared by dissolving the fluorescein (5 mg/ml) in a phosphate buffered saline PH 7.4 solution. The dilution factor was x150 (0.033 mg/ml). Therefore, all treatments presented in this study were found to be within the bounds of this expression.

Since  $V$ ,  $A$ ,  $t$ , and  $Cd$  are constant, the permeability is dependent on the concentration of the drug in the receiver compartment. Defining a constant as  $K = (V / A \cdot \Delta t \cdot Cd)$ , the equation 5 can be written as:

Eq. 3

$$P = KCr_t$$

The effect of ultrasound on permeability enhancement could eventually be estimated by the ratio between the permeability of control ( $P_c$ ) and US exposed ( $P_u$ ) tissue sample (Equation 7):

Eq. 4

$$\frac{P_u}{P_c} = \frac{[C_{r,t}]_u}{[C_{r,t}]_c}$$

The treatment duration for the sclera samples was 20 minutes. During US treatments, the samples were exposed to both the model drug (fluorescein) and ultrasound energy in the following order: 14 min rest + 2 min US + 4min rest; during sham treatments, the samples were only exposed to the model drug (n = 10 samples). The treatment regime applied to each sclera sample was chosen randomly at the time of treatment: either sham, or US-exposed. For four conditions, four different power levels at two DC% (2.5 and 5), 41 samples were treated (9-12 samples for each power level). The sample permeability to the drug compound was calculated with equation 5, and the corresponding ultrasound exposure effect from the equation 7.

This rather long drug exposure (14min) prior to US treatment is to respect the natural lag time of passive drug diffusion (Zderic et al. 2002). To further examine this, a set of nine supplementary experiments performed in the following order: 4 min rest + 2 min US + 4min r, at 3.7 W (DC 2.5%) and 11.2 MPa.

#### ***4.2.5 Preliminary studies of cavitation contribution***

A preliminary investigation has been performed to evaluate the hypothesis of inertial cavitation significant role as found in the literature. In this part of the study, a chemical detection method was chosen to validate the generation of inertial cavitation by the applied US parameters. Basically, water sonolysis leads to formation of free radicals hydroxyl OH<sup>·</sup> and hydrogen H<sup>·</sup>. The quantity of formed free radicals can be associated with inertial cavitation activity in the medium (Suslick et al. 1990, Riesz et al. 1985, Grtraud et al. 1998).

There are several chemical techniques have been practiced to dose the generated radicals caused by inertial cavitation such as the Fricke dosimeter (Price et al. 1993), the iodide dosimeter (Kratochvil et al. 2007) and the terephthalate acid (TA) dosimeter (McLean and Mortimer 1888,

Mason et al. 1994). Among them, TA dosimeter found to be the most sensitive one; therefore, it has been chosen to validate the presence of the inertial cavitation in this study.

The terephthalate dosimeter is based on the following principle: when non fluorescent terephthalate (TA) anions are in contact with hydroxyl radicals (OH), they react to form fluorescent hydroxylterephthalate (HTA) anions. As inertial cavitation produces OH radicals, the dosimetry consists in exposing a TA solution to ultrasound-induced inertial cavitation, and measuring the HTA fluorescence being generated. Similar to the set-up of Somaglino et al. (2010), a vial with 2 ml TA was placed in the focal area of the transducer and irradiated for 2 min. A prepared solution of 2mM TA, pH7.4 with 1mM phosphate buffered saline was used for these experiments. HTA concentration was then determined using a spectrofluorometer (SFM25, Kontron Instruments, Zurich Switzerland) with an excitation wavelength of 318nm, and emission wavelength of 426nm.

## 4.3 Results

### 4.3.1 Permeability measurements

At 3.2 W (DC 2.5%) and 11.2 MPa peak negative pressure, sclera permeability increased on average 2.4 fold ( $n=9$ ,  $p < 0.5$ ) with the protocol '4 min rest + 2 min US + 4min r'. By applying the same US parameters but protocol '14 min rest + 2 min US + 4min r', the permeability increased 4.9 fold compared to control ( $n=12$ ,  $p < 0.1$ ). At the same pressure level but 7.7 W (DC 5%), permeability increased 5.6 fold ( $n=11$ ,  $p < 0.05$ ). At 5.2 W (DC 2.5%) and 12.7 MPa peak negative pressure, sclera permeability increased 8.7 fold compared to control ( $n=9$ ,  $p < 0.05$ ). At the same pressure level but 14.2 W (DC 5%), samples were visibly damaged and ruptures were noticed ( $n=9$ , fig. 20).

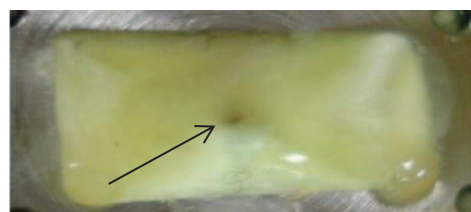
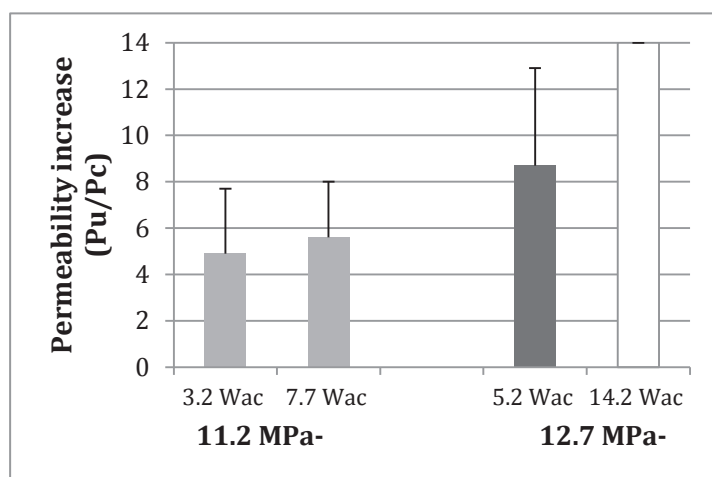


Figure 20- Permeability increase when compared to sham treatments (left); at 14.2 W and 12.7 MPa significant damage was observed in for of pits and ruptures e.g. right image.

### 4.3.2 Inertial cavitation validation

By two minutes exposure of TA solution to US energy at 11.2 MPa-, 2.5 % DC, the level of generated HTA was estimated to be 12.4% (arbitrary unit). With the same procedure, HTA levels were found to be 24.6%, 17.3% and 32.0% at 11.2 MPa-(5% DC), 12.7 MPa-(2.5 and 5% DC) respectively.

#### **4.4 Discussion**

It has been shown in the feasibility study phase that scleral permeability to a model drug compound (fluorescein) could be increased significantly with applied US parameters. The US was applied in a pulsed regime for two minutes during a 20 min treatment. At 5.4 W (DC 2.5%) and 12.7 MPa peak negative pressure, a maximum increase of 8.7 fold of permeability enhancement was achieved ( $p < 0.05$ ). No macroscopic damage was noticed for all conditions except for the highest pressure and transferred power i.e. 12.7 MPa-, 14.2 W (DC 5%). At this pressure level some visible damage in forms of pits and rupture were noticed (Fig. 20).

This delivery enhancement was achieved by respecting the lag time of compound diffusion. As previously reported (Zderic et al. 2002), the drug lag time for passive diffusion is on the order of several minutes. In case of sclera, it takes nearly 10 min for drug passive diffusion to reach a detectable concentration. It was shown that with current parameters, the compounds lag time plays a distinctive role in enhancing the treatments. To further support this fact, the supplementary experiments showed that without respecting the lag time of passive diffusion no significant permeabilization could. With this regard, it was hypothesized that in case of 20min protocol, the rest time of >10 min surpassed the lag time more efficiently; therefore, the portion of drug model which could have already overcome the scleral barriers would be released from the tight collagenic networks by application of US applying present parameters.

As been stated in the literature, both thermal and non-thermal US effects could participate in an enhanced delivery process. Although using a pulsed ultrasound exposure protocol with a low DC% reduces thermal effects, it does not completely eliminate them (ter Haar 1978). Therefore in our experiments, thermal effects were expected to increase proportionally with the applied acoustic power. The presence of cavitation in all applied exposure parameters was also validated by HTA dosimetry. As intuitively been expected the increase of pressure magnitude and the acoustic power in turn lead to increase of HTA production as a marker of inertial cavitation activity. The HTA

dosimetry in this study was more sensitive to input power and pulse duration. The magnitude of HTA detection and hence inertial bubble activity was not in complete accordance with permeability enhancement (Fig. 21).

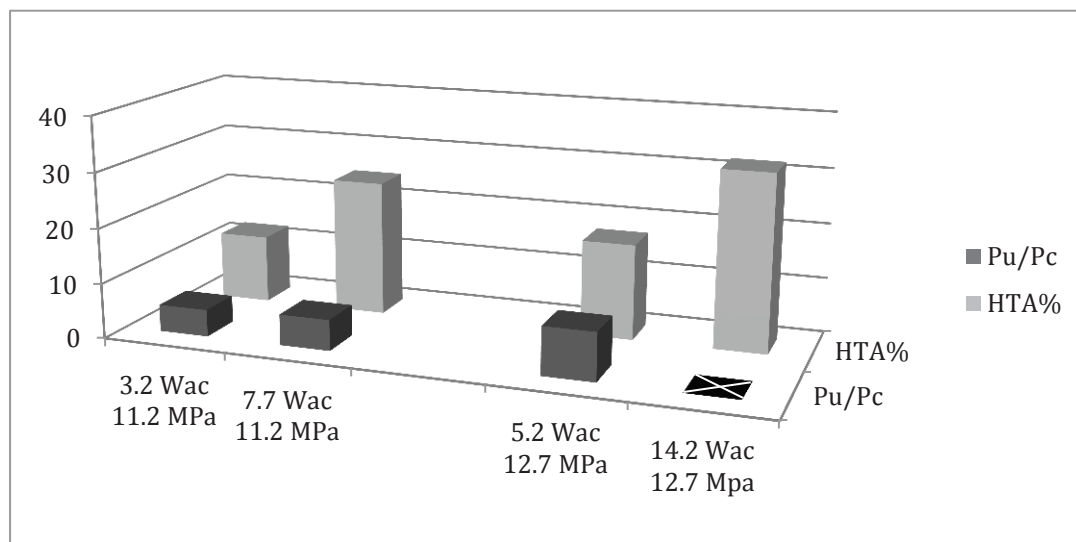


**Figure 21-** The permeability increase due to US exposure at applied powers (Pu/Pc), and corresponding HTA% production as an indicator of inertial cavitation. A macroscopic damage was found at 14.2 watts acoustic (Wac).

The limitations of this cavitation study was first, it was not validated by acoustic measurements i.e. hydrophone noise detection; and secondly, the chemical validation was performed in a free acoustic field with different experimental setup. Given the sensitivity of cavitation events to aberrations at interfaces, the amount and more importantly the type of bubble activity can differ distinctively between these two set-ups. In addition, the permeability increase cannot be associated directly to the cavitation increase which was in fact induced by applied power increase. In this way the contribution of cavitation in regard with the other acoustic phenomena to the permeability increase cannot be determined; therefore, at this point it was not possible to differentiate the contribution level of different US effects in this permeability enhancement.

## ***4.5 Conclusion***

The presented feasibility study demonstrated the potential application of US in enhancing the scleral drug delivery. There were certain limitations which affect the efficiency of the current system. For instance, applying the current exposure conditions, it was necessary to overcome the lag-time limitation hence a rather long drug exposure was needed. Considering the ophthalmologic applications, this challenge could be a major constraint. Furthermore, even though the presence of inertial cavitation was confirmed, the mechanistic part of the study was not informative enough at this stage to shed light on different aspects of US effects in permeabilization. In the following studies, some of these limitations will be addressed.

## **Chapter 5(P.I),**

### ***Action mechanisms: cavitation contribution***

#### **5.1 Introduction**

Recent research and developments have shown a wide range of potential applications for therapeutic ultrasound in the field of drug delivery. With this regard, further understanding of ultrasound physical mechanisms and its interaction with the target tissue is of pivotal importance to fulfilling this potential. Numerous mechanistic studies have tried to explore these mechanisms. Such tries are essential to better understanding a delivery system. Eventually, it is this understanding of the mechanisms that provides possibility of a safer and better exposure condition design in terms of efficiency.

In the field of ocular USDD, the potential mechanisms for enhancement of drug delivery include both thermal and mechanical effects (Zderic et al. 2004, Nabili et al. 2013, Cheung et al. 2010); however, the most effective mechanism and ultrasound parameters for inducing a therapeutically relevant effect are yet to be determined. Among the non-thermal mechanisms of action in ocular USDD, acoustic cavitation is hypothesized to play a significant role (Nuritdinov 1981, Zderic et al. 2004). This chapter of our studies aims to investigate the contribution of inertial cavitation in the enhancement of scleral drug delivery in an ocular model. To this end, tissue permeability to a model drug compound (fluorescein) was measured after ultrasound exposure. An index of inertial cavitation activity was obtained using a passive cavitation detection (PCD) system in order to correlate the permeability enhancement with inertial cavitation activity during exposures.

The choice of model for biomedical experimentation is always a contentious issue, and any choice must be justified against the aims of the experiment. The same as before several advantages with respect to the aim of the study made the *in vitro* model a clear choice. This model in turn permitted the evaluation of US and cavitation interactions with respect to the specific anatomical features of the sclera. Moreover, cavitation monitoring in situ was possible with this experimental



setup, providing data that was directly applicable to the correlation of cavitation to increases in permeability of each tissue sample. Given the chaotic behavior of cavitation activity, this case by case association of permeability and cavitation was well suited to testing the hypotheses posed here. Given that this is a mechanistic study, the actual therapeutic effect of the treatment is interesting, but of less importance, thus simplifying the model used in order to increase sample size was deemed an acceptable compromise. More importantly, a large sample size allowed for many parameters to be investigated.

The previously set-up of feasibility studies has been modified to address some of the previous issues. The new model facilitated a more controlled exposures in terms of temperature monitoring, ultrasound dosimetry, and acoustic measurements. Assessment of damage induced by ultrasound was performed by transmission electron microscopy (TEM). TEM has been instrumental in understanding the structure of outer layers of the eye i.e. connective tissues and the viability of cells through the organelles, and was thus chosen for this study (Koseki et al. 1990; Meek and Fullwood 2001; Doughty 2012).

## 5.2 Material and methods

### 5.2.1 Preparation of samples and diffusion cell

As there can be significant variations in scleral thickness even within the same eye (Norman 2010), the following sample dissection procedure was performed in order to limit variation. The eyes were divided into two pieces in the sagittal plane along the anterior-posterior axis. The equatorial region of the eye was selected for this study because it is free of major blood vessels and muscle insertions to a great extent (Doughty 2012). The posterior pole (optic nerve head) and the region near the corneoscleral limbus were avoided (Fig. 22).

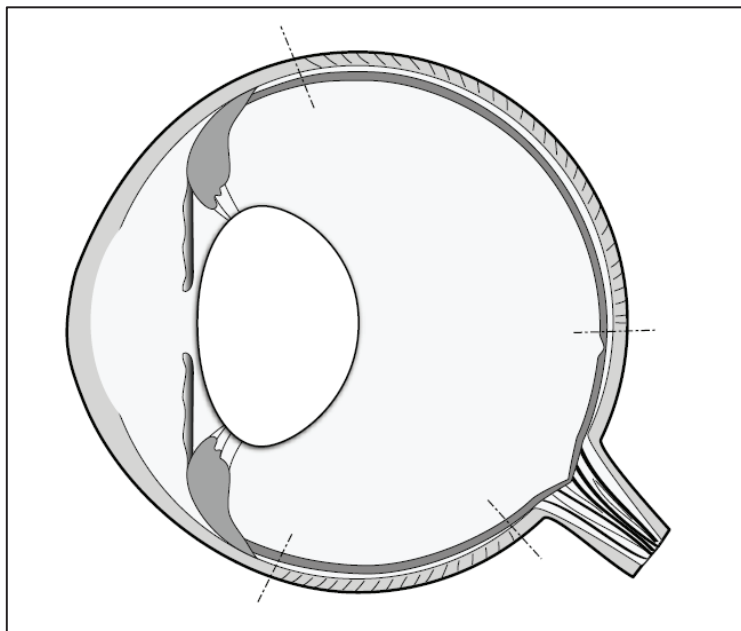


**Figure 22-** Rabbit eye is globally smaller and rounder. Contrary to the sclera surface, the cornea and lens are proportionally larger. The dotted lines indicate the dissection cuts where unhatched areas were discarded.

The experimental set-up was also modified as follows: a water tank with room temperature was assigned for the placement of the diffusion cell (Fig. 23). The receiver chamber of the cell was closed at the bottom by an ultrasound-transparent sheet to reduce the formation of standing waves within the cell. The whole cell then was placed horizontally in the tank so there would be a free passage for the propagation of the beam out of the cell. In this way, the model mimics better a real life ocular system compared to the previous model with significantly reduced formation of standing waves. This modification, reducing the standing component of the wave, in turn increases the propagating

components and facilitates to generate bubble clouds applying lower pressure ranges (Kenis et al. 2012).

In addition, a thermocouple (HI 93551, Hanna Instruments, Smithfield, RI, USA) was placed at the outer vicinity of the sample plate's orifice to measure the temperature rise in the acoustic medium within the donor chamber. The location of the thermocouple was fixed relative to the transducer based on the design of the treatment chamber. Given the sensitivity of cavitation events to aberrations at interfaces, the probe was placed proximal to the nominal focal volume, but not in the tissue sample itself in order to keep artifacts from the thermocouple minimal.

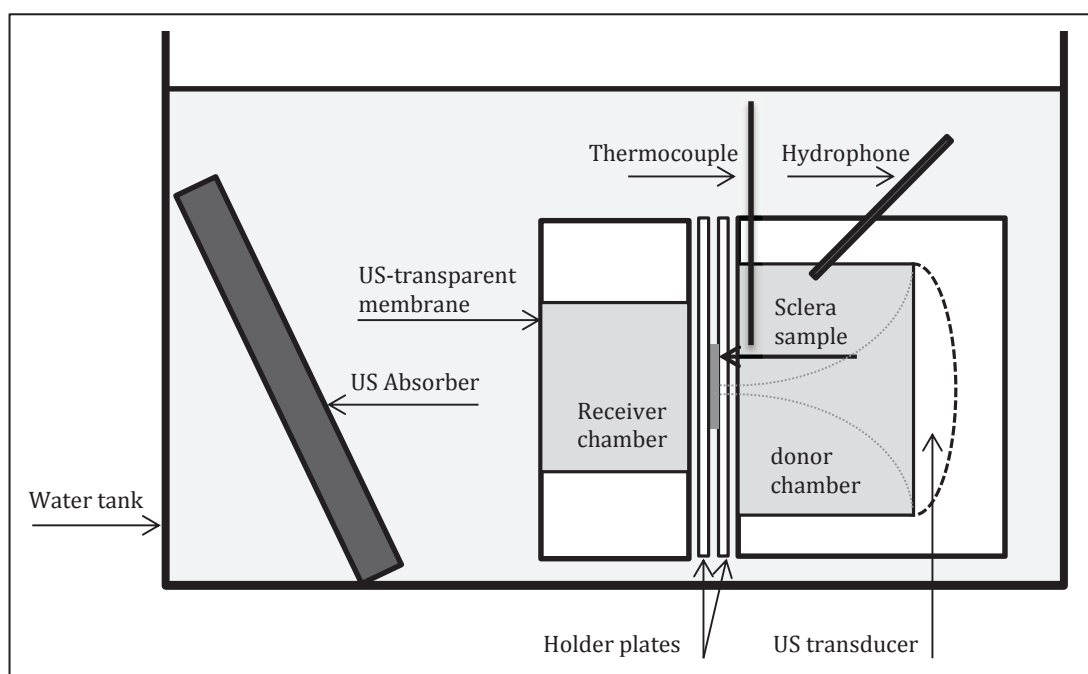


**Figure 23- Modified diffusion cell with incorporated hydrophone, thermocouple, and US transparent membrane at the bottom of the receiver chamber. The cell then placed in a water tank in order to provide an US free-passage outlet for US.**

### 5.2.2 Ultrasonic setup

The same ultrasound apparatus was used as before. Acoustic calibration and pressure measurements also followed the same procedures. In order to study the bubble activity, a passive cavitation detection (PCD) system was used to calculate a dose of inertial cavitation based on the recorded broadband noise. A needle hydrophone (VP-1.5 pinducer; piezoelectric nominal frequency: 2.5 MHz; diameter: 1.5 mm, Valpey Fisher, MA, USA) listened to bubble activity in the focal area. The

hydrophone was incorporated and fixed into the wall of the donor chamber in the diffusion cell with an angle of  $45^\circ$  to the US beam. The design of the diffusion cell allowed the hydrophone to be directed toward the geometrical center of the plates and the focal plane of the transducer. The received signal was digitized (acquisition card PXI-5620, 14 bit resolution, 32 MHz sampling frequency, National Instruments, Austin, TX, USA) and transferred to a computer to be analyzed by Labview software (National Instruments, Austin, TX, USA).

In this instantaneous spectral analysis method, two frequency domain spectra were acquired over a bandwidth of 0.1-7.1MHz: one spectrum acquired during treatment and, another acquired while the excitation signal to the transducer was off. The sampling frequency was 32 MHz. The frequency spectrum was averaged in a logarithmic scale (224 points) in order to enhance the contribution of the broadband noise (as inertial cavitation indication) and suppress the contribution of the peaks. The difference between mean values of the two spectra was then taken. This difference is defined as the inertial cavitation index (CI, Fig. 24).

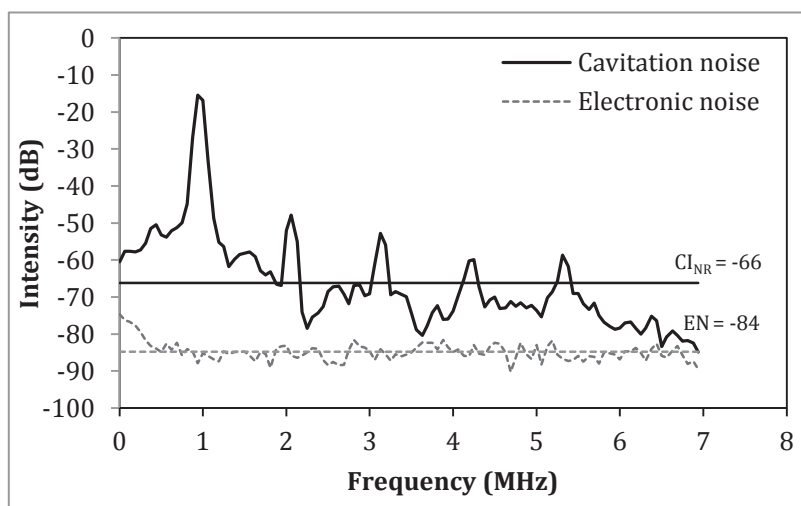


**Figure 24-** Example of instantaneous frequency-domain acoustic spectrum. The mean value of each spectra (the non-referenced cavitation index (CINR) and the electronic noise (EN)) is calculated, and the difference between the two is taken (CINR-EN). In this case, the value for the CI was found to be 18 at peak negative pressure of 12.7 MPa, PRF 100 Hz and DC 2.5%.

By application of this method, Frohly et al. (2000) showed that the contribution of peaks is negligible at relatively high pressure levels, as is the case in our study. This logarithmic method thus

does not compromise sensitivity to cavitation while conserving computational resources allowing for real-time processing in our study. In addition, this method has been chemically validated by Sabraoui et al. (2011) using a terephthalic acid (TA) dosimeter. In their studies, the CI acquired by this method was directly proportional to the production of HTA.

### ***5.2.3 US parameters***

Prior to scleral permeability measurements, a parametric study was performed to define US exposure parameters. Since the US was applied in a pulsed regime, at the first step PCD measurements were performed to investigate the effect of different pulse durations on cavitation activity. Therefore a constant duty cycle (DC: 2.5%) and total US exposure time were applied for all exposure parameters to keep the total energy dose at the same range. For this part, US was applied during two minutes at a constant pressure of 12.8 MPa for a PRF range of 100 – 1000 Hz and consequent pulse duration range of 250 – 25  $\mu$ s.

At the second step, the effect of different input powers on cavitation activity was studied at constant pulse durations or PRFs. Based on outcome of the study above, two PRFs 100 and 1000 Hz were chosen as representatives of higher and lower regimes of the cavitation activity. Following this, the cavitation evolution was monitored at these two PRFs for a range of time averaged acoustic powers from 0.2 to 7 W and sonication time of two minutes. With regards to the significance of cavitation activity, four different acoustic powers (0.5, 2.2, 3.6 and 5.4 W) were chosen for further scleral permeability studies at PRFs of 100 and 1000 Hz, DC 2.5% and US exposure time of ten minutes (details in results section).

### ***5.2.4 Measurements of permeability***

In this part the US treatment duration for the sclera samples was increased from 2 to 10 minutes but without any prior drug exposure before and after US treatment i.e. 10 min US+ drug exposure when compared to first protocol (14min drug + 2 min US + 4min drug, Section 4.2.4). The idea behind it was to define parameters that can overcome the scleral lag time in an enhanced DD

process. During US treatments, the samples were exposed to both the model drug (fluorescein) and ultrasound energy, during sham treatments, the samples were only exposed to the model drug. The treatment regime applied to each sclera sample was chosen randomly at the time of treatment: either sham, or US-exposed. For nine conditions, four different power levels at two PRF plus control, 91 samples were treated (8-13 samples for each power level).

In order to assess the transience of the effect of US on scleral permeability, a subset of tissue samples (n = 15) from both the US treated and sham treated groups were allowed to remain in the treatment chamber exposed to fluorescein without the application of ultrasound for an additional 10 minutes. For this subset of samples, the receiver chamber was sampled and had absorbance measurements, and subsequent calculation of permeability, performed twice over a period of 20 minutes.

### ***5.2.5 Assessment of damage induced by ultrasound on scleral tissue***

TEM studies were performed in order to assess US-induced damage to tissue i.e. the viability of the cells and structural alteration of collagen bundles after treatment. Immediately after each experiment, the membrane was sampled, immersed in a fixative medium (4% glutaraldehyde 0.1M, 49629, Fluka; NaCacodylate HCl, 12300, EMS, Ph7.4; volume 1:1) and stored in 4° C. Samples were prepared for TEM studies with the methods presented in Osman et al. (2012) work.

In summary, after washing 3 times (3 hours) at 4°C in 0.1 mol/l 0.1 NaCacodylate HCl ph7.4 0.2 mol/l sucrose, tissue was post fixed in 1% OsO<sub>4</sub> 0.15 mol/l NaCacodylate HCl ph7.4 for 1 hour at 4°C, they were dehydrated through a series of washes with ethanol 30,50,70, and 95% for 5 min; Then, samples were infiltrated with Epon mixture using 1:1 Epon mixture (Epon A(50%)+Epon B( 50%)) and absolute ethanol for 60 min followed by pure Epon mixture for 3 periods of 8hrs and, finally, embedded in pure Epon +DMP30(1.7%) for polymerization at 60° for 48h. Sections were made on a microtome. Area alterations were first selected on semi thin sections stained with methylene blue azurII. Consecutive ultra-thin sections (60-80 nm) were contrasted with methalonic uranyl acetate

(20 min) and lead Citrate (5min). Image acquisition was performed with a transmission electron microscope (Jeol 1400 JEM, Tokyo, Japan) equipped with a Gatan camera (Orius 600, Pleasanton, CA, USA) and Digital Micrograph Software<sup>1</sup>.

---

1- The TEM studies were performed at CeCILE - SFR / Centre Commun d'Imagerie (Lyon-Est, France).

## 5.3 Results

### 5.3.1 Evaluation of cavitation activity and scleral permeability enhancement

In order to characterize the pulse regimes studied, PCD was first used to calculate the CI for a range of PRFs at a constant pressure of 12.8 MPa. A dependence of cavitation activity on pulse duration was observed at constant pressure and DC% but different PRFs ( $n=5$ ,  $t=2$  min). Based on the results, two PRFs i.e. 100 and 1000 Hz were chosen as representatives of higher and lower regimes of the cavitation activity (Fig. 25).

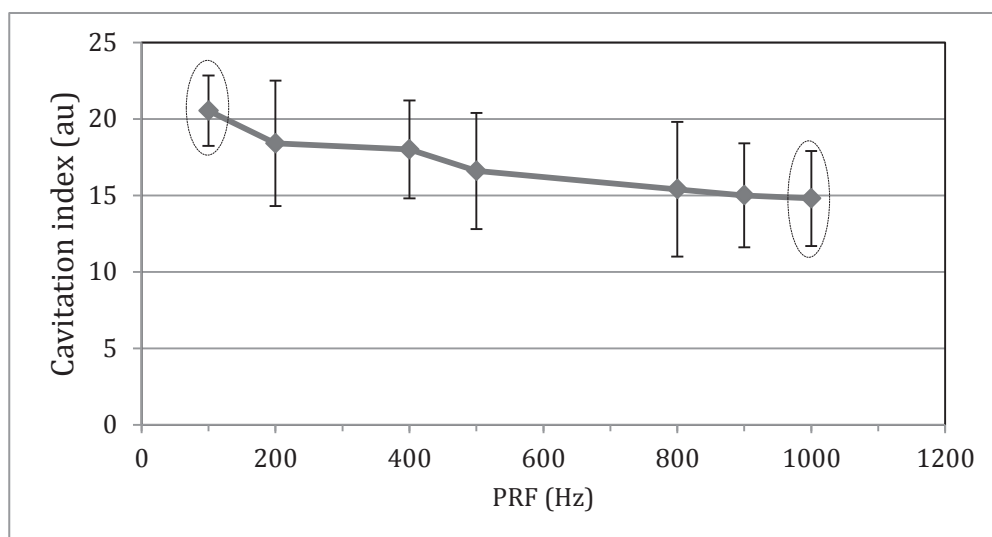


Figure 25- Evolution of CI in a PRF range of 100-1000 Hz.

Following this, the cavitation evolution was monitored at these two PRFs for a range of time averaged acoustic powers from 0.2 to 7 W and sonication time of 2 minutes ( $n = 5$  at each measured power level, Fig. 26). The different pulse regimes studied demonstrated that significant variations of CI is limited to the power range of 3.2 - 6.2 W. Based on this, four different acoustic powers were investigated for the USDD study as a function of their cavitation activity: 0.5, 2.2, 3.6 and 5.4 W, with corresponding peak negative pressure values of 6.8, 9.5, 11.3 and 12.7 MPa respectively. For the lowest two power settings chosen (time averaged acoustic power of 0.5 and 2.2 W), the CI variation was not significant between the two pulse regimes. For the higher power settings (time averaged acoustic power of 3.6 and 5.4 W), the CI was significantly different between the two pulse regimes.



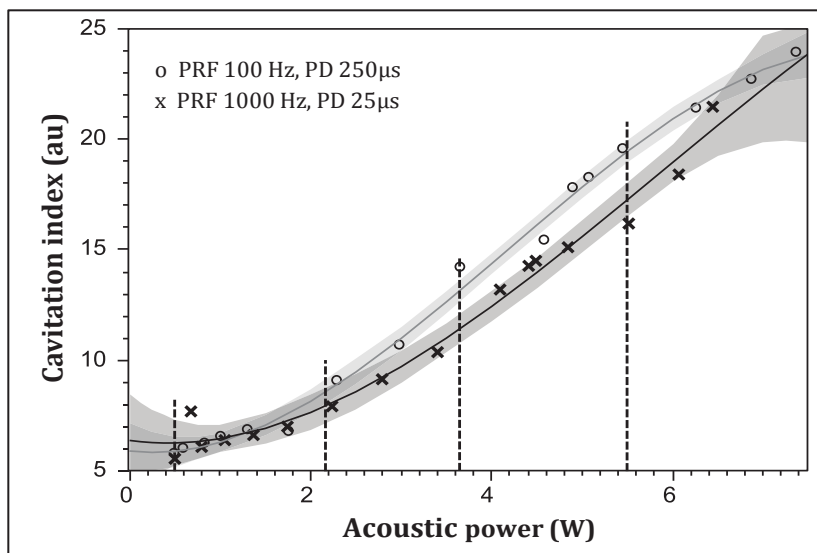


Figure 26- CI vs. acoustic power for two pulse regimes at PRFs 100 and 1000 Hz (120s US exposure at each given power,  $n = 5$  with the confidence interval demonstrated as shadows).

For the chosen parameters, the HTA measurements also were performed following the procedure of feasibility studies. The dependence of HTA concentration and input power is demonstrated in (Fig. 27). The average HTA index evolution was found in accordance with the average CI for the applied parameters. Although the average HTA% indices of PRF 100 Hz were higher than PRF 1000 Hz, the difference was not significant at none of the applied powers. In case of CI however, at both 3.6 and 5.4 W a significant difference ( $p < 0.001$ ) was registered. It is believed that HTA measurements with the current formulation and set-up lacked the necessary sensitivity.

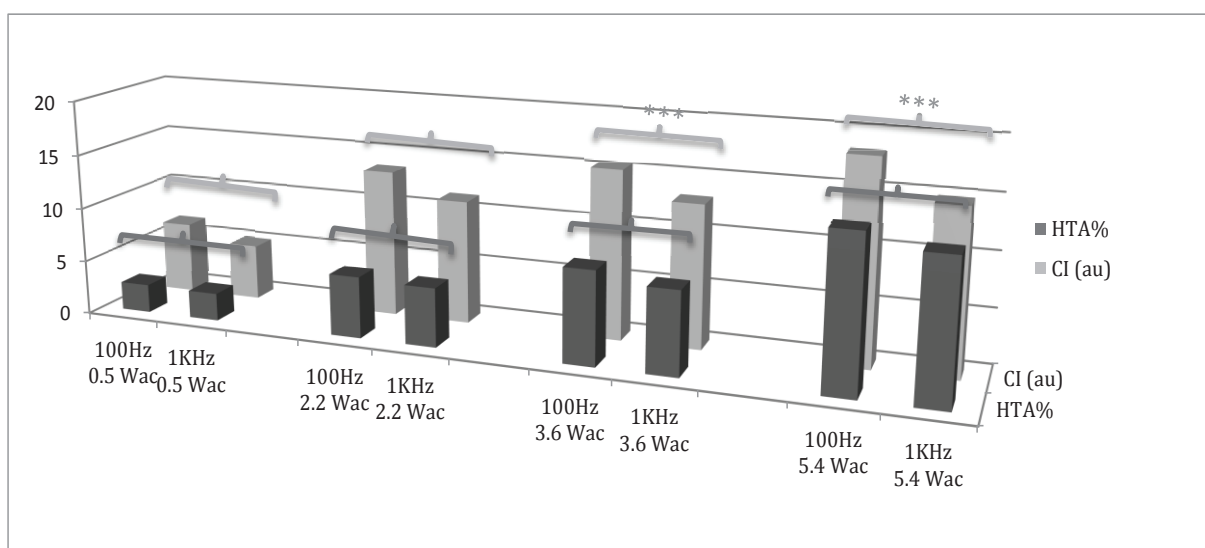


Figure 27- Cavitation index by PCD vs. HTA% by chemical validation. The only significant difference found for CI at 3.6 and 5.4 Wac (\*\*\*)  $p < 0.001$ .

In figure 28, an example of the temporal evolution of CI for the two pulse regimes of PRF 100 and 1000 Hz can be observed with constant time-averaged power of 5.4 W over the course of a 10-minute experiment. It was observed that cavitation activity was well maintained at a PRF of 100 Hz (pulse duration 250 $\mu$ s) throughout the exposure, as opposed to the more sporadic occurrence of cavitation at a PRF of 1000 Hz (pulse duration 25 $\mu$ s).

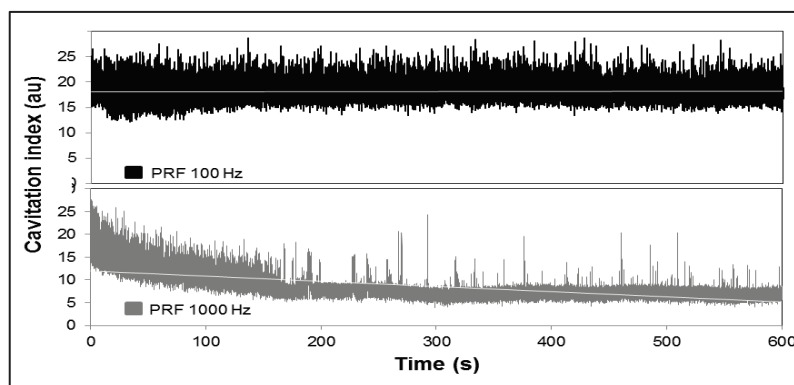


Figure 28- Temporal evolution of CI at peak negative pressure of 12.7 MPa, 5.4 W, DC 2.5%, PD 250  $\mu$ s and PRF of 100 Hz with the average value of  $18.5 \pm 1.5$  over 10 minutes of irradiation. By reducing the pulse length to 25  $\mu$ s (PRF 1000 Hz) this value for CI decreased to  $8.7 \pm 2.3$ .

The results of the permeability experiments by the above parameters are given in figure 29. Compared to sham treatments, the scleral permeability to the compound increased dependent upon the acoustic power applied. With the exception of the lowest power setting, all conditions examined resulted in a statistically significant increase in scleral permeability for both 100Hz PRF and 1000Hz PRF pulse regimes. At maximum applied power (5.4 acoustic watts, 12.7MPa peak negative pressure), permeability to fluorescein increased  $9.97 \pm 4.25$  fold compared to sham treatment ( $(1.21 \pm 0.83) \cdot 10^{-7}$  cm/s compared to  $(1.2 \pm 0.51) \cdot 10^{-6}$  cm/s, student's t-test,  $p < 0.001$ ).

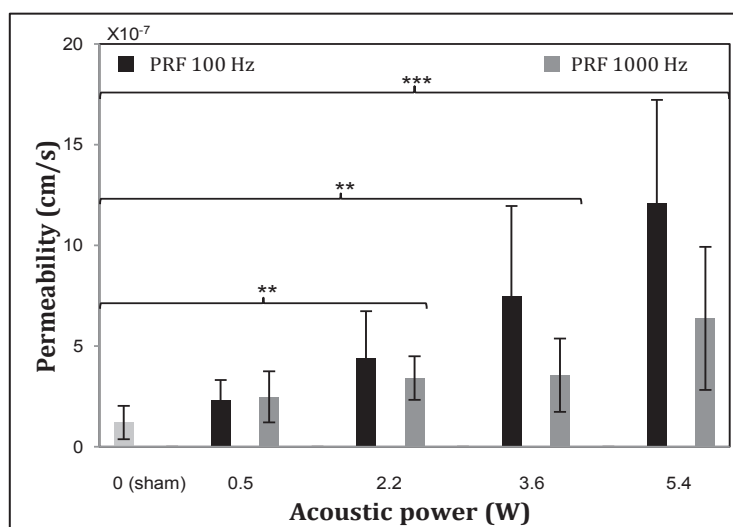


Figure 29- Average of scleral permeability measurements (n=91). Compared to sham treatments, the permeability of tissue increased significantly for all but the lowest power levels applied (student's t-test,  $**p < 0.01$ ,  $***p < 0.001$ ).

In figure 30, the increase in permeability of US-exposed sclera samples (normalized by sham treatments, equation 7) is demonstrated in a box plot, plotted together with the corresponding CI values. At 0.5 W (6.8 MPa peak negative pressure), sclera permeability increased 1.1 and 2.0 fold compared to control for the PRF 100 and 1000 Hz pulses regimes respectively, with no significant difference between either permeability enhancement or CI for each of the two regimes (CI =  $3.94 \pm 1.37$  at 100 Hz,  $2.94 \pm 0.85$  at 1000 Hz). At 2.2 W (9.5 MPa), permeability increased 3.6 and 2.8-fold at PRF 100 and 1000 Hz respectively, with no significant difference in cavitation between 2 regimes (CI =  $5.1 \pm 0.96$  at 100 Hz,  $5.03 \pm 1.35$  at 1000 Hz). At 3.6 W (11.3 MPa), permeability increased 6.1 and 2.9 fold at PRF 100 and 1000 Hz respectively, with significant difference between 2 PRFs on both permeability enhancement and CI (CI =  $13.56 \pm 2.84$  at 100 Hz,  $7.29 \pm 1.53$  at 1000 Hz). At 5.4 W (12.7 MPa), permeability increased to 9.9 and 5.2 fold at PRF 100 and 1000 Hz respectively, with significant difference between 2 PRFs on both permeability enhancement and CI (CI =  $19.89 \pm 1.14$  at 100 Hz,  $13.69 \pm 4.3$  at 1000 Hz).

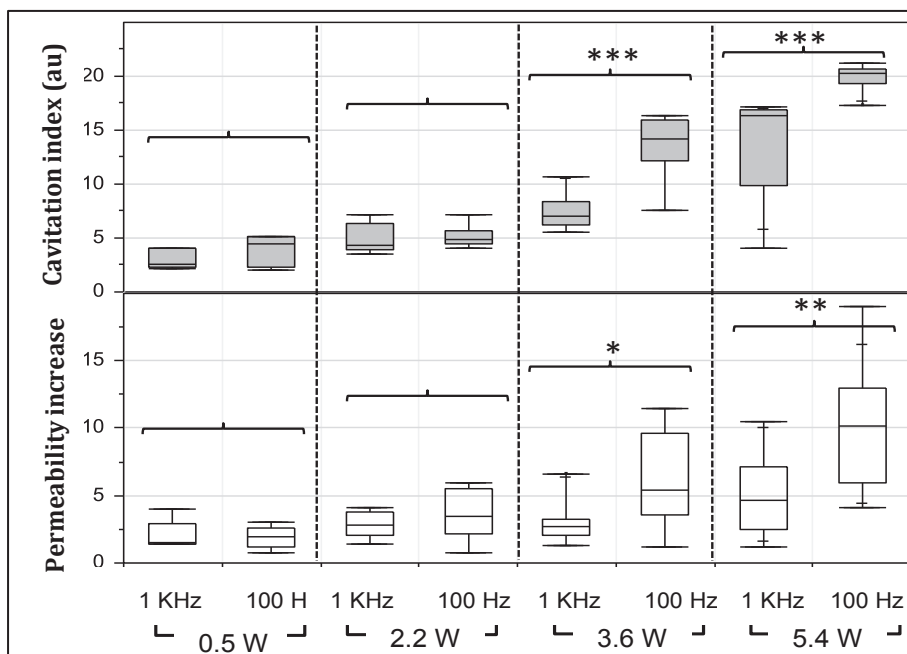


Figure 30- CI vs. Pu/Pc. At low power conditions (0.5 and 2.2 W), there was no significant difference in CI nor in permeability between the two pulse regimes; whereas for high power conditions (3.6 and 5.4 W), the cavitation activity was significantly higher for the 100 Hz PRF pulse regime compared to 1000Hz ( $p < 0.001$  for both powers), and changes in scleral permeability reflected this ( $p < 0.05$  for 3.6W and  $p < 0.01$  for 5.4W). Student's t-test: \*  $p < 0.05$ , \*\*  $p < 0.01$ , \*\*\*  $p < 0.001$ ).

In order to study the transience of US-mediated permeability alteration, 15 tissue samples were left in the diffusion cell after treatment (whether sham or US) for another 10 minutes (without US). After treatments (3.6 W) the tissue permeability increased  $5.4 \pm 0.8$  fold for these samples at 100 Hz (CI =  $14.4 \pm 1.6$ ) and  $1.9 \pm 0.6$  fold at a PRF of 1000 Hz (CI =  $7.5 \pm 0.7$ ). For the same samples after the second exposure to the model drug (without US) the tissue permeability increased  $2.4 \pm 0.8$  fold at 100 Hz and  $2.0 \pm 0.4$  fold at a PRF of 1000 Hz when compared to the sham treated samples at the same drug exposure time.

All experiments were conducted at room temperature. US treatment resulted in a moderate temperature elevation of the medium, dependent on acoustic power. For the lowest acoustic power of 0.5 W, the temperature increased by  $0.5^\circ\text{C}$ , and increased by  $4.5^\circ\text{C}$  using the highest applied acoustic power of 5.4 W. There was no significant difference in temperature increase between PRF 100 and 1000 Hz at the same power level.

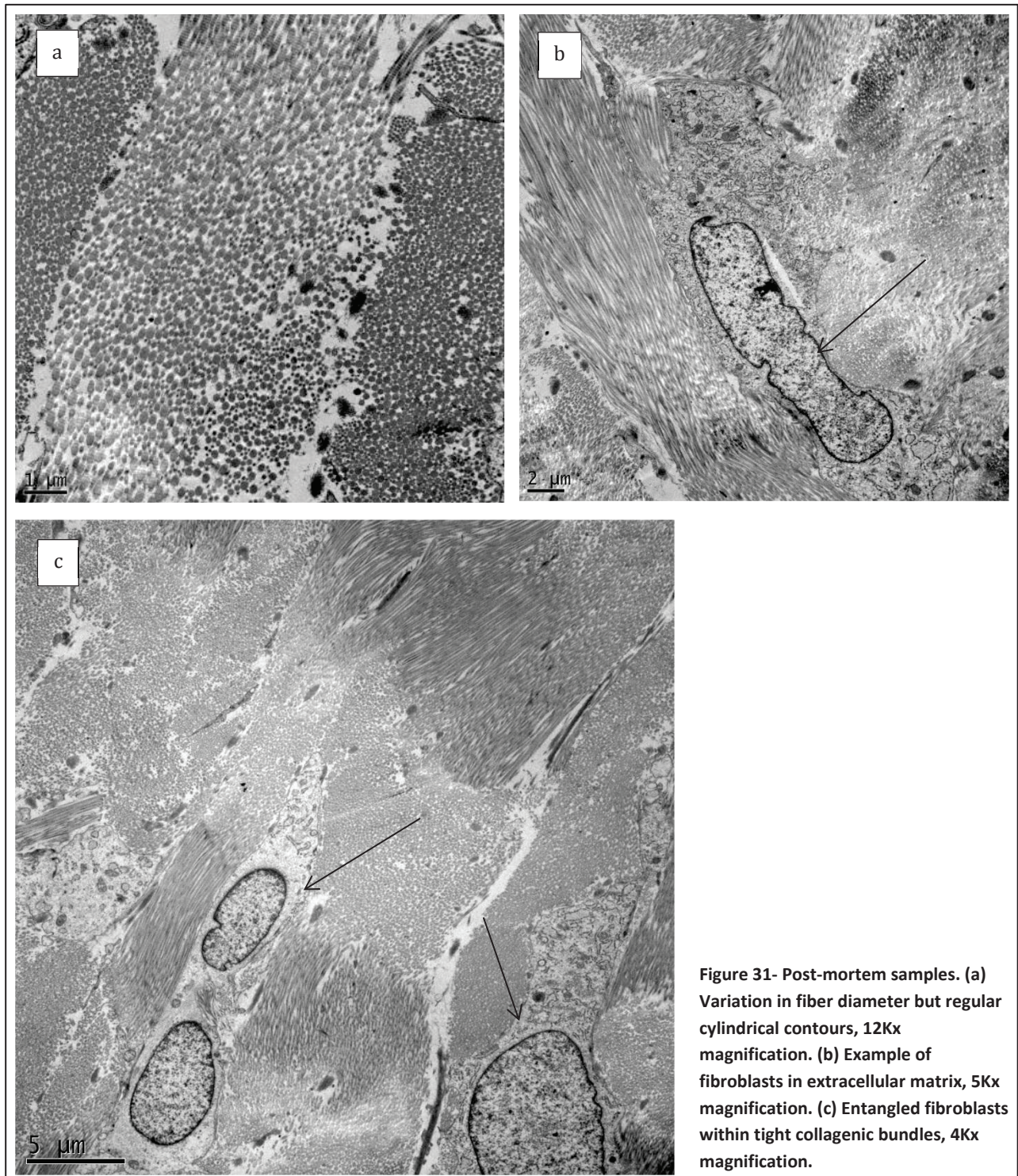
### ***5.3.2 Assessment of scleral damage induced by ultrasound***

No damage was observed at the macroscopic level for all treated samples. A TEM study was carried out for a selection of samples from all experimental conditions including samples analyzed immediately post-mortem (samples with no treatment), sham and ultrasound treated samples. In accordance with literature descriptions, the criteria of the study were carried out two levels: viability of fibroblasts and alteration in collagen fibers/bundles structure (Watson et al. 2004).

The post-mortem samples were obtained immediately after the sacrifice for TEM imaging. The results of our ultrastructure examination were in conformity with previous reports. The collagen fibrils were varied in diameters with cylindrical contours and expectedly, no irregularities or deformation (Yamabayashi et al. 1991). The parallel collagen fibrils were observed to be aligned in form of bundles. These collagenic bundles were in a crisscrossed position with each other (Raspanti et al. 1992). They were varied in width on transverse plane of observation (Meek and Fullwood 2001). A great portion of the fibroblast cells found to be in good condition, preserving the cell



membrane and organelles. These cells were observed entangled within rather tight collagenic bundles (Fig. 31). The post-mortem analysis was the reference of damage assessment for both sham and US treated samples.





*Sham and US treated samples:* In terms of fibers morphology, there was no evidence of degeneration or irregularity found in cross sectional profile of the fibers for any sample (Fig. 32a and 33a). In most of the cases the collagen bundles maintained their organized structure within sham and US exposed samples (Fig. 32b and 33b). Although in a few regions there were some level of disorganization been noticed when compared to post-mortem samples; these regions were observed both in sham and US treated samples (Fig. 32d and 32d). This disorganization was associated with regions with increased interfibrillar distance, fragmented collagens fibrils, and lack of bundelic orientation.

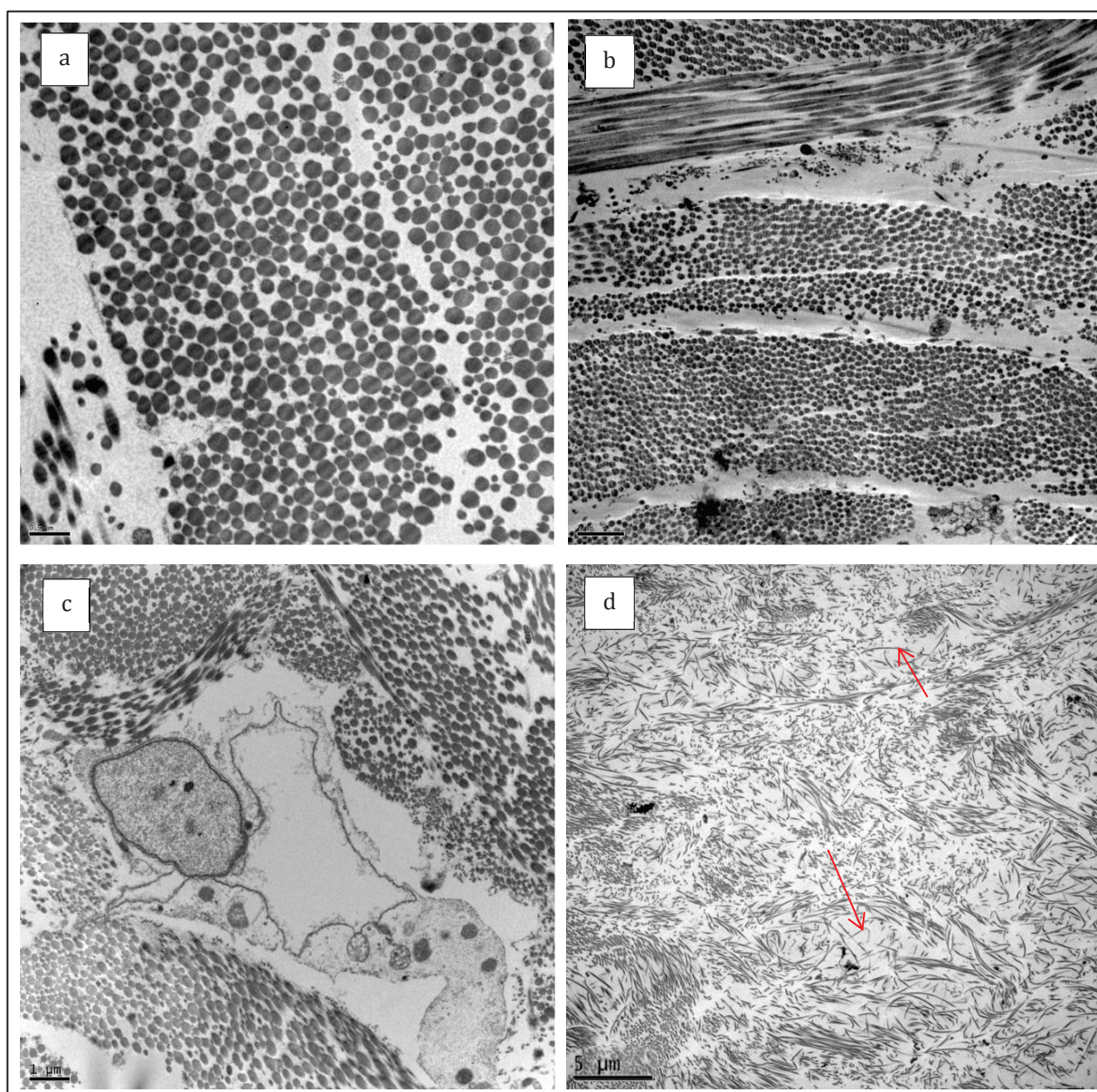


**Figure 32- Sham treatment samples: (a) collagen fibrils condition, 10kx magnification; (b) structured collagen bundles region, 6kx magnification; (c) example of damaged fibroblast, 8kx magnification; (d) fiber segmentation within disorganized region (red arrows), 4kx magnification.**



At the cellular level, within both sham (Fig. 32c) and treated samples, there was evidence of damaged fibroblasts in terms of dilution and ruptured membranes with free organelles in their vicinity within the extra-cellular matrix. On the other hand, there was also evidence of functional fibroblasts containing subcellular components with preserved cell membrane in both sham and treated samples (Fig. 33c). Comparatively, there was less evidence of damaged cells in samples examined immediately post-mortem, as opposed to the sham and US-exposed treatments.

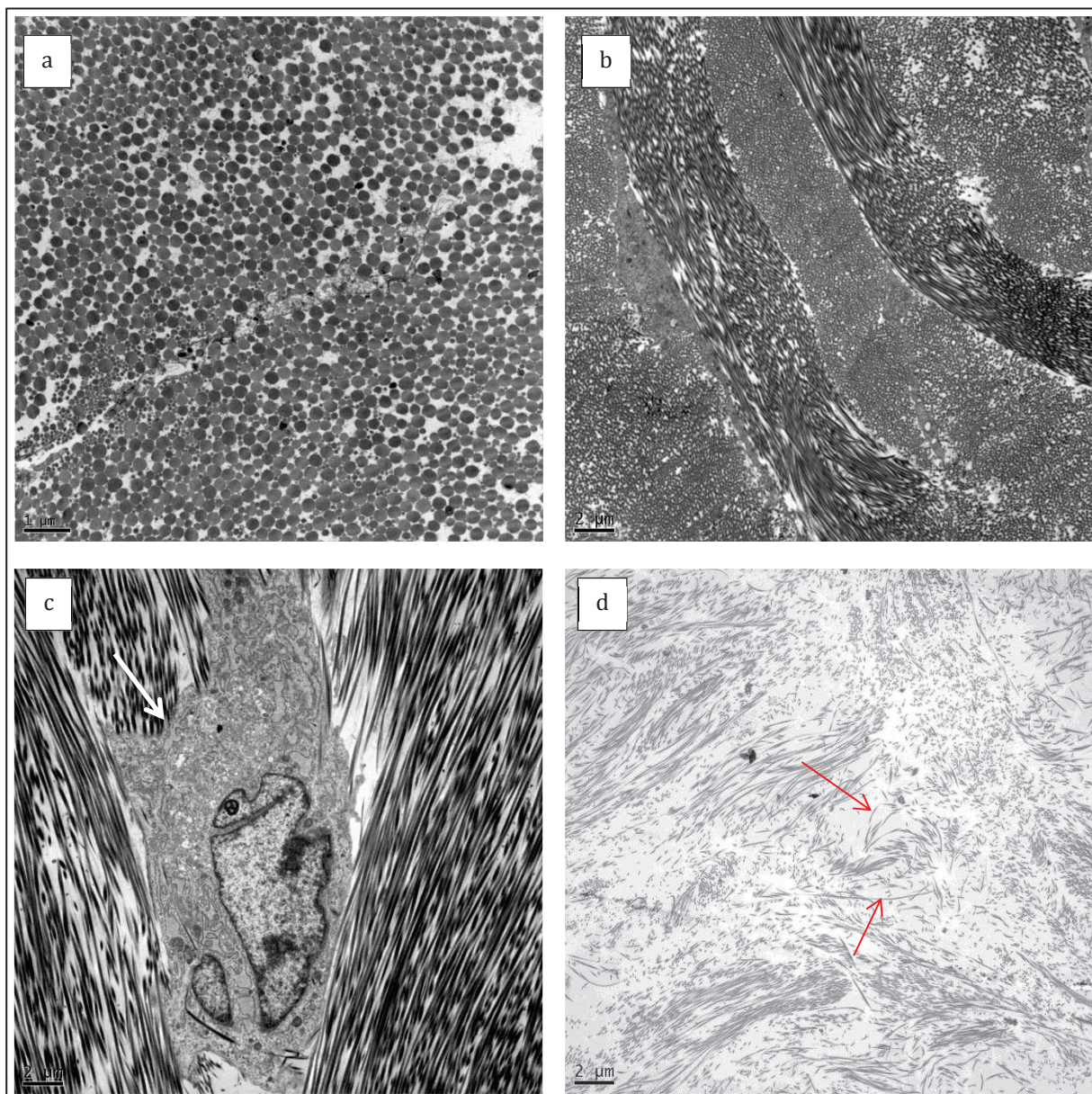


**Figure 33- US-exposed samples at 5.4 W: (a) collagen fibrils condition 10x magnification; (b) organized collagen bundles, 4kx magnification; (c) example of fibroblast in functional state containing subcellular components and well preserved cell membrane, 8kx magnification; (d) fiber segmentation within disorganized region (red arrows), 4kx magnification.**

## 5.4 Discussion

It has been shown in the feasibility study that scleral permeability to a model drug compound (fluorescein) increased significantly with application of ultrasound. This stage of the study was dedicated to explore the involving physical US mechanisms and consequent tissue interactions. As been said, a combination of US effects could potentially work in favor of an enhanced drug delivery treatment. Inertial cavitation however, is hypothesized to play a major role in this process (Nuritdinov 1981; Nabili et al. 2013). In order to study this role, an index of inertial cavitation was acquired during each exposure, and this index was in turn correlated with scleral permeability enhancement. The data presented here both supports this hypothesis, and is in agreement with previous studies using USDD for other applications.

One of the challenges of studying the role of cavitation, however, is to isolate cavitation from other effects induced by ultrasound. As shown in this work, there is a significant variation in CI between the two pulse regimes (PRFs of 100 and 1000 Hz), while the duty cycle and acoustic power remain constant (Fig. 26 and 28). In this way, it was possible to keep the impact of other non-cavitation effects relatively constant while the effects of cavitation varied significantly between the two pulse regimes at a given average power. Based on this measured difference in cavitation activity between the two pulse regimes, it was hypothesized that if cavitation plays a significant role in the enhancement of scleral permeability, then a significant difference in scleral permeability would be observed between tissues exposed to these two pulse regimes. To further support this hypothesis, inertial cavitation activity during each US treatment was obtained via a PCD (Fig. 29 and 30).

As expected, no significant difference in permeability was observed between the two pulse regimes when there was no significant difference in cavitation activity. On the other hand, when CI varied significantly as the result of the pulse regime applied, permeability enhancement varied accordingly. The measured peak negative pressure, total acoustic power (radiation force), total transferred energy dose and the average temperature increase of the test medium were



independent of PRF at each given power. This result demonstrates the significance of inertial cavitation in the enhancement of scleral permeability to the model drug compound when applying these exposure conditions.

The safety of this treatment protocol was assessed by performing a TEM study that focused on cell viability and intracellular organization of collagen bundles. The reference of comparison for both sham and US treated samples was immediate post-mortem samples (without treatment). The microscopic architecture of sham and exposed sclera tissues were found to be similar in terms of structural damage when compared to post-mortem samples. In figure 32c and 33c, the damaged compartments of sham treated samples could be seen with rather untouched ones from US exposed samples at highest power level. As mentioned, the samples were dissected from focal zone of the US where the largest possible impact is expected. Considering these observations, the damage is believed to be primarily caused by the experimental manipulation of the sclera and it was thus not fully possible to quantify the induced damage and/or to differentiate the experimental artifacts damage by treatment. Nonetheless the specific aims of the TEM investigation of present investigation, as a part of this mechanistic study, were to trace first, possible heat induced damage and then the cavitation activity within the samples.

It has been reported that heat deposition in collagenic tissues resulted in collagen denaturation and shrinkage (Vangsness et al. 1997, Kirsch et al. 1998). The role of heat in collagen denaturation and shrinkage has been variably quantified. The threshold temperature at which the phenomenon of denaturation occurs varies among different tissues. It has been demonstrated that dermal and scleral collagen shrank in a close range of 61 - 66°C (Lennox 1974, Stringer and Parr 1964). This similarity in range values could be expected since the scleral extracellular matrix is also predominantly composed of type I collagen (McBrien et el. 2006). The heat induced lineal shrinkage leads to augmentation of collagen cross-sectional diameter and consequently morphological change. These alterations could be revealed effectively by ultrastructural examination of tissue samples via TEM imaging. Figure 34

shows a region of irradiated collagenic tissue with pulsed CO<sub>2</sub> laser. The morphological change of the fibers as a result of heat energy deposition could be observed at two levels: intermediate changes assigned to increased diameter and complete denaturation where loss of recognizable fibrillar structure occurred (Kirsch et al. 1998).

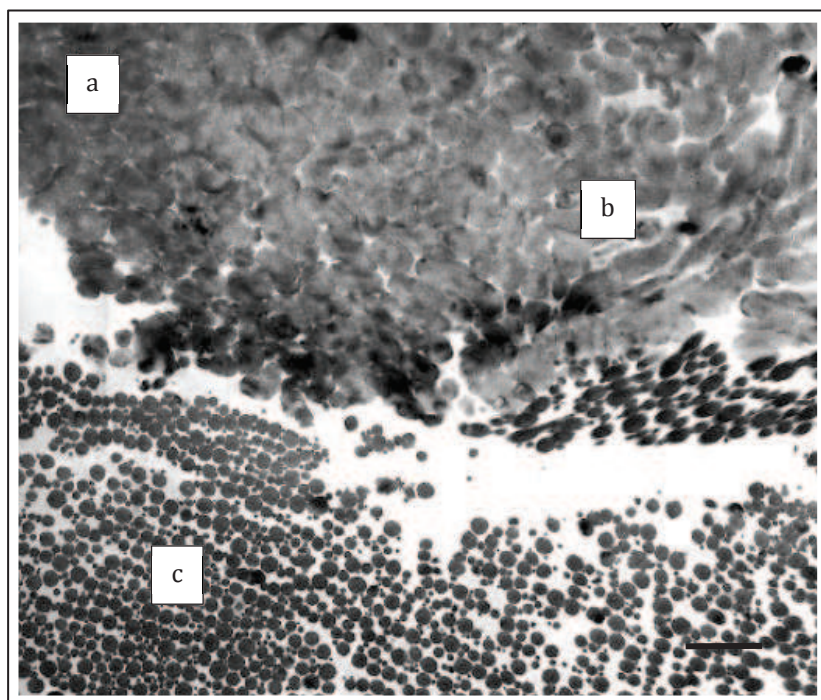


**Figure 34-** The zones of morphological change demonstrations. Zone (a) complete collagen fibril denaturation; zone (b) discrete fibrils with increased diameter; zone (c) shows normal structure and diameter collagen fibrils (6.5 kx magnification bar=1  $\mu$ m). Courtesy of Kirsch et al. 1998.

The observed denaturation was in the zone of excessive heating within the sample tissue. As been mentioned, the focal zone of our US irradiator confined well the tissue samples of TEM analysis. Therefore, it was expected that the tissue samples were encounter the most temperature increase possible. No sign of morphological change with this regard, neither intermediate nor complete, was found at all applied powers. This investigation supported the fact that the deposited thermal dose even at highest powers, was well below the collagen degradation threshold. This fact in turn, demonstrates the safety of the method at collagen fibrils level.

The next step of TEM analysis was dedicated to investigate the possibility of inertial cavitation activity within the tissue. With this concern, TEM results showed no evidence of tissue damage within the inner-sclera in the forms of pits or empty collagenic spaces, as compared to the report of

Bommannan et al. (1992) for the case of transdermal USDD (Fig. 35). In considering Bommannan's observations and with the expectation that inertial bubble activity at 1 MHz will be on the order of micron-sized growth for initial radii (Young 1989, see section 2.3.1), we surmise that no significant inertial cavitation has occurred within the inner-sclera where the collagen bundles are tightly packed (Simonin 1995). Corroborating this evidence is the fact that the membrane is covered by a medium with a plentiful supply of cavitation nuclei, thus decreasing the probability of cavitation activity within the tissue. However, more study is suggested to locate the inertial cavitation activity in ocular USDD, and to more thoroughly evaluate the effect that this treatment has on ocular tissue.

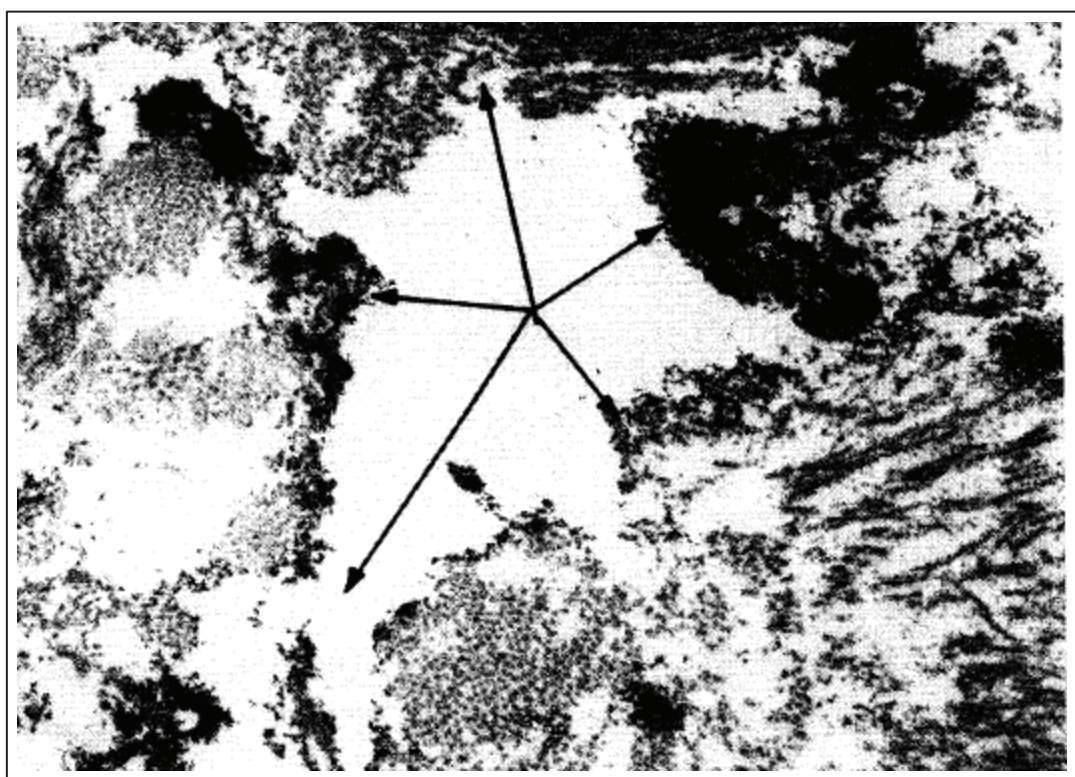


Figure 35- Electron micrograph showing the presence of the tracer in the dermis. Arrows indicate possible cavitation effect, 10kx magnification. Courtesy of Bomonnane et al. 1992.

Considering that the sclera tissue was isolated from the tissue layers which are attached to it in vivo, TEM permits us to perform a more detailed study in cellular level and collagenic intracellular structures compared to other histological methods. However, additional histological studies are suggested especially when it comes to non-isolated sclera with the choroidal and retinal layers attached. Therefore, for following ex vivo and in vivo studies, the further investigation of ultrasound

effects by light microscopy is necessary to assess the resulting condition of the other layers of the eye after US treatment. Second-harmonic generation to quantify the collagenic organization could also be useful in determining the extent of these effects (Lau et al. 2012).

In order to study the physical mechanisms of CI variation between the two pulse regimes at higher acoustic power values, the temporal evolution of CI was monitored throughout the treatment (10 minutes). It was observed that at a PRF of 100 Hz (pulse duration 250 $\mu$ s), inertial cavitation activity was well-maintained during the entire exposure. At a PRF of 1000 Hz (pulse duration 25 $\mu$ s) however, the inertial cavitation activity was not maintained throughout the entire sonication time (Fig. 28). One possible explanation is that at higher acoustic pressure levels and 1 MHz frequency, most of the bubbles likely dissolve within 100  $\mu$ s after the end of the US pulse (Mannaris and Averkiou 2012). In this way, by using a 2.5% DC, at both pulse regimes, the US off duration was too long to maintain the bubble activity memory of the preceding pulse (9.7 and 0.97 ms at a PRF of 100 and 1000 Hz respectively). Therefore, bubble growth to resonance size and inertial activation of the system may have had to build up only by each pulse (Young 1989). As stated by Lee et al. (2005), in the range of bubble radii present in the medium, smaller bubbles will require a greater number of acoustic cycles to reach the resonance size. In this way, the longer (250  $\mu$ s) pulse regime of a PRF of 100 Hz allows a greater portion of bubbles to reach the resonance size required for inertial bubble activity to happen most fiercely when compared to the short (25  $\mu$ s) pulse duration at a PRF of 1000 Hz.

In addition to an increase in cavitation activity at a PRF of 100 Hz, streaming in the experimental medium likely increases as well (Duck 1998). Thus, it is expected that bulk streaming in the experimental medium will be more significant at 100 Hz compared to 1000 Hz for a given power. This phenomenon could be a factor in scleral USDD, as was shown to be the case in both transcorneal and transdermal USDD (Zderic et al. 2004, Mitragotri et al. 1995). In addition, due to the fact that irradiation in a pulsed regime confines the cavitation activity to the focal zone, inertial collapse of

bubbles close to the membrane is likely (Coussios et al. 2006). Consequently, micro-jets near the membrane resulting from inertial-cavitation may also play a greater role in drug transportation in the case of a PRF of 100 Hz pulse regime. We therefore suggest that at the higher acoustic powers applied in this study (3.6 and 5.4 W), as the tissue permeability increases with inertial cavitation activity, bulk and micro-jet streaming may also play a greater role in scleral permeability enhancement secondary to the cavitation effects observed between the two pulse regimes.

Although using a pulsed ultrasound exposure protocol with a low DC reduces thermal effects, it does not completely eliminate them. Therefore in our experiments, thermal effects were expected to increase proportionally with the applied acoustic power. Keeping the DC constant at each given power, there was no observed difference in average temperature increase of the experimental medium between the two pulse regimes. However, we hypothesize that cavitation enhanced local heating may play a greater role at the 100 Hz PRF pulse regime compared to 1000 Hz, as the greater inertial bubble activity should convert more mechanical energy into thermal energy (Coussios and Roy 2008). However local measurement of peak temperature directly in the tissue and focal zone during treatment was not possible in this work, and further studies need to be performed to quantify such an effect.

After demonstrating that inertial cavitation plays a role in permeabilizing tissue, the characteristics and biological/anatomical mechanism of this permeabilization became questions of interest. Foremost among these questions was the transience of this permeability increase, or the permanent effects on tissue resulting from the US treatment described herein. To address the question of the transience of the observed permeability enhancement, samples which had been already irradiated were exposed to the model drug compound for another 10 minutes after the first exposure. As described in the results section, US treated tissues were twice as permeable after treatment as those exposed to sham treatments. This result shows a rather short memory effect of the US treatment. However, there was no significant difference in passive permeability after

treatment between the two pulse regimes applied. This fact suggests that the permeability enhancement mechanism of cavitation activity is in action mainly during the time of irradiation. This hypothesis was supported by an extensive TEM studies which showed no distinctive structural differences between PRF of 100 and 1000 Hz ultrasound-treated samples for all acoustic powers applied.



## 5.5 Conclusion

This chapter was primarily designed to study the effect of inertial cavitation in ultrasound-enhanced transscleral drug delivery. In order to study the contribution of inertial cavitation, the exposure conditions were defined to promote significant bubble activity at high pressure levels while maintaining a relatively constant level of non-cavitation effects. It has thus been shown that inertial cavitation could play a significant role in *in vitro* scleral drug delivery. However, these conditions are currently not optimized for relevant *in vivo* studies. For following *ex vivo* and *in vivo* studies, the further investigation of ultrasound effects will be carried out by light microscopy and second-harmonic generation method.

Although the applied acoustic pressure have not induced significant damage to the isolated sclera samples *in vitro*, some damage to the layer structure is expected *ex vivo* / *in vivo* specially at highest levels. Whether the expected damage is going to be transient or not is yet to be studied. The present work demonstrates the pivotal role of inertial cavitation in permeability enhancement; therefore, it can aid in the optimization of exposure conditions for optimal therapeutic efficacy with a controlled level of induced tissue damage. With this consideration, we speculate that by promoting the cavitation via enhancer e.g. microbubbles or US parameters e.g. frequency, similar effects could be achieved by less input power or pressure.

Concerning the upcoming *in vivo* studies, in order to have acoustic access to larger surface of sclera for USDD, several methods could be suggested. One suggestion could be the application of ring-type transducers for direct access to the sclera around the cornea similar to the previously developed systems for glaucoma treatment (Charrel et al. 2011) or iontophoresis (Behar-Cohen 2002). In addition, the possibility of some alternative transscleral routes can be explored such as the sub-conjunctival sac which is already examined in iontophoresis (Parkinson et al. 2003). The device design process, however, can address these issues better than the mechanistic study presented here.

The advantages of scleral pathway for ocular drug delivery have been explained in details (See 1.3.1). As demand of effective non-pharmaceutical modalities increases, the interest in scleral drug delivery systems is growing accordingly. By this work the feasibility of US enhanced scleral drug delivery was demonstrated. It was shown that this method potentially can be modified to achieve relevant safety for *in vivo* studies. Moreover, by a fairly well understanding of the action mechanisms, provided by this study, it is possible to optimize the exposure conditions in favor of desired effects in scleral drug delivery.



## ***Chapter 6(P.II), IR thermography***

### ***6.1 Introduction***

As been mentioned in the beginning of this manuscript, therapeutic US and HIFU systems has so far two main applications in the field of ophthalmology: drug delivery and glaucoma treatment. The topic of US mediated drug delivery has been explored in the first chapter. This chapter is dedicated to a HIFU device that has been developed and is in practice for glaucoma treatment.

This ocular disease, glaucoma, is considered to be the leading cause of visual impairment worldwide (Boland et al. 2012). In the ocular anatomy and physiology section (Section 2.2), it was demonstrated that the anterior segment is divided into two anterior and posterior chambers (Fig. 1). These two chambers are filled with aqueous humour. This fluid is produced by the ciliary bodies to provide the cornea and lens with nourishment and to remove waste products. Within a healthy eye globe, there is a balance in production and elimination of this liquid. In this way, the consequent intraocular pressure (IOP) would not undergo any distinctive variations, unless an excessive liquid production and/or lack of enough elimination terminate this balance. Glaucoma is the progressive degeneration of the retinal ganglion cells due to the increased IOP which in turn, leads to visual field defects and eventually visual loss. With these regards, the remedies could be based on two action mechanisms: reducing the production and increasing the evacuation of aqueous humour (Aptel and Lafon 2012).

The common practice for treating glaucoma respects the following steps. Mostly in non-advanced cases, the procedure starts by topical medications. In case of failure of topical administrations, a filtering surgery might be the next necessary action. In particularly stubborn cases of glaucoma, termed refractory glaucoma, a cyclo-destructive procedure can be considered as the last option for treatment. As explained in the first part of the manuscript, topical administrations are minimally effective methods due to the ocular barriers and low bioavailability. Therefore, in most

cases through a surgical procedure, an alternative channel is curved out through the sclera for better evacuation. Due to the healing power of the sclera however, the efficiency of this procedure is also limited over the long term. Therefore, as the last resort, ciliary body cyclo-destructive methods might be applied by different methods such as laser surgery, microwave therapy, or HIFU (Aptel and Lafon 2012). HIFU is one of the clinically practiced technologies in treatment of refractory glaucoma. This modality holds a specific advantage of being non-invasive compared to other approaches; given the fact that it can be focused to very small regions and induces partial coagulation without damaging the overlaying tissues.

Extensive studies on the application of HIFU to the treatment of glaucoma have been performed by different research groups in the 1980s and early 1990s (Coleman et al. 1985, Burgess et al. 1986, Valtot et al. 1989, Silverman et al. 1991). These studies focused on the ultrasonic ablation of ciliary bodies so then to reduce the excessed intraocular pressure. However, the studies diminished significantly by the mid-1990s due to the technical limitations of that era which made the procedure complex and lengthy. On top of that, severe complications were reported (Coleman et al. 1985, Silverman et al. 1991, Aptel and Lafon 2012). On the other hand, recent advances in HIFU technology once again bring the application of US into the field of glaucoma treatment. By use of miniaturized transducers, our group has developed a HIFU device, Eyeop1® (EyeTechCare, Rillieux-la-Pape, France), which operates at 21 MHz and can be used for cyclo- coagulation of the ciliary body with clinically approved results (Charrel et al. 2011, Aptel et al. 2012). This HIFU device is in post-marketing stage and is endorsed with CE marking to enter the market within the European Economic Area.

The action mode of Eyeop1 is based on transmitting a controlled amount of destructive HIFU energy to the ciliary body enough for tissue coagulation. In a general description, the EYEOP1 device consists of two compartments: command module and disposable therapy probe (Fig. 36). The treatment parameters can be set via command module. An integrated logic controller saves the

patient's data and manages safety and alarm detection throughout the treatment. This module contains all the required electronics to drive the therapy probe after the connection. The power electronics generate the electrical signal and drive the piezo-elements to precisely deliver a pre-determined energy dose and acoustic power during a designated exposure time.

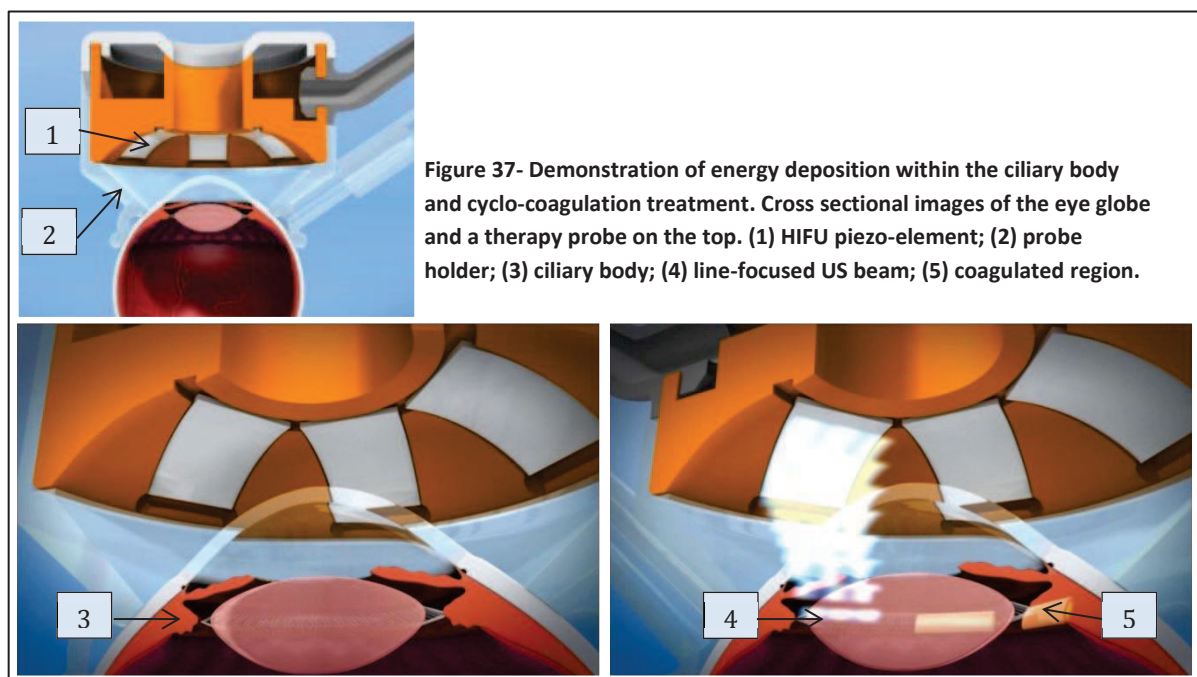


**Figure 36- Eyeop1 module (left) and HIFU therapy probe with six cylindrical piezo-elements (right).**

This therapy probe is a disposable device which contains six miniaturized piezoelectric transducers. These elements are in cylindrical form to (line-) focus the energy in six segments of a ring-shaped region corresponding the ciliary body's diameter (Fig. 37). The focal volume of the elements has approximately an elliptic cylinder shape to form selective and precise lesions within the ciliary body. In this way, the design of this therapy probe greatly reduces the risk of destructive exposure in adjacent tissues such as lens. In addition, ciliary body absorbs a great portion of the energy due the high attenuation at the frequency of 21 MHz and spares the underlying tissues such as retina in the posterior segment of the eye. The beam convergence and overlap in the posterior segment of the eye was also avoided for the sake of the retina.

As mentioned, these therapy probes are single-use. With this consideration, a large section of the production line is dedicated to these therapy probes. Dealing with the patient safety and treatment efficacy, the HIFU induced coagulations and ablations need to be assessed prior to any clinical treatment. On the other hand, the quality control of these probes is an expensive procedure

in terms of time and resources. Consequently, efficient testing of these HIFU devices in all aspects is of a major importance (Shaw and Hodnett 2008).



## 6.2 HIFU characterization

Generally speaking, characterization of HIFU devices is a challenging process especially in industrial formats. Several modalities have been developed for US field characterization such as magnetic resonance imaging (MRI), hydrophone pressure field measurement, and thermography methods; however, each holds certain drawbacks which make them not fully responsive to industrial requirements. The MRI and Shlieren ultrasonic field visualization methods are quite expensive; beside the fact that it can hardly be considered as a precise method due to rather low spatial resolution; especially in this particular application at frequency a range of 21 MHz. The conventional hydrophone field measurement can provide high resolution field maps; however, it is prohibitively slow especially in case of multi-element and phased array devices; moreover, the specific hydrophones for US field measurements are fragile, expensive, and in range of therapy parameters, they are susceptible to be damaged easily. A similar modality has been developed which applies fiber

optic hydrophone. In this way it can address some of the hydrophone issues more effectively especially in therapy fields, but again it is as slow as hydrophone method (Shaw et al. 2011, Khokhlova et al. 2013).

There are also several thermography methods developed for US field visualization. In principle, the partial energy absorption of a propagating US wave would be translated to heat, proportional to the US intensity. Assuming medium to be homogenous, the rate at which acoustical energy is irreversibly lost per unit volume by conversion into heat is equal to the rate at which heat ( $q_v$ ) is produced per unit volume (Wu and Nyborg 2006):

Eq. 5

$$q_v = 2\alpha I$$

where  $\alpha$  is absorption coefficient and  $I$  is US intensity ( $W/cm^2$ ). By this equation, fastest local temperature increase could be expected where the local intensity is highest. This is assuming the US to be mono-frequency in a linear regime thus a uniform absorption rate occurs where no other heat loss/generating mechanisms are involved. Although this is a simplified model, temperature distribution field still can provide a qualitative assessment of intensity/pressure field distribution in complex situations (Shaw and Nunn 2010).

The modalities such as US thermometry, thermometric cholesteric liquid crystals (TLC), thermocouple, and infrared thermography apply the above principle for visualizing the US field distribution. The same as non-thermic methods, most of thermography approaches are not potentially applicable in industry. For instance, the ultrasound thermometry method has poor accuracy and low spatial resolution. The same as hydrophone, thermocouple is a local sensor and scanning a field with high resolution is slow; moreover, it can be applied only in solid body mediums where the cooling effect of US streaming is cancelled, contrary to hydrophone methods. TLC, on the other hand, could be applied for fast US field mapping (Cook and Werchan 1971). However, the thermal resolution in terms of color range is limited; beside the fact that the color-temperature

relationship is not linear. On the other hand, considering some potential advantages of IR thermography to address the issues above, the interest in this modality for US field visualization is growing in R&D and pre-clinical studies (Hand et al. 2009, Bobkova et al. 2010, Shaw and Nunn 2010, Myers and Giridhar 2011, Khokhlova et al. 2013).

### ***6.3 Eyeop1® therapy probes quality control, current methods***

Currently, there are two control methods for detecting defective therapy probes in terms of field distribution: gel method and hydrophone measurement. As a therapeutic HIFU device, these testing procedures are of a major importance. Dealing with the patient safety, the HIFU induced coagulations needs to be assessed prior to any treatments to avoid any extra damage or less than desired damage so not to compromise the efficiency of the system.

The same as rest of the HIFU devices, quality assessment of these therapy probes is a challenging process. Although traditional hydrophone methods provide pressure maps of ultrasonic field distributions, it is not fully informative about the US effects in terms of lesion dimensions given the clinical parameters. Furthermore, it is prohibitively slow. In recent days, ultrasonic phantom gels are applied as a complementary modality to hydrophone measurements both in R&D and industry. These crystal clear synthetic gels can be customized to produce lesions of almost the same characteristics as those induced in biological tissues by HIFU exposure.

In R&D applications, these gels are capable of evaluating the ultrasonic radiator parameters such as frequency, power profiles and exposure time. In addition, the temporal progression of lesion growth can be recorded for further analysis. The industrial application of this modality is also increasing due to the immediate detection of defective HIFU systems in manufacturing quality control since variations in lesion shape and dimension in gel is measurable. In addition, the alignment and focus quality is also assessable by this method.

The Eyetechcare Company is one of the first HIFU system manufacturers using this modality on an industrial scale. These phantom gels (Onda, CA, USA) have their attenuation coefficient and thermal conductivity in a close range with biological tissues but with a homogeneous structure. The combination of gel lesion and hydrophone measurements provides a quality control tool for testing the Eyeop1 probes. Based on internal specifications, the conformity of piezo-ceramics is evaluated in terms of gel lesion dimensions (prior to sterilization for clinical use). In figure 38, a representation of this system with gel lesions could be observed. These protein-based gels are sensitive to temperature and if the thermal deposition of energy passes the coagulation threshold via a HIFU exposure, the color of corresponding areas turns to white.

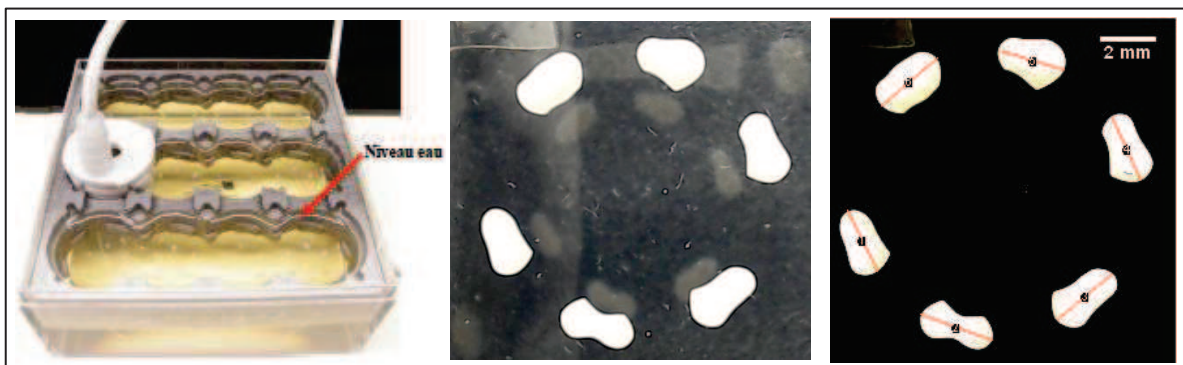


**Figure 38- Gel inspection tool (left); six gel lesions corresponding six ceramics of a probe (middle); a separate example of imageJ measurement (right).**

An image processing program such as image J (open source) could provide the dimensions of this coagulated area in terms of surface and width. These measurements provide an assessment tool, since lesion size is in accordance with the piezo-element size. For example, in an ideal case, a homogeneous power distribution or vibration would focus the energy in a line of almost the same width of the ceramic and thus induce a lesion of the same size. In this way a smaller lesion than a defined size could reveal a dysfunctional element.

With all the advantages of this system, there are several shortcomings for industrial applications. For example in our case: the shelf-life of these gels is limited due to its protein-based contents; the whole control process is time consuming with very limited automation capability; the storage and

environmental uncertainties are challenging to control and could compromise the precision of the method to a considerable extent; the uncertainties concerning the gel structural variations could not be controlled except by the manufacturer which at this time is not following any quality standard; and last but not least, on an industrial scale they are expensive as a single-use material. With these regards, the need of an alternative modality with similar functionality immersed. That said, the prospective modality needs to address the above concerns. For example, the set-up must be constituted from non-disposable materials with automation and time-saving capabilities; the experimental uncertainties have to be controllable with high precision; furthermore, as a detection tool for defective transducers, a good conformity with gel lesion and hydrophone measurements is essential.

#### **6.4 IR thermography**

The application of IR technology in healthcare has been expanded over many different fields as a control tool. One of the main applications of so called digital infrared thermal imaging technique (DITI) is monitoring dermal physiological changes, for instance inflammation or responses to external stimuli (Jones and Plassmann 2002). As this method is capable of detecting subtle changes in skin surface temperature, DITI has been applied in recent years for breast cancer diagnosis. The Clinical studies showed that DITI is a valuable modality complementary to mammography and ultrasound imaging (Arona et al. 2008). This technique has found its way also to breast cancer research as a prognostic tool (Xie et al. 2004). In the field of ophthalmology, IR thermography could be applied for evaluation of ocular surface temperature. This evaluation could be applied to detect impaired retrobulbar haemodynamics in patients with glaucoma (Galassi et al. 2007). The feasibility of DITI is also demonstrated in determining inflammatory state in patients with Graves' ophthalmopathy which is an autoimmune disease (Chang et al. 2008).

One application of IR thermography, in industry, is when it combines with US for nondestructive evaluation. Basically, the subsurface defects have locally inhomogeneous thermal properties which



can be revealed by temperature gradient and detected by IR imaging as US energy propagates through the sample medium (Shu-Yi 2004). On the other hand, IR thermography can be applied for quality control assessments of US devices themselves. For example, the maximum surface heating of therapeutic ultrasound transducers can be assessed by IR imaging when they are derived directly in the air. This quality control measure is of an important clinical importance where an US transducer is in touch with the patient's body (Kollmann et al. 2005).

#### ***6.4.1 IR thermography and Ultrasonic field visualization-state of the art***

Referring to the literature, the common motivation for application of IR systems in US field mapping is that this method is a distinctively fast assessment tool. In addition, the recent advances in IR technology make this modality a precise thermography tool with high thermal/temporal/spatial resolution. Although this technology is not fully tamed yet for HIFU field characterization, studies by different research groups achieved encouraging results (Bobkova et al. 2010).

The main challenge of IR thermography application is the fact that IR recorders could only register the temperature field of the surface of an object of interest. This fact poses a problem: contrary to hydrophone method, there need to be an air interface between the plane of interest and the IR camera. As the US refuses to continue its propagation through the air along the beam axis, it will be reflected back to the medium by the air interface, due to a distinctive impedance mismatch. With this regard, different groups have addressed this issue in different ways.

One of the first applications of thermography in therapeutic US field was done by ter Haar and Carnochan (1982). The objective of their study was to compare the thermal patterns of RF inductive and an US heating system designed for clinical application. This qualitative comparison was performed in two phases, theoretical modeling and experimental. For the experimental purpose, the mentioned challenge above was tackled by use of two phantom gel blocks which were stacked on each other, with a thin oil layer in between for acoustic coupling. The interface of the blocks was then placed along or across the beam axis. In this way, immediately after the exposure the blocks

could be split and the temperature field distribution of the surface be recorded by an IR camera. A similar method was applied for visualization of HIFU induced temperature rise in biological tissue (Khokhlova et al. 2002). As it could be seen in figure 39, tissue interface was placed along the beam axis of a HIFU transducer. By application of these methods, a good qualitative agreement between the predicting model and the temperature profile obtained after US exposures at 0.7, 1, 2, and 3 MHz.

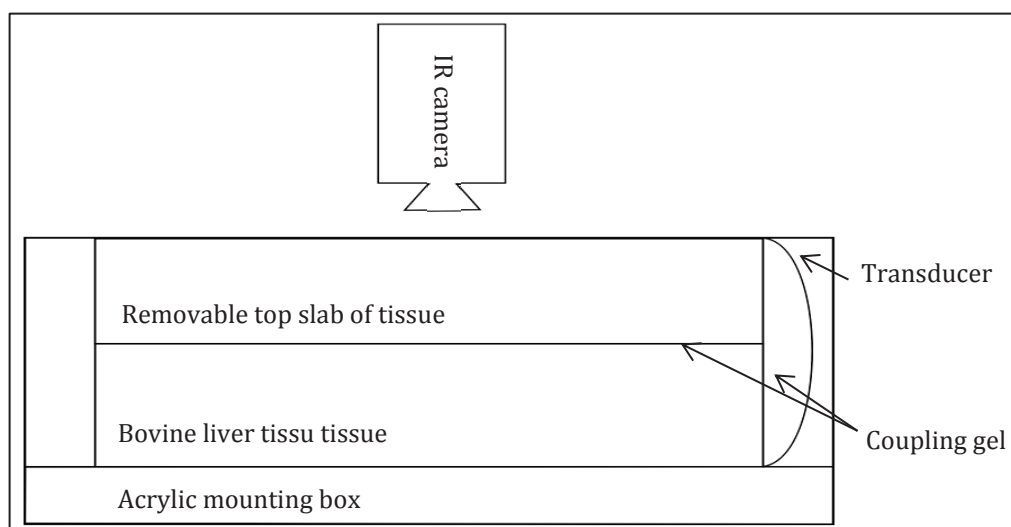


**Figure 39- Experimental set-up of Khokhlova et al. (2002) for IR thermography.**

The direct proportionality between incident intensity and the rate of temperature increase was defined above in equation 1. Based on this concept, several methods have been developed to obtain a qualitative assessment of intensity field distribution. Shaw and Nunn (2010) immersed their HIFU system in a water tank with the angle of  $45^\circ$  relative to the water surface where a polyacetate film was laid. In this way a great portion of the US energy was reflected off the air interface towards the tank wall. An ultrasound transparent film (Mylar) was mounted close to the US target to avoid the cooling effects of acoustic streaming in the water bath. The temperature field distribution was infrared imaged by a fixed camera above the tank. The thermal images then reconstructed for any desired orientation in post-processing phase. It was also possible to achieve a 3D map by transducer repositioning. The major constrain of this study was that the target (plastic film) was not placed at perpendicular focal. In this way field interpretation and image reconstruction were performed with

high accumulated uncertainties. The reason to use such configuration was to avoid energy reflection back to the transducer and also to reduce the acoustic field perturbation. In addition, the available acoustic target was not absorptive enough at 45° angle to reveal the field distribution effectively; and in perpendicular focal plane, it got melted due to double absorption.

The following studies compensate for these drawbacks by substituting the acoustic target with specific 2mm thick ultrasonic absorber (Aptflex F28, Precision Acoustics, Dorchester, UK); and repositioning into perpendicular plane to the beam axis with normal incident. Moreover, US was applied in the burst regime (0.1-0.3 s) to reduce the acoustic disturbance due to the reflection along the acoustic axis (Bobkova et al. 2010). The main objective of this study was to demonstrate a method for acoustic focusing through a rib cage that aimed to minimize heating of the ribs. For that matter a 2D, 1 MHz phased array with 254 randomly distributed elements was applied. The large number of focusing conditions in addition to being a very slow process left no room for application of hydrophone methods. A previously developed IR thermography by the same group was extended to provide estimations of ultrasonic fields both qualitatively and quantitatively. Following this, Khokhlova et al. (2013) extended the method further. The main goal of this recent work was to evaluate the suitability of the IR thermography for rapid intensity estimation in US fields radiated by a flat physiotherapy transducer and two focused HIFU transducers. A calibration coefficient was defined between IR measurement data versus hydrophone data in one selected plane. This coefficient was specific to each transducer. By this coefficient conversion the temperature distribution field to corresponding intensity field was possible also in other planes of interest. A good agreement then achieved between the two methods.

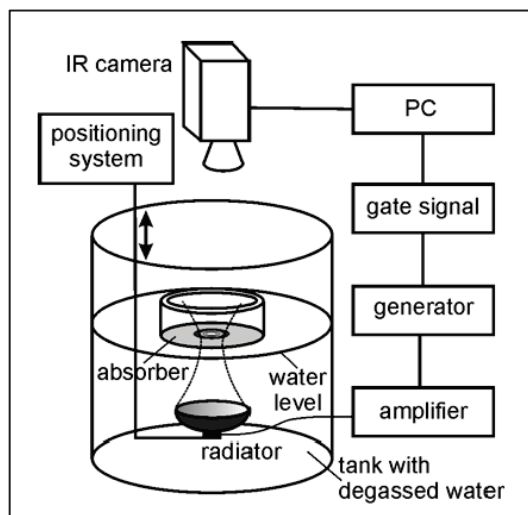


Figure 40- Experimental set-up of Khokhlova et al. (2013) for IR thermography.

Myers and Giradhar (2011) also developed a prediction tool for intensity estimation within a phantom tissue base on IR imaging. For the experimental validation of numerical model (Giradhar et al. 2012) a rather thick cylindrical block of phantom gel (40 mm in diameter and thickness). The geometrical focal plane of the HIFU was then aligned with the gel/air interface. Again the numerical predications and experimental data were in good correlation. However, their intensity assessment model found to be not fully compatible to other HIFU set-ups such as the ones of Bobkova et al. and Khokhlova et al. which were discussed briefly above.

Upon reviewing the publications of different research groups reveals that all the developed IR assessment methods for US field characterization are customized to one specific HIFU set-up, even though they are based on the same principle. Therefore, stands to reason to perform a feasibility study in order to evaluate IR thermography application for Eyeop1 probe characterization. Here, the set-up was customized and extended for Eyeop1. On the other hand, the quantitative methods have more applications in R&D and pre-clinical studies where exposure condition variations assessment or absolute intensity evaluation is necessary. As been explained, in our case, the need of a rapid assessment tool in the quality control of therapy probes emerged in production line of the HIFU systems. Given the automation capability, IR thermography was a good candidate for qualitative

control procedure. With this regard, this study sets out to extend this R&D technique to an industrial application.

## ***Chapter 7(P.II),***

### ***Ultrasonic field characterization via IR thermography: A feasibility study***

#### ***7.1 Introduction***

The advantages of IR thermography application in qualitative US field characterization were described previously. Referring to literature, previous studies have developed for lower frequency HIFU systems (1-5 MHz) when compared to Eyeop1 ( $21\pm 1.5$  MHz). Here, the method is extended for Eyeop1 therapy probes characterization in terms of beam profile at the focal line. The feasibility study was initiated applying available tools and materials. This investigation first aimed to show the coherency of this method with other applied control tools such as pressure field measurements and gel phantom method. Then, by adjusting the exposure parameters, we tried to obtain close field distribution estimations with hydrophone measurements. The promising results encouraged us to up-grade the system to a more advanced one. During this process the acquisition and analysis techniques have also been improved. Following this, it has been shown that IR method is in good agreement with both gel and hydrophone qualitative measurements. This system exhibited also a good reliability. Satisfying the needs of a control tool for field distribution control such as being fast and precise, the gel method and qualitative hydrophone method could potentially be replaced by IR inspection modality.

## 7.2 Materials and methods

### 7.2.1 Acoustic set-up

#### 7.2.1.1 EYEOP1 therapy probes

Prior to this, it was explained that IR systems were developed for thermal characterization of the EYEOP1 therapy probes. Each probe consists of six piezo-elements. The positioning of the elements inside the probe was with spacing of  $55^\circ$  except in the nasal and temporal meridians, in which a spacing angle of  $70^\circ$  was applied in order to preserve untouched areas of ciliary body; ensuring a sufficient production of aqueous humour and nourishment of the interior segment. The  $21 \pm 1.5$  MHz elements had a cylindrical form and were designed to focus the energy in a thin line at focal distance of  $10.1 \pm 0.4$  with the curvature radius of  $40.36^\circ$  (Fig. 41). For clinical applications there were two different types of piezo-elements in terms of active surface, while they all had the same bulk size. One type of elements had a larger active surface of  $35 \text{ mm}^2$  with a length of  $7.24 \text{ mm}$  and a width of  $4 \text{ mm}$  (dimensions in a plane, Fig. 41a). With the same length, the other type of elements had a width of  $2.5 \text{ mm}$  thus a smaller active surface of  $18.5 \text{ mm}^2$  (Fig. 41b). Both of these two types of transducers were applied in the following studies and they are referred as '4mm' and '2.5mm' in this text.

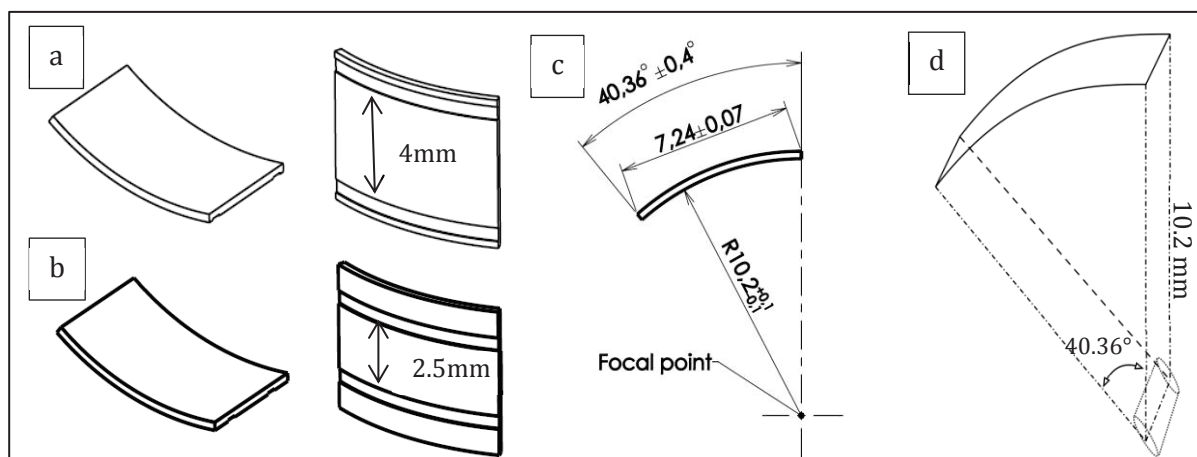


Figure 41- Isometric view of piezo-elements with 4 mm (a) and 2.5 mm (b) widths; geometrical dimensions (c); and demonstration of elliptical focal line (d).

### 7.2.1.2 Acoustic measurements

The acoustic field characterizations were performed by hydrophone method in a free field water tank (similar to measurements of the first part of the manuscript subsection 4.2.2); details of the measurements are explained later in the text (See 7.2.2). The acoustic power measurements were done applying force radiation balance method (Davidson 1991). This method is generally developed for normal incident of US beam relative to a horizontal target been laid on a balance. In our case however, beam incident is with an angle of  $20.76^\circ$  relative to the absorber sheet, due to the position of elements within the probes (Fig. 42). Therefore direct translation of radiation force measurements to acoustic power leads to an over estimation of the power. For angled incident, the transmitted acoustic power is given by (N'Djin et al. 2008):

Eq. 6

$$P_{ac} = \frac{\Delta m}{k} \quad \text{with } K = \frac{(70 \cos^2 \alpha)}{1000}$$

where  $P_{ac}$  is the acoustic power (W),  $\Delta m$  is mass variation (g), and  $k$  ( $\text{gW}^{-1}$ ) is a constant which takes into account the radius of curvature of the transducer and the angle of incidence ( $\alpha$ , rad) between the ultrasonic wave and the norm of the interface, in our case the absorber. After applying the correction factor, the acoustic power range used in this study was 0.96-2.28 W.

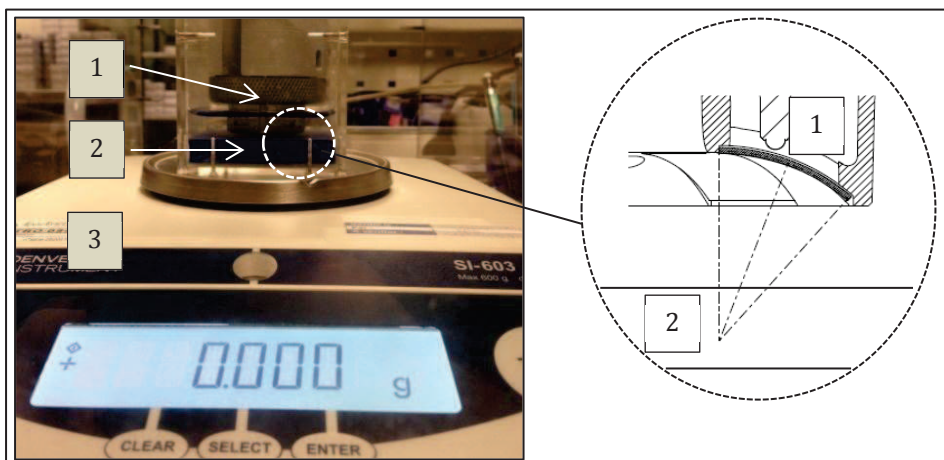


Figure 42- Force balance measurement set-up. (1) therapy probe; (2) ultrasonic absorber; (3) balance.



## 7.2.2 IR systems

The first part of the feasibility study was performed applying the Optris IR system (Optris PI160, Berlin, Germany). This system was already available in the laboratory for basic applications. The feasibility results were found to be encouraging to upgrade the system for further studies. With this regard, FLIR camera (Research SC655, FLIR Systems, Boston, MA, USA) was a clear choice. Similar systems in Research FLIR family were applied in prior studies. This system possessed some advanced measuring features and industrial capabilities in terms of automation.

### 7.2.2.1 Acquisition with Optris system

The therapy probe contained six piezo-ceramic transducers which were driven sequentially with adjustable pause-time between each sector. In order to have a good spatial resolution for IR imaging, it was necessary to reposition the camera for each sector since a larger field of view would compromise the spatial resolution of images distinctively. During the acquisition process, this camera was set to record radiometric videos at frame rate of 120 f/s.

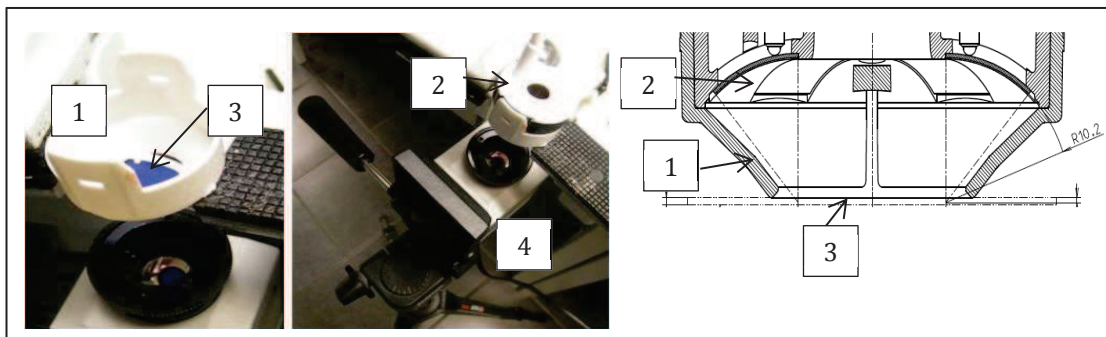


Figure 43- Optris experimental set-up. (1) probe holder ; (2) therapy probe; (3)absorber sheet ; (4) IR camera.

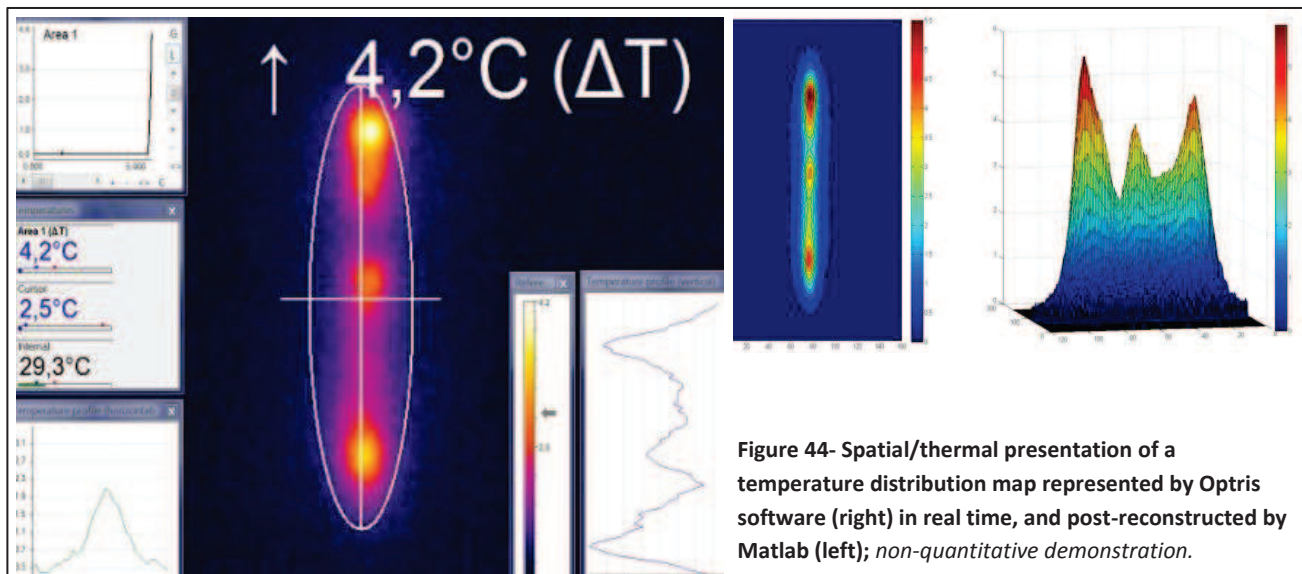
The IR camera was set to map the resultant temperature change induced in a specific acoustic absorber (Aptflex F28, Acoustic Precisions Ltd, Dorchester, UK) from below at the distance of  $22 \pm 0.5$  mm. At this distance the frame width and height were 8.8 and 6.6 mm respectively (160x120 pixels with a pitch of 0.06 mm). Therapy probes could be placed inside a cone shaped holder at a fixed position and distance to the absorber (Fig. 43). The absorber sheet was attached to the cone at the focal distance of the elements. Aptflex F28 was a suitable choice for the requirements of IR thermography (single-pass attenuation coefficient of 3 dB/MHz/mm). Considering the reflection at

the water/absorber interface of -25 dB, a significant portion of the US wave propagates into the absorber due to matched acoustic impedance and wave speed to a water medium (1.5 MRayls and 1500 m/s at room temperature). In addition, this material is highly stable and suitable for multiple usages due to the cross-linked polyurethane structure. In principle, the thermal diffusion in thinner absorbers is less prominent thus the temperature field is more in conformity with pressure field. Therefore, this sheet was customized to be homogeneous at considerably short thickness of  $0.7 \pm 0.1$  mm (corresponding  $\sim$  ten wavelengths of  $0.075 \pm 0.005$  mm at 21 MHz). This was the thinnest sheet possible to be achieved by this material.

Once a probe was attached, the cone was filled with degassed water at room temperature (21-23° C). The probe and piezo-elements were controlled and driven by the Eyeop1 integrated generator module. The US was applied in continuous regime and the exposure time was set to be in the range of 100 - 200 ms. After each US exposure by an element, the heat deposition spread out due to thermal diffusion which preheated the adjacent area of the next element. To avoid this pre-heat effect, a sufficient pause-time was defined for a full heat dissipation prior to the next shoot (One minute pause). In this way, the initial temperature ( $T_0$ ) of the absorber was the same for all elements within one probe. After each exposure, the temperature distribution field could be recorded in a radiometric format (ravi) in which the thermal/spatial/temporal information was encoded. For post processing, a frame of interest could be decoded and analyzed with analysis tools e.g. Microsoft Excel® or Matlab®. The Optris software (PI connect) also had a real-time monitoring option which was handy for repositioning and adjustment of the camera. Figure 44 demonstrates an example of Optris acquisition.

*Summary of Optris system & procedure:*

- Set-up: Optris camera, probe holder, 0.7mm absorber, Eyeop1 module
- Exposure time (continuous regime): 100-200 ms
- Acoustic power: 0.96-1.84 W



### 7.2.2.2 Acquisition with FLIR system

FLIR system was used for the next phase of the feasibility studies. During the thermal recording, the camera was set to record radiometric videos at frame rate of 50 Hz and thermal resolution of 50mK. This frame rate was a good compromise for reducing the IR movie size, yet acquiring all the necessary temporal field distribution data. In order to achieve a high spatial resolution a close-up IR lens (FLIR T198059, 2.9 $\times$ ,) was utilized. By this lens a field of view of 32x24 mm (640x480 pixel of 50  $\mu$ m) was achievable at the working distance of 84 mm from the absorber sheet. By this setting, it was possible to contain the whole absorber area in one frame, thus immobilizing the acquisition system in the sequence of six exposures for one therapy probe. This set-up in turn reduced the previous experimental errors due to the camera repositioning between each sector. The IR camera was attached to a 3D positioner for micro adjustments. Once adjusted, it could be immobilized at the desired distance. For the IR acquisition the positioner and camera were placed inside a glassy box (polycarbonate) to cut out the IR noise from the environment. A temperature sensor (multi-thermocouple) was applied to monitor the temperature inside and outside of the box. A modified probe holder with an attached absorber sheet was fixed on the top of the box where camera could see the absorber through an open window.

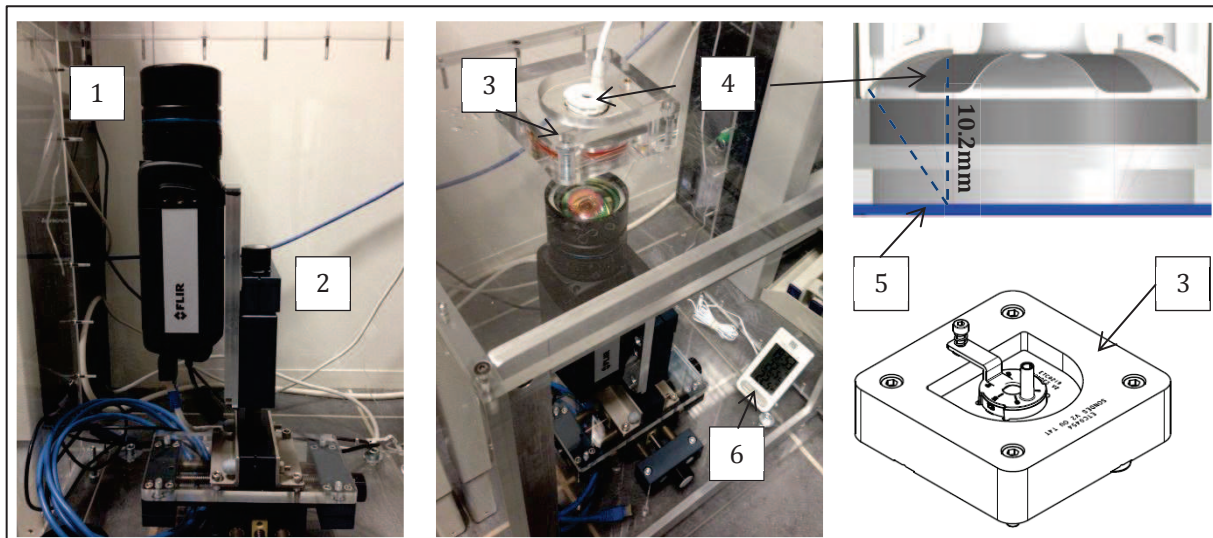


**Figure 45- FLIR experimental set-up. (1) IR camera; (2) 3D positioner; (3) probe holder; (4) therapy probe (5) absorber sheet at 10.2mm distance (dashed line); (6) temperature double-sensor for outside and inside the container box.**

Once a probe was attached, the holder was filled with degassed water at room temperature (Fig. 45). For this part of the study, US was applied in a tone-burst regime (See discussion). With 23.3% DC and a PRF of 33.3kHz, short bursts of 150 cycles per 30  $\mu$ s were generated for an exposure time of 600 ms; the duration of 150 cycles correspond 7.1-7.9  $\mu$ s regarding the frequency variations of elements in frequency range of  $21 \pm 1.5$  MHz (the reason for these US parameters choice is described in the discussion section). The generation of tone bursts was provided by a function generator (Agilent 33250A, Santa Clara, CA, USA). The signals then were amplified by an RF amplifier (VectaWave VBA200-30, Isle of Wight, UK) and passed through a matching circuit and a communication module built in house for driving the elements in pre-set sequences. The IR camera and electronics were controlled by a PC. The pause-time between driving each element was three seconds. In order to avoid any pre-heat memory effect, the adjacent sectors were avoided to be driven in a successive sequence; instead the sectors were driven in non-sequential order. In this way, after driving an element, the necessary time for heat dissipation would not interfere with the successive element.

The experimental system and software managed the acquisition system and data post-processing. The application software was developed in a cross-platform application framework, Qt (in C++) by an internal software-engineering section. The camera interface was written in a generic

programming interface for machine vision cameras (GenICam™ standard, European Machine Vision Association).

Summary of FLIR system & procedure:

- Set-up: FLIR camera, container box and probe holder, PC and lab instruments
- Exposure time and Burst duration: 600 ms and 150 cycle each 30  $\mu$ s (7.1-7.9  $\mu$ s)
- PRF and DC: 33.3 KHz and 23.3%
- Acoustic power: 2.28 W

### 7.2.3 Data analysis

The IR systems were applied to map the resultant temperature change induced in the acoustic absorber. In this way, for each exposure, a radiometric sequence of images was accessible. The general protocol for post-processing procedure was as follows: in order to obtain relative temperature distribution fields, the initial absolute temperature value of the absorber i.e. first frame before any exposure, was subtracted from all the successive images. The product of this forward subtraction ( $\Delta T$ ) provided relative temperature distribution and used for further qualitative thermal analysis.

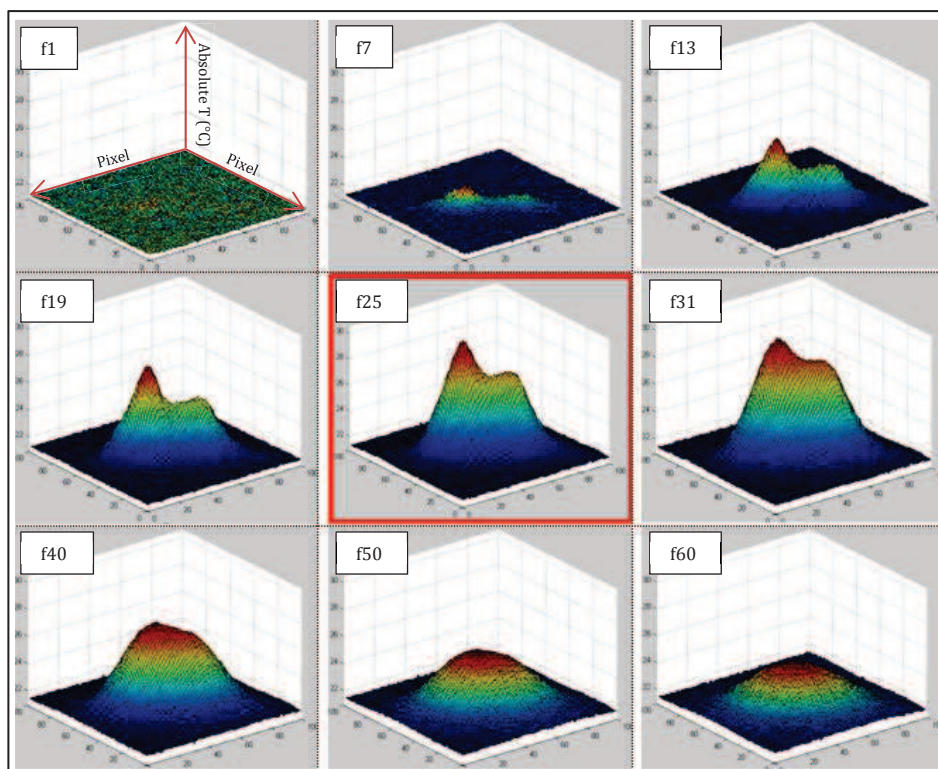


Figure 46- Evolution of temperature field distribution in 60 frames recorded by FLIR (frame rate 50Hz); non-quantitative demonstration.



Among the thermal images, the frame with the maximum temperature ( $T_{\max}$ ) was chosen for mapping the field distribution. A non-quantitative demonstration of this process could be seen in figure 46: starting from the first frame, the temperature evolution reaches its maximum value in the 25th frame (f25); this would be chosen for further analysis. With thermal-spatial data encoded in this frame, it was then possible to define the region of interest in terms of width or area. Thus, temperature profile was measured in two different regions of interest: the area encompassed by 70.7%  $T_{\max}$ , and also full width at half maximum. In a qualitative field assessment, these values correspond to either intensity ( $I$ ) field at -1.5dB and -3dB or pressure ( $p$ ) field at -3dB and -6dB respectively; as US intensity is directly proportional to the squared pressure. In figure 47, an example of this comparison method is demonstrated.

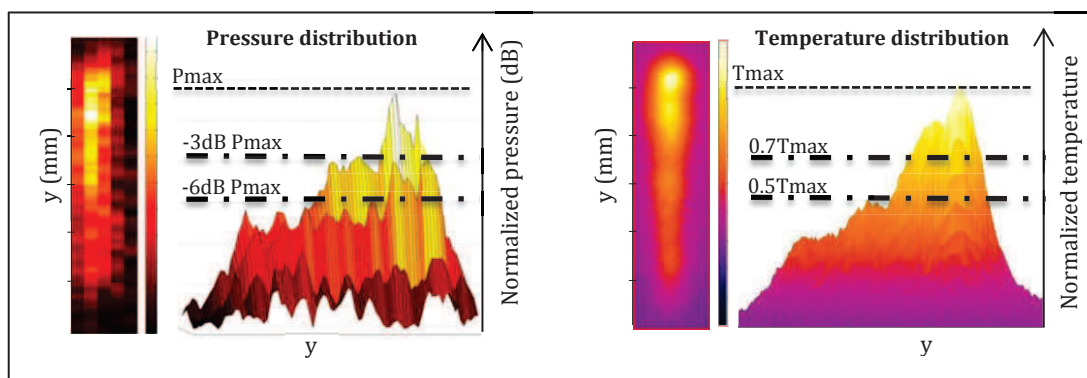


Figure 47- Relative comparison of pressure field hydrophone measurement (left) and temperature distribution field recorded by Optris camera (right); *non-quantitative demonstration*.

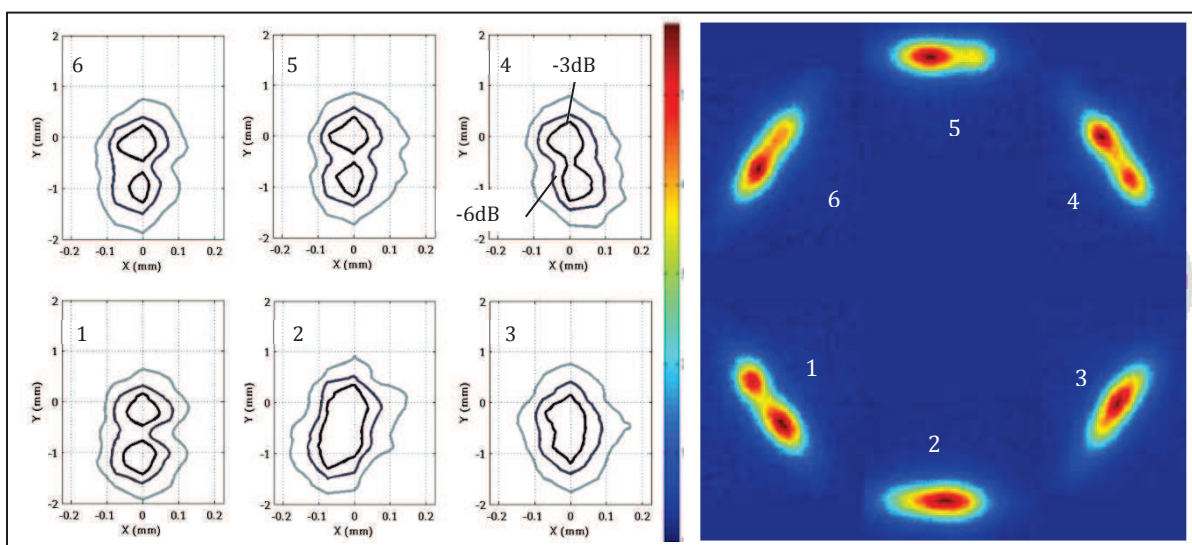


Figure 48- Pressure field map of six piezo-elements/one probe measured in focal plane (right); thermal distribution map taken from the surface of the absorber sheet (left); *non-quantitative demonstration*.

The US parameters for IR inspection were tried to be adjusted in accordance with the pressure field measurements. Several experiments have been performed with this aim. For comparison reason, pressure profile was taken as reference and its absolute difference with temperature profiles was taken for further assessments ( $|y_T - y_p| \cdot 1/y_p$ ). In statistical analysis, the relative standard deviation or variation coefficient (VC) were used as an indication of repeatability. VC was calculated by dividing the standard deviation of a population by their mean value (expressed as percentage).

#### **7.2.4 Overview of feasibility studies**

The final provisioned IR thermography tool has to meet certain requirements. This system has to possess the inspection capacities of both phantom gel and hydrophone measurements. In this way, a good correlation with hydrophone pressure field is a must. It needs also to have the inspection capabilities of gel lesion method since traditional hydrophone method alone is not fully capable to detect all sorts of nonconformities when it comes to clinical US parameters. Contrary to gel method however, this future system has to function with very good repeatability and reproducibility. With this road map on mind, an overview of feasibility studies could be found bellow.

##### **7.2.4.1 IR thermography: an inspection tool (I)**

The very first feasibility study was performed applying the Optris set-up. One R&D probe (6 elements, 4mm) and a phantom gel block from the control section were used. The induced lesion by each element was compared to corresponding temperature and pressure field distributions. For IR imaging, US was applied at 1.96 W, continuous regime for 200ms. Free field hydrophone measurements were carried out in focal plane (normal incident, varied among elements  $10.1 \pm 0.4$  mm) and absorber plane (at distance of 10.2 with  $20.76^\circ$  angle of incident, Fig. 49). The comparative parameters of IR inspections were width of temperature profile at 0.707 and 0.5 of  $T_{max}$ ; corresponding -3 and -6 dB of pressure profile respectively.

This initial study was aimed to investigate:

- If IR inspection could potentially be considered as an inspection tool similar to gel method.

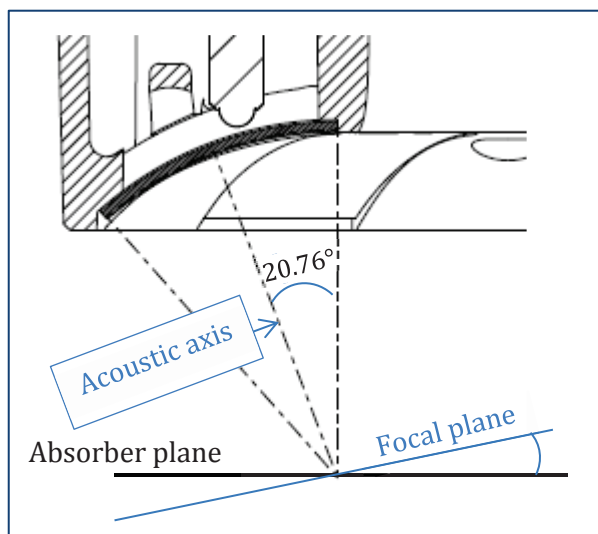


Figure 49- Demonstration of 20.76° inclination of the absorber plane to the normal incident.

#### 7.2.4.2 IR thermography/ pressure hydrophone measurement (I):

The studies were continued applying *Optris system and procedure*. There were four probes (24 ceramics of 2.5mm) available which had been used previously for clinical studies. In this way, they had already passed the quality control section. In addition, the result of clinical studies was approved; therefore their efficiency was proven in terms of lesion inducing. For IR imaging US was applied at 0.96 and 1.84 W, continuous regime with two exposure lengths of 100 and 200ms. The acquired temperature fields were then compared with hydrophone measurements as reference. The parameters of comparison were temperature profile at 0.707 and 0.5 of  $T_{max}$ , corresponding -3 and -6 dB of pressure profile respectively.

This study aimed to investigate:

- If accordance of IR and hydrophone method could be modified with exposure parameters adjustment.



### **7.2.4.3 US parameters adjustment for IR inspection method:**

A parametric study was performed for adjusting the US exposure parameters for FLIR system based on the requirements of the quality control inspection. 20 sample probes (120 elements of 2.5mm) were chosen from the production line. These probes had already passed the control. In order to reduce field perturbation between the elements and absorber, a tone burst regime was applied for further studies with pulse repetition period (PRP) of 30 $\mu$ s (See discussion).

Three different exposure durations were tested with almost equal total energy dose. The thermal distribution of each element was IR imaged for three successive times for the same applied exposure duration. Between each exposure the therapy probe was removed and repositioned back to the holder; the average and standard deviation of them were taken for further analysis. The examined exposure durations were:

- 200ms, continuous
- 400ms, PRP 30 $\mu$ s, 280 cycles (~ 50% DC)
- 600ms, PRP 30 $\mu$ s, 200 cycles (~ 25% DC)

Based on the outcome, 600 ms was chosen for further studies. The next parameter to adjust was the burst duration:

- 600ms, 30 $\mu$ s, 50 cycles
- 600ms, 30 $\mu$ s, 100 cycles
- 600ms, 30 $\mu$ s, 150 cycles

It was expected that reproducibility of the system got influenced by these variations; therefore the aim of this investigation was to choose a set of parameters that could provide more reproducibility.

### **7.2.4.4 IR thermography/ pressure hydrophone measurement (II):**

By application of *FLIR system & procedure*, a few studies were carried out to investigate the influence of plane inclination (normal incident to 20.76°) on pressure field measurements. The

hydrophone measurements were performed for 20 production probes (120 elements of 2.5mm) in three different planes:

1. Acoustic focal plane (10.1±0.4mm on acoustic axis) and normal beam incident
2. Acoustic focal plane and angled beam incident (20.76°)
3. Absorber plane (10.2mm) and angled beam incident (20.76°, the same plane of absorber)

Prior to this, all the probes passed the quality control test with gel method and then IR inspection was performed. The parameters of comparison were temperature profile at 0.707 and 0.5 of  $T_{max}$ , corresponding -3 and -6 dB of pressure profile respectively. A clinical acoustic power of 2.28 was applied for IR imaging.

In this way, this part of the feasibility study was aimed to answer the following questions:

- Could temperature width profile at absorber plane be compared with the pressure profile of the focal plane, considering the 20.76° angle of incident on the absorber?
- Could applying clinical US powers for IR method keep its correlation with hydrophone method?

#### **7.2.4.5 IR thermography: an inspection tool (II)**

The second phase of this study has performed applying the *FLIR system and procedure*. For this matter, three probes (18 elements) from production (2.5mm) were chosen for IR inspection. These probes were already tested by control section using the gel method. The lesion width and FWHM of temperature profile were compared with each other; sector by sector their absolute difference was calculated with gel taken as reference. A preliminary bound of conformity was defined according to gel method's specification (2.5 mm) previously defined in the control section. Based on this specification, the elements with width of lesion outside the bound of 1.4-2.5 mm would be considered as defective or nonconforming. In order to test the detection capability of IR inspection, four R&D probes were also examined with different ceramic dimension in width: 1.5 and 4 mm. For comparison reason, these probes were considered as "defective 2.5mm probes".

#### **7.2.4.6 IR thermography: a reliability survey of current set-up**

The reliability of the current set-up was measured through repeatability and reproducibility examinations. In four separate procedures, repeatability, influence of probe positioning within the set-up, influence of renewing/replacing the US absorber, and room temperature on reproducibility were investigated as follows. The comparative parameters of IR inspections were  $T_{\max}$ , width and area of temperature profile at FWHM.

1. **Repeatability:** 20 probes (120 elements, 2.5mm) randomly were chosen from the production line. Each probe passed the IR inspection three successive times; the testing probe was immobilized during three measurements within the holder.
2. **Influence of probe repositioning on reproducibility:** the same probes and procedure were applied; the testing probe however, was removed from set-up and then replaced back to the set-up to examine the repositioning reproducibility.
3. **Influence of renewing/replacing the US absorber on reproducibility:** the same probes were tested for another time but with a newly installed US absorber sheet (the same material and properties). The thickness of the new absorber was measured to be 0.6 i.e. 0.1 thinner than the previous one (0.7 mm). The outcome was compared to corresponding ceramics from the first procedure.
4. **Influence of room temperature on reproducibility:** five probes from the same group were examined at five different room temperature adjusted in a period of five successive days at 20, 20.5, 22, 23.5, and 25° C. The IR inspection of each sector then analyzed with regard to these variations.

This survey **aimed to shed light on this question:**

- Is method potentially reliable to be applied for an industrial application?

## 7.3 Results

### 7.3.1 IR thermography: an inspection tool (I)

One R&D probe (4mm) was utilized to be inspected by gel lesion method. In figure 50, the color change from surroundings signifies a region which became coagulated after the US exposure. The exposure parameters were adjusted for the elements to transfer the same acoustic power. However, a distinctive lesion variation could be observed in terms of dimension. Considering elements 2, 3, and 4 the lesion width was on average  $4.05 \pm 0.07$  mm; and elements 1, 5, and 6 on average  $2.68 \pm 0.50$  mm. The results of IR inspection and hydrophone measurements for these elements could be seen in table 2.

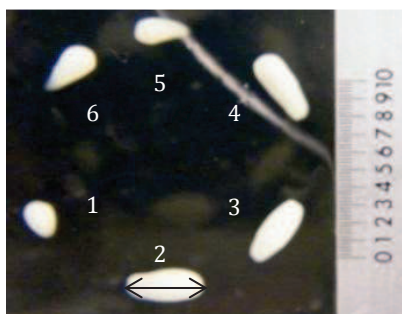


Figure 50- Gel lesions, 6 elements (4mm).

Element	parameter	IR method	P: acoustic focal, normal incident	P: absorber plane, angled incident	Gel lesion
#2,3,4	0.707T:-3dB	$3.48 \pm 0.56$	$3.97 \pm 0.13$	$4.05 \pm 0.01$	$4.05 \pm 0.07$
	0.5T:-6dB (mm)	$4.27 \pm 0.25$	$4.42 \pm 0.12$	$4.37 \pm 0.08$	
#1,5,6	0.707T:-3dB	$1.61 \pm 0.55$	$2.15 \pm 0.16$	$3.27 \pm 0.82$	$2.68 \pm 0.50$
	0.5T:-6dB (mm)	$2.43 \pm 0.79$	$4.32 \pm 0.16$	$4.42 \pm 0.01$	

Table 2- Relative profile measurements of temperature and pressure field.

A good agreement could be seen among P at -6dB,  $0.5T_{\max}$  and gel lesions; except for the pressure measurement of the mal- functioning elements.

### 7.3.2 IR thermography/ pressure hydrophone measurement (I)

The hydrophone pressure field measurements at the focal plane for 4 probes (24 elements, 2.5mm) was on average  $1.22\pm 0.32$ mm and  $1.86\pm 0.31$  mm at -3dB and -6dB respectively. The corresponding temperature profile of US exposures at 0.84 W and duration of 100ms was on average  $1.12\pm 0.11$ mm and  $1.67\pm 0.17$  mm at 0.7 and 0.5 of  $T_{max}$  respectively. By increasing the exposure time to 200ms the corresponding values were  $1.15\pm 0.18$  and  $1.69\pm 0.19$  mm at 0.7 and 0.5 of  $T_{max}$  respectively. In next step the transferred acoustic power was increased to 1.96 W. Applying the same protocol, temperature profile of 100ms of US exposures was on average  $1.29\pm 0.32$  and  $1.93\pm 0.41$  mm at  $0.7T_{max}$  and FWHM respectively. By increasing the exposure time to 200ms the corresponding values were  $1.35\pm 0.33$  and  $1.95\pm 0.36$  mm at 0.7 and 0.5 of  $T_{max}$  respectively (Fig. 51).

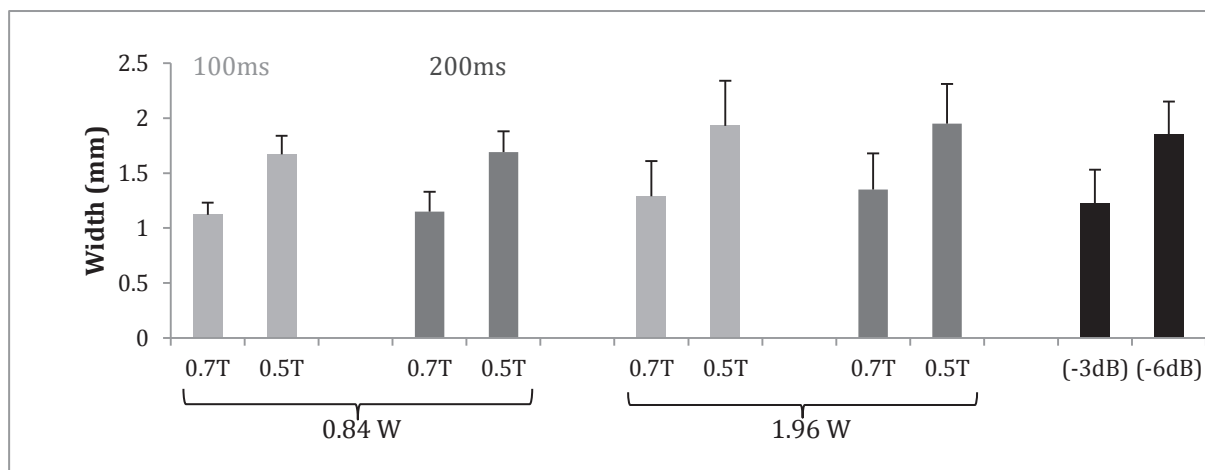


Figure 51- Width of temperature profile applying US power at 0.84 and 1.96 W and exposure time of 100 and 200ms (bars in gray scale); width of pressure profile at -3 and -6 dB (black bars).

In figure 53, width of temperature profile at 0.7 and 0.5 of  $T_{max}$  could be compared with corresponding -3 and -6 dB of pressure profile respectively. The values are representing the average of six elements in each probe. The absolute width difference of temperature and pressure profile ( $\Delta y$ ) was calculated for each element, taken the pressure field width ( $y_p$ ) as reference ( $\Delta y / y_p$ ). The lowest value of this comparison was  $8.15\% \pm 4.63$ , corresponding the temperature profile at FWHM, 0.96 W, 100ms; the highest was  $27.92\% \pm 18.66$  at  $0.7T_{max}$ , 1.84W, 200 ms (Fig. 52).

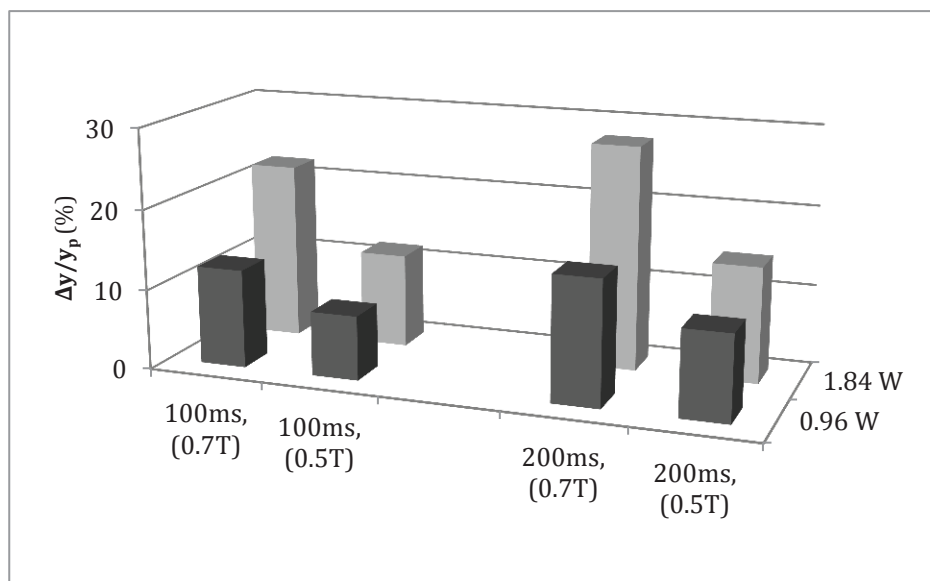


Figure 52- Comparison of width of temperature and pressure profiles for four different probes (average of six elements each).

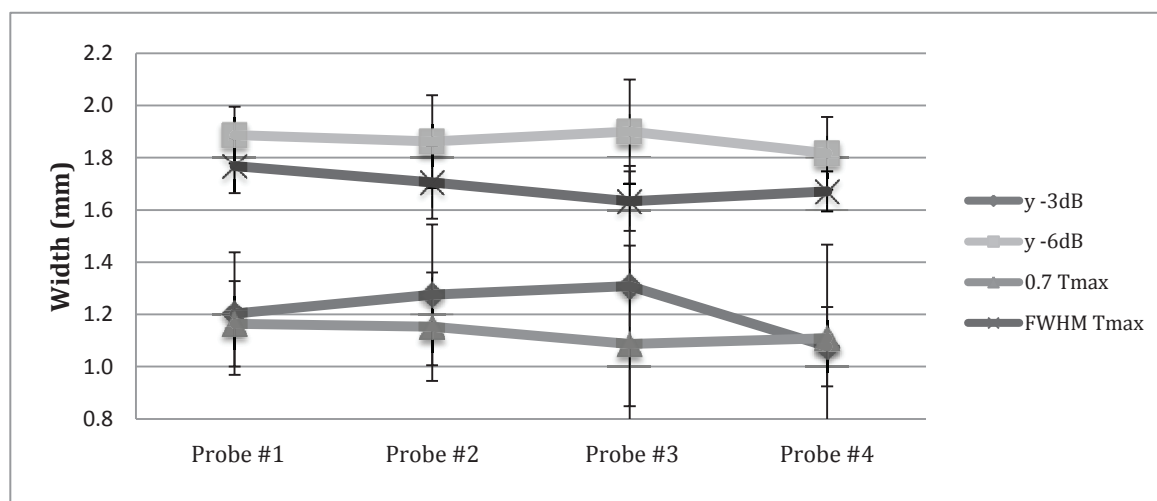


Figure 53- The absolute width difference of temperature and pressure profile ( $\Delta y$ ), taken the pressure field width as reference ( $\Delta y/y_p$ ). The US for IR method was applied at 0.96 W (dark bars) and 1.84 W (gray bars).

### 7.3.3 US parameters adjustment for IR inspection method

The highest reproducibility was achieved by applying 600ms of US exposure in a burst mode (PRP 30 $\mu$ s, 200 cycles) with VC of 1.11 $\pm$ 1.06 % (Fig. 54 and 55). A highest dispersion was in case of continuous application of US for 200ms with occasional VC > 90%. Even with significant variations of  $\Delta T_{max}$  among different burst durations (Fig. 58), no significant variation was observed in terms of temperature profile at FWHM (Fig. 56 and 57).

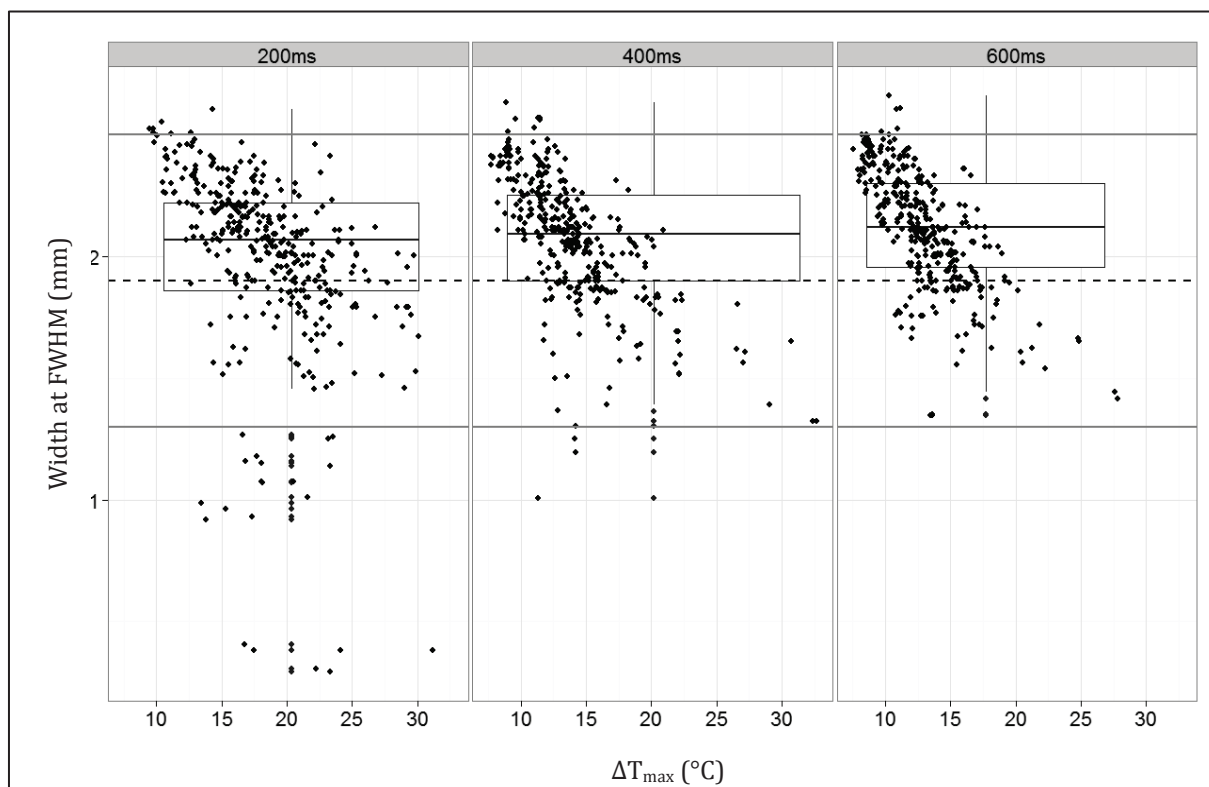


Figure 54- Box plot presentation of temperature profile at FWHM applying US exposure durations of 200ms (continuous), 400ms (280 cycles/30 $\mu\text{s}$ ), and 600ms (200 cycles/30 $\mu\text{s}$ ). The black lines indicate the bounds of conformity (1.4-2.6 mm).

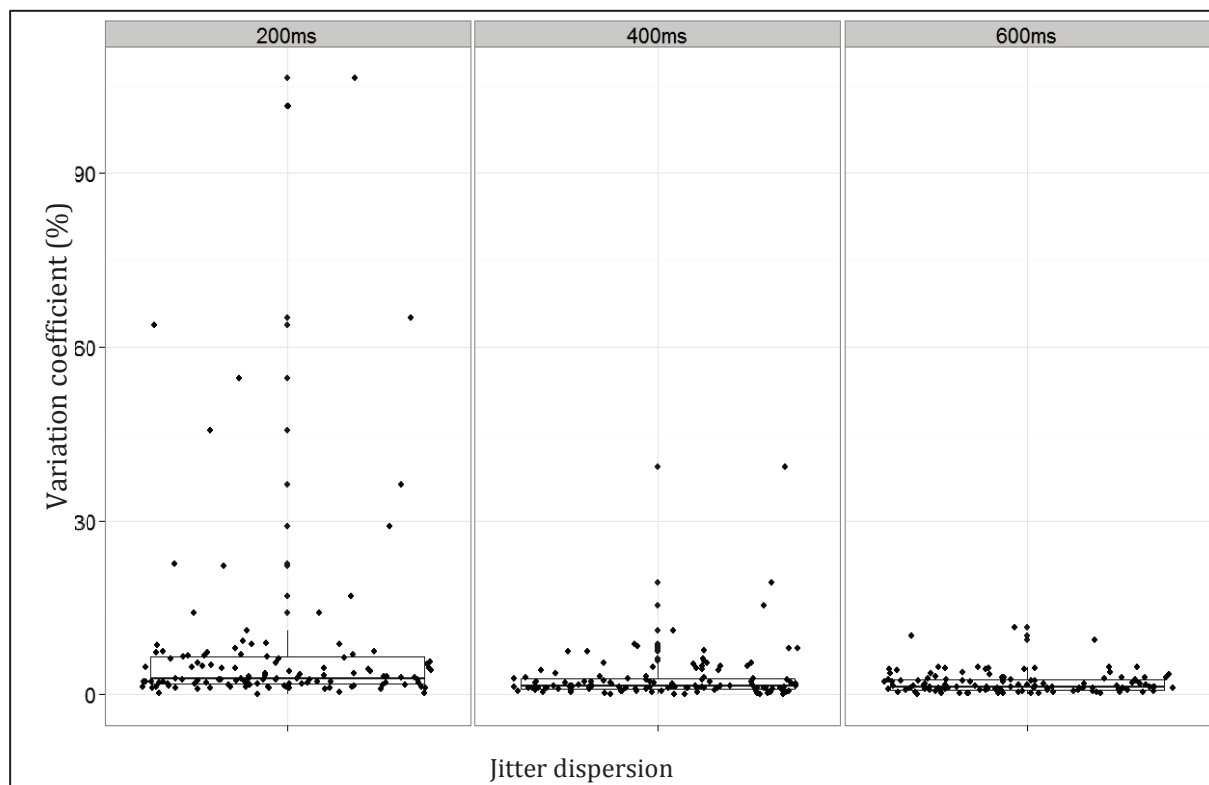


Figure 55- Variation coefficient of three successive reproducibility experiments for each group.

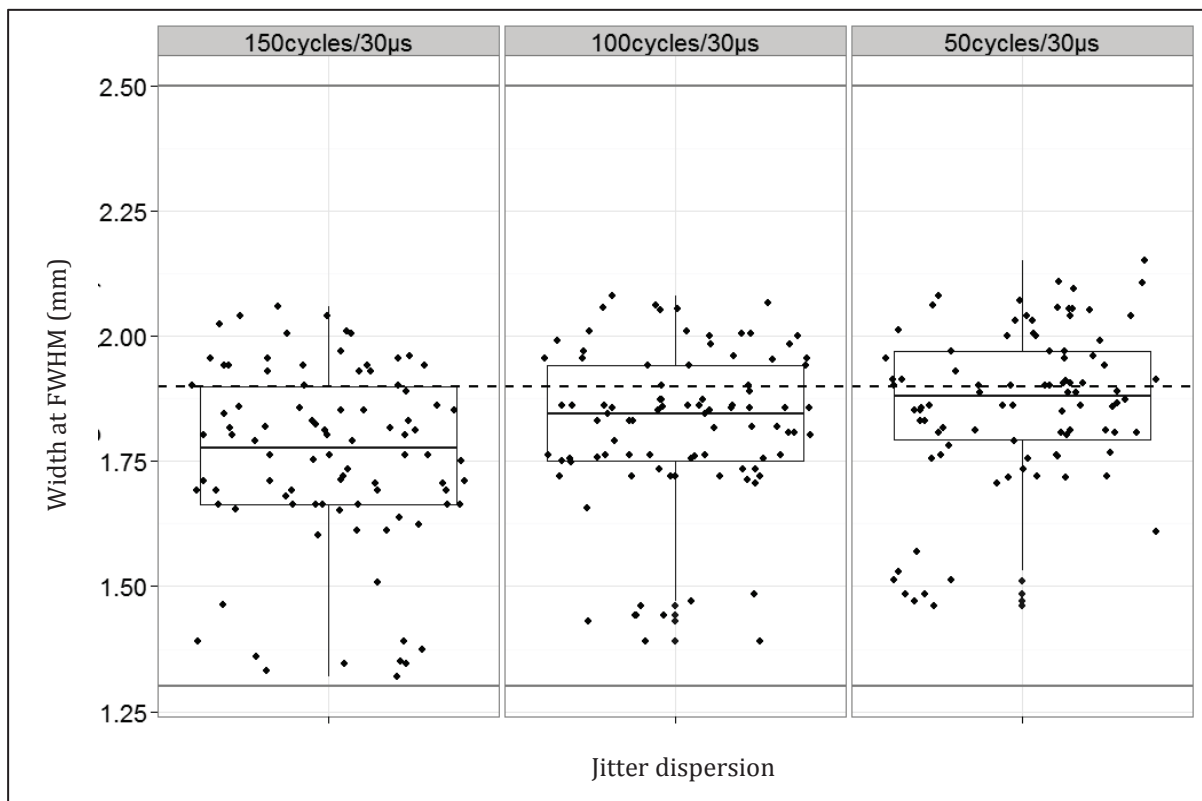


Figure 56- Box plot demonstration of temperature profile at FWHM for PRP 30µs and three burst durations.

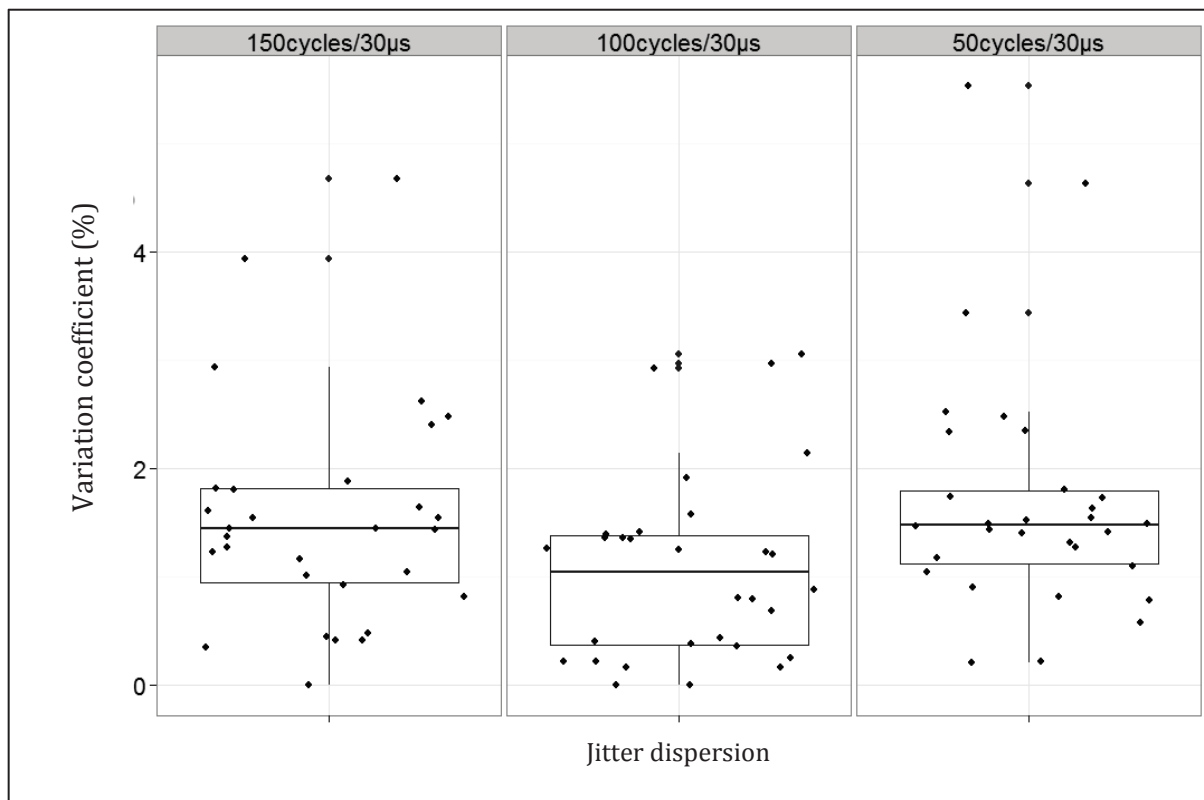


Figure 57- Variation coefficient of three successive reproducibility experiments for each group.



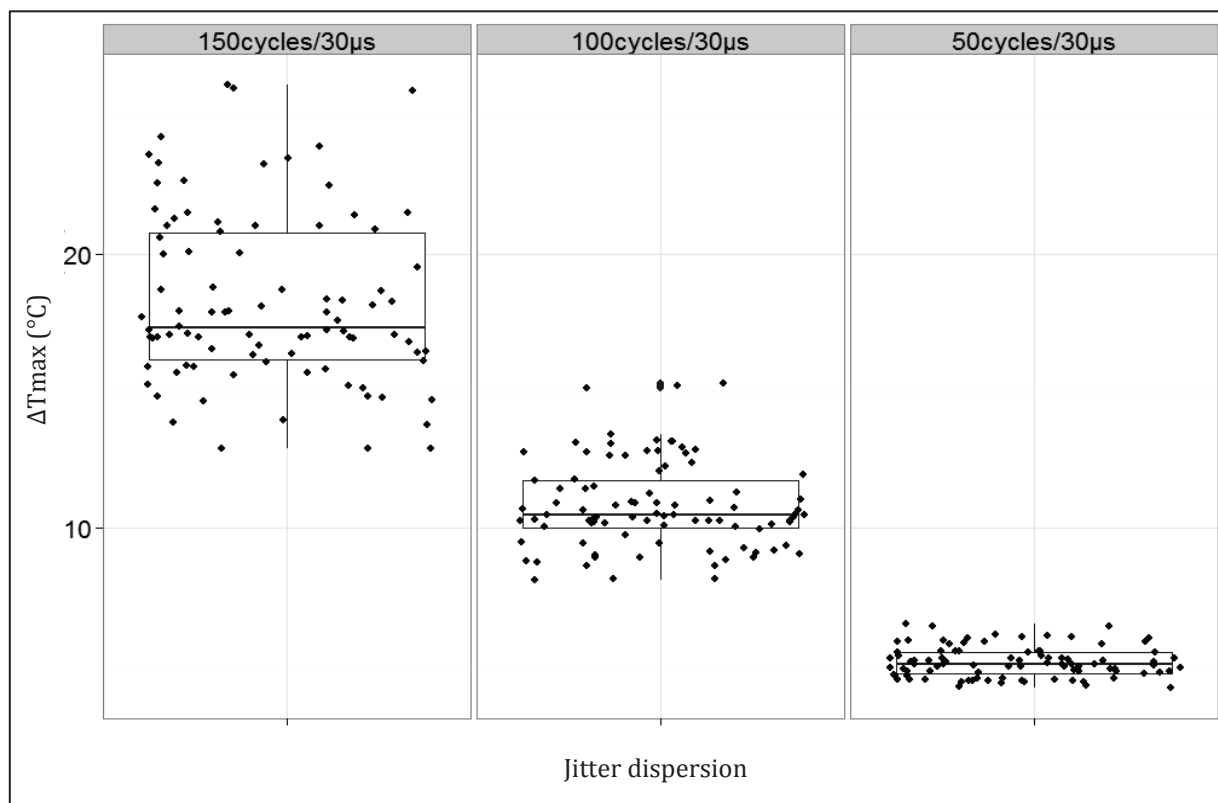


Figure 58- Box plot demonstration of maximum temperature PRP 30 $\mu$ s and three burst durations.

### 7.3.4 IR thermography/ pressure hydrophone measurement (II)

All the 120 elements and eventually probes were in conformity with gel method specification of control section with no rejected element. The width of lesions on average over 120 elements was  $1.97 \pm 0.18$  mm. For three different acoustic planes, the results of hydrophone measurements could be seen in table 3. The plans were: focal plane with normal beam incident, focal plane with angled ( $20.76^\circ$ ) beam incident, and at the absorber plane (10.2 mm) with angled ( $20.76^\circ$ ) beam incident. No significant difference was achieved for pressure profiles among all three acoustic planes ( $p > 0.5$ ). The relative -3 and -6 dB of these pressure profiles could be compared with corresponding width of temperature profile at 0.707 and 0.5 of  $T_{max}$  respectively. The absolute width difference of temperature profile and each of the pressure profiles explained above could be compared in table 4.

Parameter (width)	IR method	P: Ac. focal plane, normal incident	P: Ac. focal plane, angled incident	P: Absorber plane, angled incident
0.707Tmax:-3dB (mm)	1.32±0.17	1.42±0.27	1.43±0.28	1.38±0.23
0.5T:-6dB (mm)	1.79±0.18	1.86±0.13	1.86±0.13	1.81±0.12

**Table 3- Field distribution profile by IR method and hydrophone measurements in three planes (average of 120 elements, Ac: acoustic).**

Method	Abs. difference (-3dB)	S. deviation (-3dB)	Abs. difference (-6dB)	S. deviation (-6dB)
P: Ac. focal plane, normal incident	13.50%	20.24%	6.39%	4.16%
P: Ac. focal plane, angled incident	19.23%	19.69%	7.41%	5.93%
P: Absorber plane, angled incident	18.57%	18.05%	7.19%	5.42%

**Table 4- Absolute difference and standard variation of IR method with hydrophone measurements in three planes (average of 120 elements, Ac: acoustic).**

Here, before providing the rest of the results the summary of ‘*FLIR system & procedure*’

condition is reintroduced:

- Set-up: FLIR camera, container box and probe holder, PC and lab instruments
- Exposure time and Burst duration: 600 ms and 150 cycle each 30  $\mu$ s (7.1-7.9  $\mu$ s)
- PRF and DC: 33.3 KHz and 23.3%
- Acoustic power: 2.28 W
- IR imaging from the surface of the absorber placed at the geometrical focal plane (10.2 mm).

### **7.3.5 IR thermography: an inspection tool (II)**

Three production probes (18 elements of 2.5mm) were passed the IR inspection (*FLIR system & procedure*). The bound of conformity was based on the quality control specifications (1.4-2.5 mm, Fig.60, horizontal lines). The elements with width (FWHM) bellow or above this range would consider as defective in the control section. To examine the detection capability of IR inspection method, one R&D 1.5mm probe and three 4mm probes were examined expected to be inspected as “defective probes”. Figure 59 demonstrates an example of IR thermography for these three different element sizes: 4, 2.5, and 1.5 mm. As it was expected, all 18 elements of 4mm probes were above the specified max limit; five sectors of 1.5mm probe were below the specified min limit; one element of

this probe unexpectedly was within the bound of specification. Following gel and hydrophone measurement confirmed this strange behavior (Fig. 61).

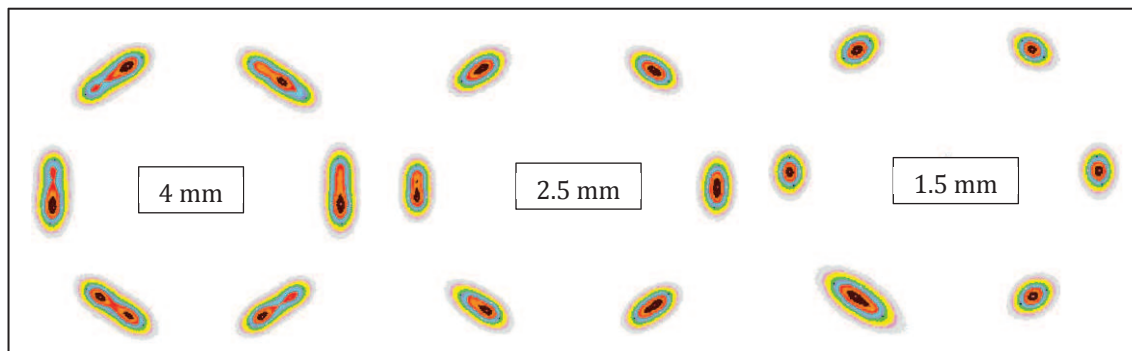


Figure 59- Example of IR images of the frame  $T_{max}$  for probes 1.5, 2.5, and 4mm.

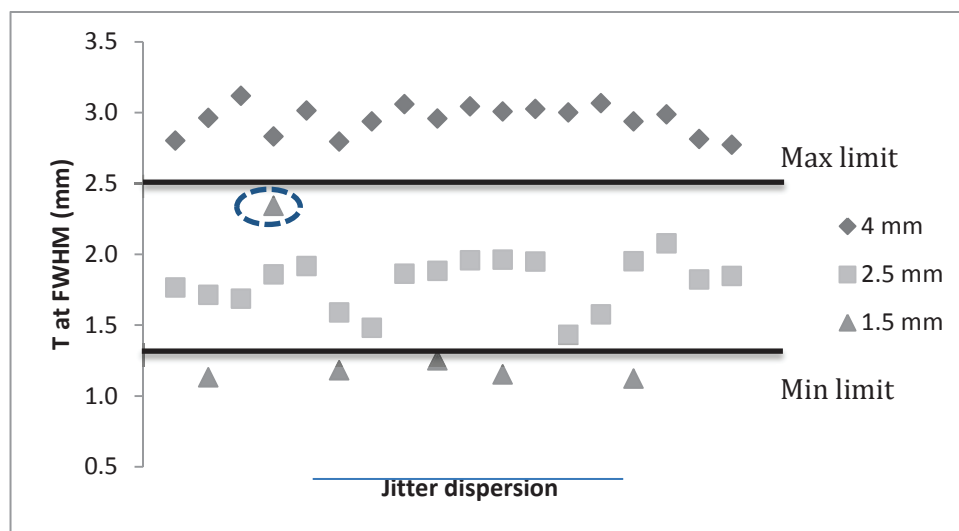


Figure 60- IR inspection of ceramics with different width (1.5, 2.5, and 4mm). Jitter dispersion is a random demonstration of elements in the graph with relation to the temperature profile at FWHM. The horizontal lines are the specification bound for 2.5 elements. One element from 1.5 mm showed an exceptionally large temperature width.

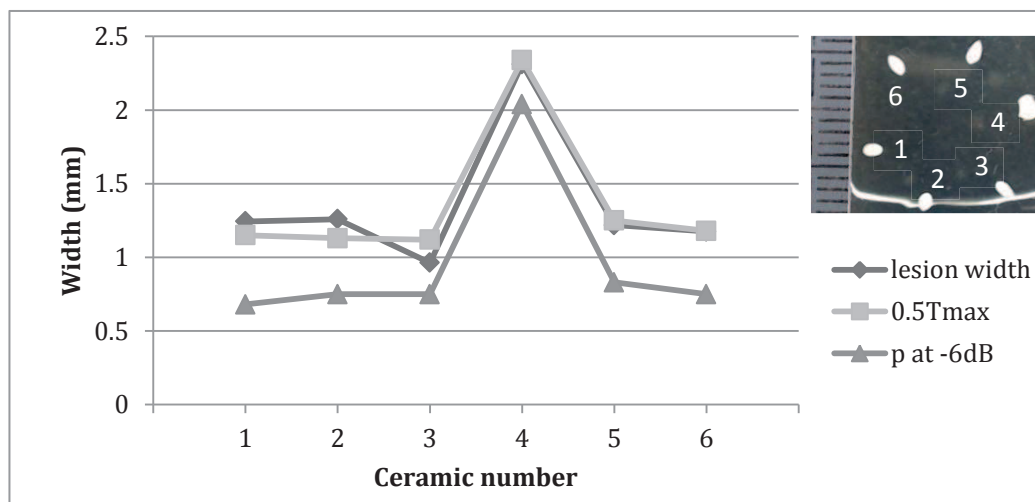


Figure 61- Gel/IR/hydrophone measurements for six 1.5mm elements of one probe. The element number 4 exhibits a distinctively large width in all methods.

### 7.3.6 IR thermography: a statistical reliability survey of current set-up

The data pool consisted of standard deviation and variation coefficient of related experiments on each ceramic. Here, the statistical dispersion data is presented by averaging over the corresponding population. The results of each procedure could be seen below in an arrangement according to subsection.

1. **Repeatability:** 120 elements (20 production probes), 3 measurements for each element, FLIR system & procedure. A very high repeatability with less than 0.5% variation coefficient was achieved for all the parameters after successive IR inspections at the same condition.
2. **Influence of probe repositioning within the set-up:** 120 elements (20), 3 measurements for each element, FLIR system & procedure. A very good reproducibility of IR inspection (VC <1%) was achieved by width measurements at FWHM of  $T_{\max}$  (Table 5).

Parameter	Standard deviation	Variation coefficient
Width at FWHM (mm)	0.015±0.009	0.9±0.5
Area at FWHM (mm <sup>2</sup> )	0.028±0.016	2.1±1.3
$\Delta T_{\max}$ (°C)	0.098±0.093	0.7±0.6

Table 5- Influence of probe repositioning on reproducibility.

3. **Influence of renewing/replacing the US absorber on reproducibility:** 120 elements, 2 different absorber blocks with the same properties, 1 measurement for each element per absorber, FLIR system & procedure. The reproducibility of the system, in terms of area of the temperature field, was influenced the most by replacing the absorber (Table 6, Fig. 62).

Parameter	Standard deviation	Variation coefficient
Width at FWHM (mm)	0.06±0.051	3.5±3.1
Area at FWHM (mm <sup>2</sup> )	0.091±0.076	7.4±6.4
$\Delta T_{\max}$ (°C)	0.074±0.053	3.5±2.6

Table 6- Influence of replacing the US absorber on reproducibility.

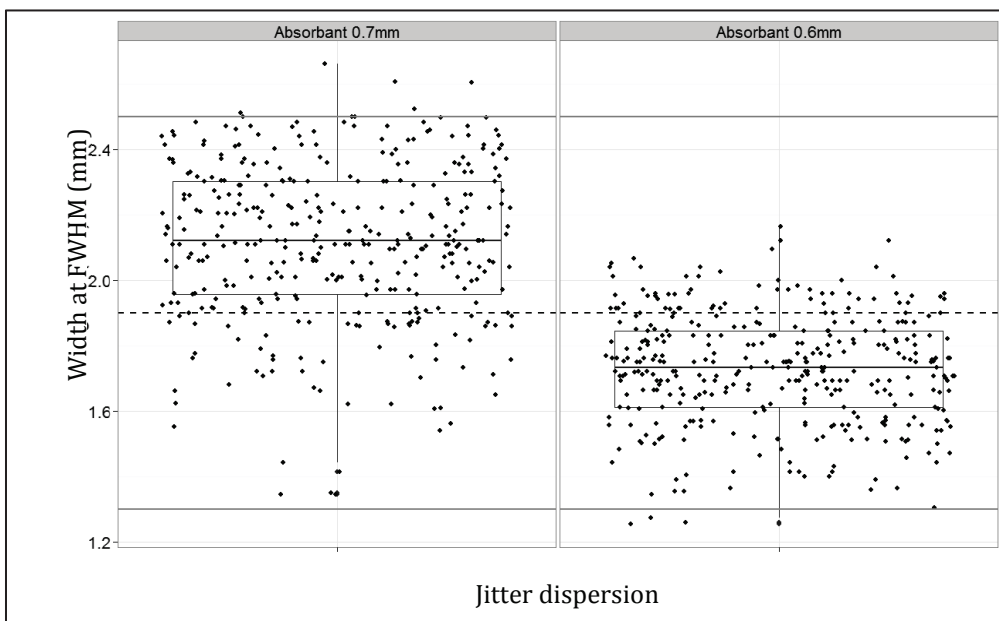


Figure 62- Temperature profile at FWHM of the same probes but US absorbers with different thickness.

4. **Influence of room temperature on reproducibility:** 120 elements, 5 different room temperature values (20-25 °C), 3 measurements for each element per temperature, FLIR system & procedure. The variations in the room temperature in this range did not have a significant influence on reproducibility of the system (Table 7, Fig. 63).

Parameter	Standard deviation	Variation coefficient
Width at FWHM (mm)	0.003±0.018	1.6±1.1
Area at FWHM (mm <sup>2</sup> )	0.035±0.017	2.8±1.4
ΔTmax (°C)	0.026±0.020	1.2±0.8

Table 7- Influence of room temperature on reproducibility.

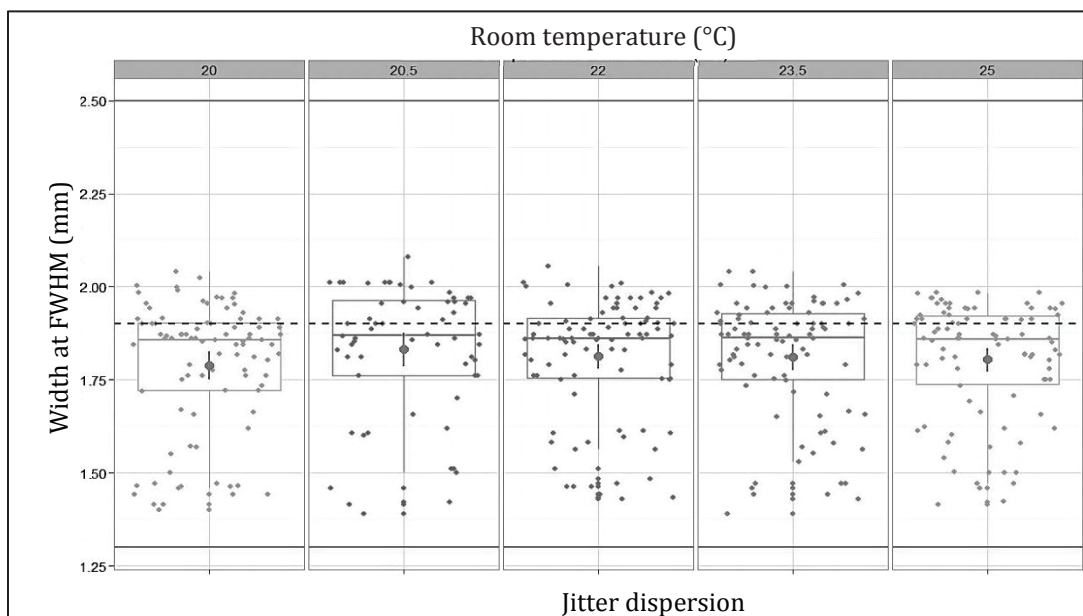


Figure 63- Influence of room temperature variations on temperature profile at FWHM

## **7.4 Discussion**

In this study feasibility application of IR thermography was assessed as a potential tool for quality control. As been said previously, the current method: traditional hydrophone and gel have several disadvantages in large scale applications; disadvantages such as being prohibitively slow and expensive. On the other hand, studies of other research groups have shown the capability of IR thermography for rapid US field characterization. The developed method however was limited to low US frequency regime and standard HIFU devices. In our studies, this method was extended and adjusted to the specifics of the Eyeop1. In this way, a system of IR inspection and an analysis technique were developed and a series of feasibility studies were carried out by an available IR camera (Optris). The general method of characterization was based on the temperature profiles similar to pressure field method. The outcome was promising; therefore, the following studies were performed using a more advanced system with automation capability (FLIR). Consequently, the IR method was modified and evolved though out this process. Currently, the inspection of a probe of six elements takes two minutes; whereas in case of hydrophone scanning it takes more than 45 minutes.

The initial motivation for exploring IR thermography was to assess if this method could potentially substitute the gel method for testing HIFU therapy probes. The IR methods needed to be designed in a way that it would be in a good correlation with the hydrophone method i.e. temperature map needed to be in accordance with pressure field distribution of the focal plane in case of HIFU (Shaw et al. 2012). One of the limitations of our set-up however, was that US absorber could not be place in the focal plane where the beam incident would be perpendicular to the plane. This was due to the ceramics' placement within a probe; these ceramics were positioned to irradiate with an angle of  $20.76^\circ$  for therapeutic reasons. Therefore, the hydrophone measurements initially performed in both planes for further assessments: acoustic focal plane ( $10.1 \pm 0.4$ ) with normal beam incident and in absorber plane at  $z=10.2$  mm with angle of  $20.76^\circ$  in a free field water tank.

As can be seen in figure 49, the 20.76° tilt of plane is around the focal line which is constant in width. The US was focused all along this line in accordance with the active width of the ceramics. In this way, although the pressure distribution in length (x) and depth (z) would differ by tilting the pivotal axis, focal width (y) was not expected to undergo any significant changes. Therefore, for thermal inspection the relative width of this focal line were measured for further assessments. The temperature profile of the focal line in this way would be in accordance with first, pressure profile of the line and also width of the corresponding gel lesion which follows the width of the focal line; in case of a balanced power distribution along the ceramic width. As been explained before, the width of the gel lesion was compared to temperature and pressure profiles at 0.707 and 0.5 of the maximum (corresponding the -3dB and -6dB of the maximum in case of pressure).

In the preliminary study, one probe was used to be characterized with all three methods gel, IR, and hydrophone. The choice of this R&D probe was due to its three defective piezo-elements. This fact provided a good opportunity to assess the IR thermography. Shown by gel method, the lesions of these three were distinctively shorter than the rest (Section 7.3.1). The pressure profiles of both planes (normal and angled beam incident), were in accordance with gel only at -3dB. The temperature profiles were in accordance with gel both at 0.707 and 0.5 of  $T_{max}$ . The spatial pattern of temperature field distribution was in a very good agreement with pressure field. In case of dysfunctional ceramics, the corresponding distribution maps revealed a heterogeneous energy deposition pattern along the focal line which is believed to be due to an unbalanced power distribution on the transducer surface; this could also explain the lesions were not at the full width. The following IR inspection could very well discriminate these three elements from the others which were fully functional.

It was then shown that exposure conditions could be adjusted to provide closer estimations of field distribution with pressure field. For this matter, a set of probes were chosen that previously passed the quality control tests and then were applied in clinical operations with approved results.

With these regards, their pressure field distribution could be considered as a reference for adjustment of IR method parameters. Among the examined parameters, the one with shorter exposure time and applied power was in more conformity with the pressure field (with  $8.15\% \pm 4.63$  error at 100 ms, 0.84W). The calculated error increased as the time of exposure and power increased (Section 7.3.2.2).

To explain this effect, we can refer to the fact that the increase of exposure time also increased the rate of lateral diffusion of energy which in turn led to less accordance of temperature and pressure fields (Shaw and Nunn 2010). By applying higher power level, it was also expected that distortion of wave propagation also increased. This distortion is due to a non-constant propagation speed where higher-pressure portions of the US wave travel faster than lower-pressure portions (Canney et al. 2010). In this way, a portion of energy would be transferred at higher frequencies (harmonics) which leads to a higher absorption rate. This absorption is not uniform and would eventually reduce the accordance of the temperature field of the absorber's surface with the intensity field distribution. In other words, this effect could be considered as an extra heat source which is not directly proportional to the incident intensity; thus could result in intensity distribution modulation and generate artifacts in thermal field characterization, given the very fine spatial distribution structure of these high frequency piezo-ceramics (Khokhlova et al. 2013). As the power increased these artifacts generated more errors;  $27.92\% \pm 18.66$  in case of 200 ms, 1.94 W.

In less degree, this effect could generate artifacts also in linear regime by continuous insonation depending on relative phase of forward and reflected waves. The modulation in intensity distribution is sensitive to micron-sized changes (< one quarter wavelength) in ceramic/absorber distance. This is especially important in reproducibility of our system since the relative distance of element/absorber could be varied due to the repositioning.

The following parametric studies with FLIR system demonstrated the effect of this field perturbation on reproducibility of the system. For comparison reasons, the parameter '200ms,



continuous US' was compared with 400 and 600ms pulsed US with a PRP of  $30\mu\text{s}$  to avoid any overlap of a successive burst at the ceramic surface ( $> 4z/c$ , where  $z$  is focal distance=10.2 and  $c$  is the speed of sound in water  $\sim 1500$  m/s). The cycle-number of 280 and 200 were chosen per  $30\mu\text{s}$ -burst for '400 and 600ms exposure durations' respectively. In this way the dose of energy delivery would be close to the case of '200ms, continuous US'. The results showed a very low reproducibility of continuous application of US contrary to 600ms US in a burst mode. Furthermore, in order to avoid any self-interference within the absorber several burst durations were tested which were less than  $13\mu\text{s}$  or 273 cycles per burst ( $< 2z/c$ ). No significant difference was observed among 50, 100, 150 cycles per burst; however the temperature elevation for shorter bursts was not sufficient for the inspection method. Therefore, for the following studies (*FLIR system & procedure*), US was applied in a tone burst mode at a PRP of  $30\mu\text{s}$  and 150 cycles per burst for duration of 600ms (Khokhlova et al. 2013).

In following studies the issue of angled beam incident in IR set-up was addressed after the modifications to the IR method procedure and up-grading the set-up to FLIR system. In this way, less reflection induced artifacts were expected due to insonation in a tone burst regime; in addition, the acquired thermal fields were with higher spatial resolution.

At the first step, the free field hydrophone measurements were done in three different planes: acoustic focal plane with normal beam incident, acoustic focal plane and angled beam incident, and geometrical focal plane with angled beam incident (the same plane of absorber). There was no significant difference found in pressure profile of the focal line ( $p>0.5$ ). The possibility of relative profile comparison between temperature and pressure fields was validated in this way for absorber plane and acoustic focal plane with normal beam incident. In the following statistical studies, the best agreement was found between the temperature and pressure profiles at FWHM and -6dB respectively (error:  $6.39\pm 4.16\%$ ); they were also in better agreement with gel width compare to

0.707T and -3dB. Therefore for the following studies this parameter (FWHM) of comparison was chosen as the main IR inspection parameter.

A back up for this choice was provided by the reliability tests in terms of repeatability and reproducibility. The successive measurements were producing field characterization with a very high repeatability of  $\Delta T_{\max}$ , FWHM, and 0.707T (<0.5 % variation). In case of reproducibility however, the parameters  $\Delta T_{\max}$  and 0.707T were more influenced by set-up conditions and environmental changes. With these regards, the parameter FWHM for IR inspection was a clear choice at this point. However, each of these parameters such as  $\Delta T_{\max}$ , area, length and etc. could be informative for field characterization depending on the application. Therefore, more studies are highly suggested.

At the next step, IR method was applied for the inspection a pool of elements with different focal line width (1.5, 2.5, and 4mm). An experimental bound of conformity was defined the same as gel method's specification for 2.5 mm elements. Based on this specification, the elements with width of lesion outside the bound of 1.4-2.5 mm would be considered as defective. Although the 1.5 and 4mm probes were not "defective" in the sense, however, their gel lesions were shorter or larger than 2.5mm due to their ceramic width. The IR inspection with current configuration could discriminate the 2.5mm probes from the rest very well.

Another modification for IR set-up was using the lab instruments instead of Eyeop1 module. The integrated generator of eyeop1 module had a stabilization-time of 50-200 ms for the signals to reach a stable magnitude. This rise-time would not affect the delivered energy dose in clinical parameters with 4-6 s; however, for thermal characterization with a few hundred milliseconds, this rise-time could compromise the magnitude of energy delivery. Therefore to increase the reliability of the system, a lab generator was used with negligible stabilization time. As been said, the IR inspection system initially exhibited a good reliability. More studies need to be carried out for a complete assessment for industrial tools.

## 7.5 General discussions and Conclusion

This part of the study is concluded by answering some initial questions that were posed in the beginning of this project.

- *Can IR thermography provide qualitatively close estimations to hydrophone method of quality control considering the acoustic specifics of Eyeop1?*
- ✓ It was shown in this study that our method of characterization and set-up of acquisition could provide close estimations with hydrophone measurements of focal line profile.

The issue of high absorption at 21MHz can be addressed by very short bursts and choice of very thin yet homogeneous and stable absorber. At this stage of the work, the focal line characterization is the aim of IR inspection and control tests. At the current configuration, direct estimation of area or length of the field is not possible due to the angled plane of characterization relative to the focal plane. On the other hand, the absorber could not be placed at the focus for normal incident and contain all six elements in an immobilized system. This is due to the geometrical specifics of the probe. In terms of width of the field profile however, it was shown that an inclination of 20° is not a determining factor in pressure and temperature distribution. Of course any change in application objective may result in set-up reconfiguration.

- *Can the IR method be used in an industrial capacity for Eyeop1 probe production? Can IR inspection replace the gel method?*
- ✓ It is distinctively rapid and reliable in terms of repeatability and reproducibility. It also conforms to the gel method.

In this study, it has been shown that the IR inspection could detect defective elements almost flawlessly. On the other hand, the disadvantages of gel method were mentioned before. Therefore it could be replaced by IR inspection system. Frequent use of hydrophone as a control tool is also expensive in terms of time and resources in a production line. For instance, a current procedure for hydrophone field measurement (2D) takes 45 minutes for one therapy probe (six ceramics). With the current system the IR inspection takes less than two minutes. It was shown that IR method is in a

good agreement with the hydrophone method in terms of spatial pattern and focal line profile; therefore the control aspect of hydrophone application could potentially be replaced by IR system.

As been demonstrated, by application of IR thermography it is possible to monitor the evolution of temperature field distribution during an US exposure (Fig. 64). One application of this in our case for example, is as a reference tool for classification of the therapy probes based on their field distribution patterns. Furthermore, the effect of different exposure parameters on field distribution could be monitored and adjusted due to the requirements of (pre-) clinical studies.

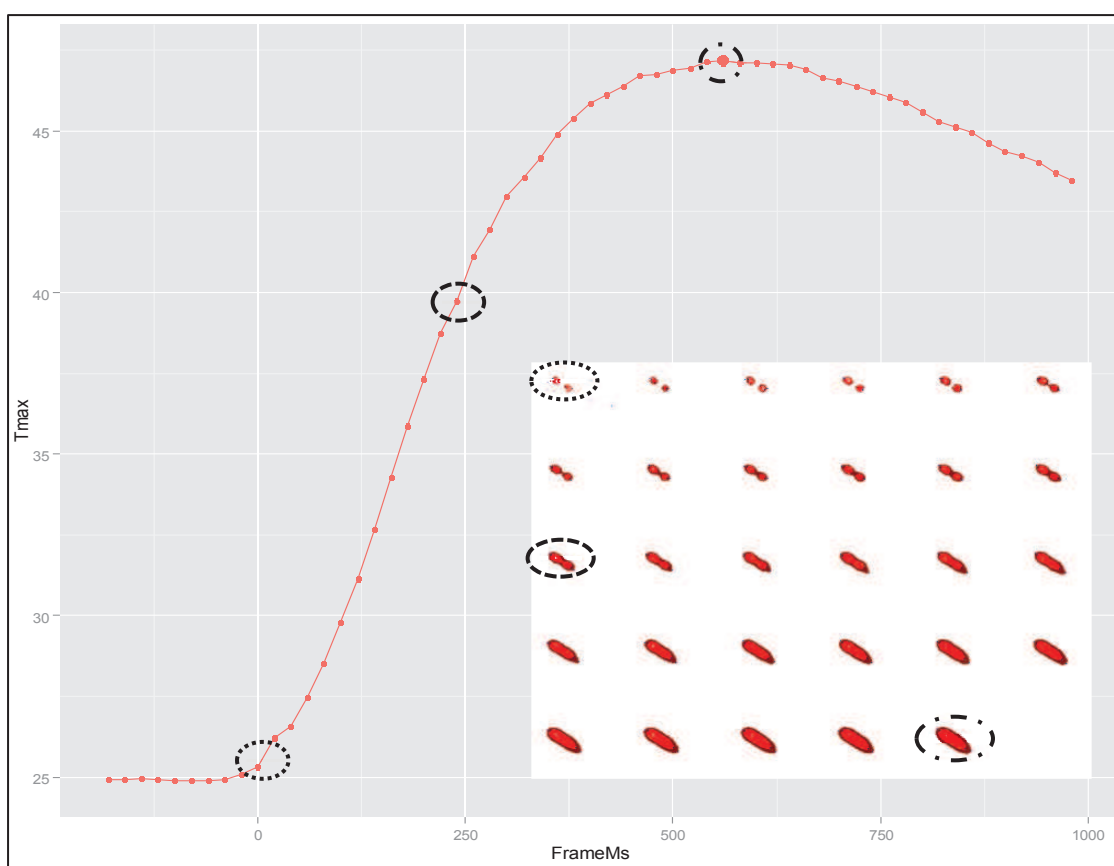


**Figure 64- Evolution of temperature distribution and Tmax during a sequence of thermal images.**

In these types of applications however, there is no need for characterization method to be necessarily in high accordance with hydrophone measurements; given the fact that hydrophone measurements themselves are estimations of pressure fields and are not fully applicable in terms of HIFU lesions at clinical US parameters assessment. In our group, this potential application of IR

system has been explored and the results are promising. Of course, IR thermography is a new method in HIFU field and many potential aspects of it are yet to be explored.

In conclusion, this study was aimed to expand the application of a R&D technique for ultrasonic field characterization to an industrial scale.

## ***List of figures***

Figure 1- Schematic diagram of human eye. ....	9
Figure 2- Histologic section of human cornea .....	10
Figure 3- Histologic section of human corneascleral junction and iridial angle .....	11
Figure 4- Histologic section of human sclera, choroid, and retina (www.udel.edu). ....	12
Figure 5- Topical administration and ocular barriers against drug delivery. ....	15
Figure 6- Intravitreal injection. ....	16
Figure 7- Subtenon injection. ....	17
Figure 8- Subconjunctival injection. ....	17
Figure 9- Retrobulbar injection in two steps. ....	18
Figure 10- Schematic presentation of intravitreal injection .....	20
Figure 11- Fluid microstreaming around oscillating bubble .....	29
Figure 12- Formation of microjet during inertial cavitation .....	29
Figure 13- Asymmetric bubble collapse near the membrane .....	31
Figure 14- Custom diffusion cell .....	44
Figure 15- Placement of sclera sample while maintaining the natural outward curvature. ....	45
Figure 16- US field characterization set-up. ....	46
Figure 17- Pressure field maps .....	47
Figure 18- Peak pressure value corresponding the input voltage. ....	47
Figure 19- Example of calibration curve. ....	48
Figure 20- Permeability increase .....	52
Figure 21- The permeability increase due to US exposure .....	54
Figure 22- Rabbit eye is globally smaller and rounder .....	58
Figure 23- Modified diffusion cell with incorporated hydrophone .....	59
Figure 24- Example of instantaneous frequency-domain acoustic spectrum .....	60

Figure 25- Evolution of CI in a PRF range of 100-1000 Hz. ....	64
Figure 26- CI vs. acoustic power for two pulse regimes at PRFs 100 and 1000 Hz.....	65
Figure 27- Cavitation index by PCD vs. HTA% by chemical validation .....	65
Figure 28- Temporal evolution of CI .....	66
Figure 29- Average of scleral permeability measurements.....	66
Figure 30- CI vs. Pu/Pc .....	67
Figure 31- Post-mortem samples.....	69
Figure 32- Sham treatment samples.....	70
Figure 33- US-exposed samples.....	71
Figure 34- The zones of morphological change demonstrations .....	74
Figure 35- Electron micrograph showing the presence of the tracer in the dermis .....	75
Figure 36- Eyeop1 module.....	83
Figure 37- Demonstration of energy deposition within the ciliary body.....	84
Figure 38- Gel inspection tool.....	87
Figure 39- Experimental set-up of Khokhlova et al. (2002) for IR thermography. ....	90
Figure 40- Experimental set-up of Khokhlova et al. (2013) for IR thermography. ....	92
Figure 41- Isometric view of piezo-elements.....	95
Figure 42- Force balance measurement set-up.....	96
Figure 43- Optris experimental set-up.....	97
Figure 44- Spatial/thermal presentation of a temperature distribution map.....	99
Figure 45- FLIR experimental set-up.....	100
Figure 46- Evolution of temperature field distribution .....	101
Figure 47- Relative comparison of pressure field hydrophone measurement.....	102
Figure 48- Pressure field map of six piezo-elements/one probe.....	102
Figure 49- Demonstration of 20.76° inclination of the absorber plane to the normal incident. .	104
Figure 50- Gel lesions, 6 elements (4mm). ....	108

Figure 51- Width of temperature profile .....	109
Figure 52- Comparison of width of temperature and pressure profiles .....	110
Figure 53- The absolute width difference of temperature and pressure profile .....	110
Figure 54- Box plot presentation of temperature profile.....	111
Figure 55- Variation coefficient of three successive reproducibility experiments.....	111
Figure 56- Box plot demonstration of temperature profile at FWHM for PRP 30 $\mu$ s.....	112
Figure 57- Variation coefficient of three successive reproducibility experiments.....	112
Figure 58- Box plot demonstration of maximum temperature PRP 30 $\mu$ s .....	113
Figure 59- Example of IR images of the frame $T_{max}$ for probes 1.5, 2.5, and 4mm.....	115
Figure 60- IR inspection of ceramics with different width (1.5, 2.5, and 4mm).....	115
Figure 61- Gel/IR/hydrophone measurements for six 1.5mm elements of one probe.....	115
Figure 62- Temperature profile at FWHM, US absorbers with different thickness.....	117
Figure 63- Influence of room temperature variations on temperature profile at FWHM .....	117
Figure 64- Evolution of temperature distribution .....	124



***List of tables***

Table 1- US parameters applied in feasibility study. ....	48
Table 2- Relative profile measurements of temperature and pressure field. ....	108
Table 3- Field distribution profile by IR method and hydrophone measurements ....	114
Table 4- Absolute difference of IR method and hydrophone measurements.....	114
Table 5- Influence of probe repositioning on reproducibility.....	116
Table 6- Influence of replacing the US absorber on reproducibility.....	116
Table 7- Influence of room temperature on reproducibility. ....	117

## ***Bibliography***

Achouri D, Alhanout K, Piccerelle P, Andrieu V. Recent advances in ocular drug delivery. *Drug Dev Ind Pharm*. 2013 Nov;39(11):1599-617.

Ahmed I, Gokhale RD, Shah MV, Patton TF. Physicochemical determinants of drug diffusion across the conjunctiva, sclera, and cornea. *J Pharm Sci* 1987a;76:583-586.

Ahn JS, Jeong MB, Park YW, Lee YS, Lee ER, Kim SH, Lee I, Seo K. A sub-Tenon's capsule injection of lidocaine induces extraocular muscle akinesia and mydriasis in dogs. *Vet J*. 2013 Apr;196(1):103-8.

Allen TM. Long-circulating (sterically stabilized) liposomes for targeted drug delivery. *Trends in pharmaceutical sciences*. 1994 Jul; 15(7):215-220.

Arora N, Martins D, Ruggerio D, Tousimis E, Swistel AJ, Osborne MP, Simmons RM. Effectiveness of a noninvasive digital infrared thermal imaging system in the detection of breast cancer. *The American Journal of Surgery*. 2008 Oct; 196 (4): 523-526

Aptel F, Charrel T, Lafon C, Romano F, Chapelon JY, Blumen-Ohana E, Nordmann JP, Denis P. Miniaturized high-intensity focused ultrasound device in patients with glaucoma: a clinical pilot study *Invest Ophthalmol Vis Sci*. 2011 Nov;52(12):8747-53.

Aptel F, Lafon C. Therapeutic applications of ultrasound in ophthalmology. *Int J Hyperthermia*. 2012;28(4):405-18.

Bailey MR, Khokhlova VA, Sapozhnikov OA, Kargl SG, Crum LA. Physical mechanisms of the therapeutic effect of ultrasound (a review). *Acoustical Physics*. 2003 Jul; 49(4): 369-388.

Baker KG, Robertson VJ, Duck FA. A review of therapeutic ultrasound: biophysical effects. *Physical Therapy*. *Phys Ther*. 2001 Jul;81(7):1351-8.

Bazan-Peregrino M, Arvanitis CD, Rifai B, Seymour LW, Coussios CC. Ultrasound-induced cavitation enhances the delivery and therapeutic efficacy of an oncolytic virus in an in vitro model. *J Control Release*. 2012 Jan 30;157(2):235-42.

Bazan-Peregrino M, Rifai B, Carlisle RC, Choi J, Arvanitis CD, Seymour LW, Coussios CC. Cavitation-enhanced delivery of a replicating oncolytic adenovirus to tumors using focused ultrasound. *J Control Release*. 2013 Apr 4;169(1-2):40-47.

Bennett J, Maguire AM. Gene therapy for ocular disease. *Mol Ther*. 2000;1:501-505.

Blana A, Walter B, Rogenhofer S, Wieland WF. High-intensity focused ultrasound for the treatment of localized prostate cancer: 5-year experience. *Urology*. 2004 Feb;63(2):297-300.

Blomley MJ, Cooke JC, Unger EC, Monaghan MJ, Cosgrove DO. Microbubble contrast agents: a new era in ultrasound. *BMJ*. 2001 May 19;322(7296):1222-5.

Bobkova S, Gavrilov L, Khokhlova V, Shaw A, Hand J. Focusing of high-intensity ultrasound through the rib cage using a therapeutic random phased array. *Ultrasound Med Biol*. 2010 Jun;36(6):888-906.

Bommannan D, Okuyama H, Stauffer P, Guy RH. Sonophoresis. I. The use of high-frequency ultrasound to enhance transdermal drug delivery. *Pharm Res*. 1992 Apr;9(4):559-64.

Bommannan D, Menon GK, Okuyama H, Elias PM, Guy RH. Sonophoresis. II. Examination of the mechanism(s) of ultrasound-enhanced transdermal drug delivery. *Pharm Res*. 1992b Aug; 9(8):1043-7.

Boland MV, Ervin AM, Friedman D, Jampel H, Hawkins B, Volenweider D, Chelladurai Y, Ward D, Suarez-Cuervo C, Robinson KA. Treatment for Glaucoma: Comparative Effectiveness [Internet]. Source Rockville (MD): Agency for Healthcare Research and Quality (US); 2012 Apr. Report No.: 12-EHC038-EF.

Byl NN. The use of ultrasound as an enhancer for transcutaneous drug delivery: phonophoresis. *Phys Ther.* 1995 Jun;75(6):539-53.

Burgess SE, Silverman RH, Coleman DJ, Yablonski ME, Lizzi FL, Driller J, et al. Treatment of glaucoma with high intensity focused ultrasound. *Ophthalmology* 1986;93:831-838.

Canney MS, Khokhlova VA, Bessonova OV, Bailey MR, Crum LA. Shock-induced heating and millisecond boiling in gels and tissue due to high intensity focused ultrasound. *Ultrasound Med Biol.* 2010 Feb;36(2):250-67.

Cevc G, Schätzleina A, Blumeb Transdermal drug carriers: Basic properties, optimization and transfer efficiency in the case of epicutaneously applied peptides. *J Controlled Release.* 1995 Sep; 36(1-2):3\_16.

Chakravarti S, Paul J, Roberts L, Chervoneva I, Oldberg A, Birk DE. Ocular and scleral alterations in gene-targeted lumican-fibromodulin double-null mice. *Invest Ophthalmol Vis Sci.* 2003 Jun;44(6):2422-32.

Chang TC, Hsiao YL, Liao SL. Application of digital infrared thermal imaging in determining inflammatory state and follow-up effect of methylprednisolone pulse therapy in patients with Graves' ophthalmopathy. *Graefes Arch Clin Exp Ophthalmol.* 2008 Jan;246(1):45-9.

Chari RV. Targeted cancer therapy: Conferring specificity to cytotoxic drugs. *Accounts of Chemical Research* 2008;41(1):98-107.

Charrel T, Aptel F, Birer A, Chavrier F, Romano F, Chapelon JY, Denis P, Lafon C. Development of a miniaturized HIFU device for glaucoma treatment with conformal coagulation of the ciliary bodies. *Ultrasound Med Biol.* 2011 May;37(5):742-54.

Cherkasov IS, Marmur RK, Radkovskaia AI. Phonophoresis of hypotensive agents in the treatment of simple glaucoma. *Oftalmol Zh* 1974;29(2):114-118.

Cheung AC, Yu Y, Tay D, Wong HS, Ellis-Behnke R, Chau Y. Ultrasound-enhanced intrascleral delivery of protein. *Int J Pharm.* 2010 Nov 30;401(1-2):16-24.

Coleman DJ, Lizzi FL, Driller J, Rosado AL, Chang S, Iwamoto T, et al. Therapeutic ultrasound in the treatment of glaucoma. I. Experimental model. *Ophthalmology* 1985; 92:339–346.

Coleman DJ, Lizzi FL, Driller J, Rosado AL, Burgess SE, Torpey JH, et al. Therapeutic ultrasound in the treatment of glaucoma. II. Clinical applications. *Ophthalmology* 1985; 92:347–353.

Coleman AJ, Saunders JE. A review of the physical properties and biological effects of the high amplitude acoustic field used in extracorporeal lithotripsy. *Ultrasonics.* 1993;31(2):75-89.

Cook BD, Werchan RE. Mapping ultrasonic fields with cholesteric liquid crystals. 1971 Apr; 9(2): 88-94.

Coussios CC, Collin JRT, Muckle AJ. Non-invasive monitoring and control of inertial cavitation dynamics during HIFU exposure in vitro. 6th Int. Symp. Ther. Ultrasound, Oxford: Am. Inst. Phys. 2006; 316–21.

Coussios CC, Roy R. Applications of acoustics and cavitation to noninvasive therapy and drug delivery. 2008. *Annual review of fluid mechanics.* 40: 395-420

Davidson F. Output measurements for medical ultrasound. Springer Veelag, Berlin, Germany. P: 75-90. 1991.

Davies NM. Biopharmaceutical considerations in topical ocular drug delivery. *Clin Exp Pharmacol Physiol.* 2000 Jul;27(7):558-62.

Davis JL, Gilger BC, Robinson MR. Novel approaches to ocular drug delivery. *Curr Opin Mol Ther.* 2004 Apr;6(2):195-205.

Del Amo EM, Urtti A. Current and future ophthalmic drug delivery systems. A shift to the posterior segment. *Drug Discov Today*. 2008 Feb;13(3-4):135-43.

Delius M, Ueberle F, Gambihler S. Destruction of gallstones and model stones by extracorporeal shock waves. *Ultrasound Med Biol*. 1994;20(3):251-8.

Doughty MJ. Observations on the ultrastructure of equatorial scleral collagen fibrils in sheep eyes. *Vet Ophthalmol*. 2012 Mar;15(2):71-80.

Duck FA. Radiation Pressure and Acoustic Streaming. *Ultrasound in medicine; Chapter 3*; P:39-56. 1998.

Duvvuri, S., Majumdar, S., Mitra, A.K., Drug delivery to the retina: challenges and opportunities. *Expert Opinion on Biological Therapy* 2003; 3 (1), 45–56.

Elder SD. Cavitation microstreaming. *J. Acoust. Soc. Am*. 1959; 31, 54.

Escoffre JM, Zeghimi A, Novell A, Bouakaz A. In-vivo gene delivery by sonoporation: recent progress and prospects. *Curr Gene Ther*. 2013 Feb;13(1):2-14.

Fellinger K, Schmid J. Klinik und merapie des Chmnischen Gelenkhuematismum. Maudrich (Austrian); 1954:549-552

Feril LB Jr, Tachibana K. Use of ultrasound in drug delivery systems: emphasis on experimental methodology and mechanisms. *Int J Hyperthermia*. 2012;28(4):282-9

Filippenko VI, Tret'iak VV. The treatment of eye diseases using the Gamma-G ultrasonic apparatus. *Voen Med Zh*. 1989 Aug;(8):30-1.

Fry WJ. Mechanism of acoustic absorption in tissue. *J. Acoust. Soc. Am*. 1952 Jan; (24):412-15.

Galassi F, Giambene B, Corvi A, Falaschi G. Evaluation of ocular surface temperature and retrobulbar haemodynamics by infrared thermography and colour Doppler imaging in patients with glaucoma. *Br J Ophthalmol*. 2007 Jul;91(7):878-81.

Gaudana R, Ananthula HK, Parenky A, Mitra AK. Ocular drug delivery. *AAPS J*. 2010 Sep;12(3):348-60.

Giridhar D, Robinson RA, Liu Y, Sliwa J, Zderic V, Myers MR. Quantitative estimation of ultrasound beam intensities using infrared thermography-Experimental validation. *J Acoust Soc Am*. 2012 Jun;131(6):4283-91.

Guzmán HR, Nguyen DX, Khan S, Prausnitz MR. Ultrasound-mediated disruption of cell membranes. I. Quantification of molecular uptake and cell viability. *J Acoust Soc Am*. 2001 Jul;110(1):588-96.

Halhal M, Renard G, Courtois Y, BenEzra D, Behar-Cohen F. Iontophoresis: from the lab to the bed side. *Exp Eye Res*. 2004 Mar;78(3):751-7.

Hamilton MF. Fundamentals and applications of nonlinear acoustics. V III: background materials. *Physical acoustics summer school*, 1986.

Hand JW, Shaw A, Sadhoo N, Rajagopal S, Dickinson RJ, Gavrilov LR. A random phased array device for delivery of high intensity focused ultrasound. *Phys Med Biol*. 2009 Oct 7;54(19):5675-93.

Hughes PM, Olejnik O, Chang-Lin JE, Wilson CG. Topical and systemic drug delivery to the posterior segments. *Adv Drug Deliv Rev*. 2005 Dec 13;57(14):2010-32.

Hynynen K, Jolesz FA. Demonstration of potential noninvasive ultrasound brain therapy through an intact skull. *Ultrasound Med Biol*. 1998 Feb;24(2):275-83.

Hynynen K, McDannold N, Vykhodtseva N, Jolesz FA. Noninvasive MR imaging-guided focal opening of the blood-brain barrier in rabbits. *Radiology*. 2001 Sep;220(3):640-6.

Hynynen K, McDannold N, Vykhodtseva N, Raymond S, Weissleder R, Jolesz FA, Sheikov N. Focal disruption of the blood-brain barrier due to 260-kHz ultrasound bursts: a method for molecular imaging and targeted drug delivery. *J Neurosurg*. 2006 Sep;105(3):445-54.

Hynynen K. Ultrasound for drug and gene delivery to the brain. *Adv Drug Deliv Rev*. 2008 Jun 30;60(10):1209-17.

Iakimenko SA, Chalanova RI, Artemov AV. The use of lekozim phonophoresis for the treatment of eye burns. *Oftalmol Zh* 1989:492-7.

Jones BF, Plassmann P. Digital infrared thermal imaging of human skin. *Engineering in Medicine and Biology Magazine, IEEE* 2002 Dec; 21(6): 41-48.

Kam AW, Wang H, Farahani K, Thomasson D, O'Neill B, Angstadt M, Jesson J, Li KCP. Safety of pulsed high intensity focused ultrasound for enhanced drug and gene delivery. 6th Int. Symp. Ther. Ultrasound, 2006. 455-461.

Kato A, Kimura H, Okabe K, Okabe J, Kunou N, Ogura Y. Feasibility of drug delivery to the posterior pole of the rabbit eye with an episcleral implant. *Invest Ophthalmol Vis Sci*. 2004 Jan;45(1):238-44.

Kenis AM, Grinfeld J, Zadicario E, Vitek S. Impact of propagating and standing waves on cavitation appearance. *Ultrasound Med Biol*. 2012 Jan;38(1):99-108. doi: 10.1016/j.ultrasmedbio.2011.08.002. Epub 2011 Nov 21.

Keshavarzi A, Vaezy S, Noble ML, Chi EY, Walker C, Martin RW, Fujimoto VY. Treatment of uterine leiomyosarcoma in a xenograft nude mouse model using high-intensity focused



ultrasound: a potential treatment modality for recurrent pelvic disease. *Gynecol Oncol*. 2002 Sep;86(3):344-50.

Khan P, Khan L, Mondal P. Cluster endophthalmitis following multiple intravitreal bevacizumab injections from a single use vial. *Indian J Ophthalmol*. 2013.

Khokhlova VA, Miller N, Ollos R, Martin RW, Bailey MR, Mohammadian Y, Naghavi M. Visualization of temperature rise induced by high intensity ultrasound in tissue. 17th International Congress on Acoustics, Rome University "La Sapienza". 2002; (7): 186-187

Khokhlova VA, Shmeleva SM, Gavrilov LR, Martin E, Sathoo N, Shaw A. Infrared mapping of ultrasound fields generated by medical transducers: feasibility of determining absolute intensity levels. *J Acoust Soc Am*. 2013 Aug;134(2):1586-97.

Kirsch KM, Zelickson BD, Zachary CB, Tope WD. Ultrastructure of collagen thermally denatured by microsecond domain pulsed carbon dioxide laser. *Arch Dermatol*. 1998 Oct;134(10):1255-9.

Kitchen SS, Partridge CJ. A review of therapeutic ultrasound, part 1: background and physiological effects. *Physiotherapy*. 1990;76:593-595.

Kollmann C, Vacariu G, Schuhfried O, Fialka-Moser V, Bergmann H. Variations in the output power and surface heating effects of transducers in therapeutic ultrasound. *Arch Phys Med Rehabil*. 2005 Jul;86(7):1318-24.

Koseki T, Wood RL, Kelly DE. Structural analysis of potential barriers to bulk-flow exchanges between uvea and sclera in eyes of rabbits. *Cell Tissue Res*. 1990 Feb;259(2):255-63.

Kuo HK, Lai IC, Fang PC, Teng MC. Ocular complications after a sub-tenon injection of triamcinolone acetonide for uveitis. *Chang Gung Med J*. 2005 Feb;28(2):85-9.

- Kuruvilla R, Sahu PD, Meltzer MA. Systemic uptake of chlorpromazine after delivery via retrobulbar injection. *Arch Ophthalmol*. 2012 Oct 1;130(10):1348-9.
- Lafon C, Zderic V, Noble ML, Yuen JC, Kaczkowski PJ, Sapozhnikov OA, Chavrier F, Crum LA, Vaezy S. Gel phantom for use in high-intensity focused ultrasound dosimetry. *Ultrasound Med Biol*. 2005 Oct;31(10):1383-9.
- Lau TY, Ambekar R, Toussaint KC. Quantification of collagen fiber organization using three-dimensional Fourier transform-second-harmonic generation imaging. *Opt Express*. 2012 Sep 10;20(19):21821-32.
- Lee J, Kentish S, Matula TJ, Ashokkumar M. Effect of surfactants on inertial cavitation activity in a pulsed acoustic field. *J Phys Chem B*. 2005 Sep 8;109(35):16860-5.
- Lee SB, Geroski DH, Prausnitz MR, Edelhauser HF. Drug delivery through the sclera: effects of thickness, hydration, and sustained release systems. *Exp Eye Res*. 2004 Mar;78(3):599-607.
- Lee SY, Chee SP, Balakrishnan V, Farzavandi S, Tan DT. Surodex in paediatric cataract surgery. *Br J Ophthalmol*. 2003 Nov;87(11):1424-6.
- Leighton TG. *The acoustic bubble*. San Diego: Academic Press, 1994.
- Lennox FG. Shrinkage of collagen. *Biochem J*. 1947;41(4):xivii.
- Leslie T, Ritchie R, Illing R, Ter Haar G, Phillips R, Middleton M, Bch B, Wu F, Cranston D. High-intensity focused ultrasound treatment of liver tumours: post-treatment MRI correlates well with intra-operative estimates of treatment volume. *Br J Radiol*. 2012 Oct;85(1018):1363-70.
- Levy g, Jusko wj. effect of viscosity on drug absorption. *J Pharm Sci*. 1965 Feb;54:219-24.

Liu J, Lewis TN, Prausnitz MR. Non-invasive assessment and control of ultrasound-mediated membrane permeabilization. *Pharm Res.* 1998 Jun;15(6):918-24.

Lizzi FL, Coleman DJ, Driller J, Franzen LA, Jakobiec FA. Experimental, ultrasonically induced lesions in the retina, choroid, and sclera. *Invest Ophthalmol Vis Sci.* 1978 Apr;17(4):350-60.

Lizzi FL, Coleman DJ, Driller J, Franzen LA, Leopold M. Effects of pulsed ultrasound on ocular tissue. *Ultrasound Med Biol.* 1981;7(3):245-52.

Marmur RK, Moiseeva NN, Korkhov SS. Current state and perspectives of further development of phonophoresis of drugs in ophthalmology. *Oftalmol Zh.* 1979;34(2):68-73.

Mannaris C, Averkiou MA. Investigation of microbubble response to long pulses used in ultrasound-enhanced drug delivery. *Ultrasound Med Biol.* 2012 Apr;38(4):681-91.

Mason TJ, Lorimer JP, Bates DM, Zhao Y. Dosimetry in sonochemistry: the use of aqueous terephthalate ion as a fluorescence monitor, *Ultrason. Sonochem.* 1994; 1: 91–95.

Maurice DM. Drug delivery to the posterior segment from drops. *Surv Ophthalmol.* 2002 Aug;47 Suppl 1:S41-52.

McBrien NA, Metlapally R, Jobling AI, Gentle A. Expression of collagen-binding integrin receptors in the mammalian sclera and their regulation during the development of myopia. *Invest Ophthalmol Vis Sci.* 2006 Nov;47(11):4674-82.

McLean JR, Mortimer AJ. A cavitation and free radical dosimeter for ultrasound. *Ultrasound Med Biol.* 1988;14(1):59-64.

Meek KM, Fullwood NJ. Corneal and scleral collagens--a microscopist's perspective. *Micron.* 2001 Apr;32(3):261-72.

Milani JK, Verbukh I, Pleyer U, Sumner H, Adamu SA, Halabi HP, Chou HJ, Lee DA, Mondino BJ. Collagen shields impregnated with gentamicin-dexamethasone as a potential drug delivery device. *Am J Ophthalmol.* 1993 Nov 15;116(5):622-7.

Mitragotri S, Blankschtein D, Langer R. Ultrasound-mediated transdermal protein delivery. *Science.* 1995b Aug 11;269(5225):850-3.

Mitragotri S, Edwards DA, Blankschtein D, Langer R. A mechanistic study of ultrasonically-enhanced transdermal drug delivery. *J Pharm Sci.* 1995a Jun;84(6):697-706.

Mitragotri S, Blankschtein D, Langer R. Transdermal drug delivery using low-frequency sonophoresis. *Pharm Res* 1996;13(3): 411-420.

Molokhia SA, Jeong EK, Higuchi WI, Li SK. Transscleral iontophoretic and intravitreal delivery of a macromolecule: study of ocular distribution in vivo and postmortem with MRI. *Exp Eye Res.* 2009 Mar;88(3):418-25.

Myers MR, Giridhar D. Theoretical framework for quantitatively estimating ultrasound beam intensities using infrared thermography. *J Acoust Soc Am.* 2011 Jun;129(6):4073-83.

Nabili M, Patel H, Mahesh SP, Liu J, Geist C, Zderic V. Ultrasound-enhanced delivery of antibiotics and anti-inflammatory drugs into the eye. *Ultrasound Med Biol.* 2013 Apr;39(4):638-46.

N'Djin WA, Melodelima D, Parmentier H, Chesnais S, Rivoire M, Chapelon JY. Utility of a tumor-mimic model for the evaluation of the accuracy of HIFU treatments. results of in vitro experiments in the liver. *Ultrasound Med Biol.* 2008 Dec;34(12):1934-43.

Norman RE, Flanagan JG, Rausch SM, Sigal IA, Tertinegg I, Eilaghi A, Portnoy S, Sled JG, Ethier CR. Dimensions of the human sclera: Thickness measurement and regional changes with axial length. *Exp Eye Res.* 2010 Feb;90(2):277-84.

Nuritdinov VA. Phonophoresis and cavitation. *Vestn Oftalmol.* 1981 Jan-Feb;(1):56-8.

Onami H, Nagai N, Kaji H, Nishizawa M, Sato Y, Osumi N, Nakazawa T, Abe T. Transscleral sustained vasohibin-1 delivery by a novel device suppressed experimentally-induced choroidal neovascularization. *PLoS One.* 2013;8(3):e58580.

Osman O, Zanini LF, Frénéa-Robin M, Dumas-Bouchiat F, Dempsey NM, Reyne G, Buret F, Haddour N. Monitoring the endocytosis of magnetic nanoparticles by cells using permanent micro-flux sources. *Biomed Microdevices.* 2012 Oct;14(5):947-54.

Oude Blenke E, Mastrobattista E, Schiffelers RM. Strategies for triggered drug release from tumor targeted liposomes. *Expert Opin Drug Deliv.* 2013 Jun 25.

Park J, Zhang Y, Vykhodtseva N, Akula JD, McDannold NJ. Targeted and reversible blood-retinal barrier disruption via focused ultrasound and microbubbles. *PLoS One.* 2012; 7(8):e42754.

Parkinson TM, Ferguson E, Febbraro S, Bakhtyari A, King M, Mundasad M. Tolerance of ocular iontophoresis in healthy volunteers. *J Ocul Pharmacol Ther.* 2003 Apr;19(2):145-51.

Patton TF, Francoeur M. Ocular bioavailability and systemic loss of topically applied ophthalmic drugs. *Am J Ophthalmol.* 1978 Feb;85(2):225-9.

Pescina S, Santi P, Ferrari G, Nicoli S. Trans-scleral delivery of macromolecules. *Ther Deliv.* 2011 Oct;2(10):1331-49.

Pitt WG, Hussein GA, Staples BJ. Ultrasonic drug delivery--a general review. *Expert Opin Drug Deliv.* 2004 Nov;1(1):37-56.

Prausnitz MR, Noonan JS. Permeability of cornea, sclera, and conjunctiva: a literature analysis for drug delivery to the eye. *J Pharm Sci* 1998; 87:1479-1488.

- Raspanti M, Marchini M, Della Pasqua V, Strocchi R, Ruggeri A. Ultrastructure of the extracellular matrix of bovine dura mater, optic nerve sheath and sclera. *J Anat.* 1992 Oct;181 (Pt 2):181-7.
- Rudnick DE, Noonan JS, Geroski DH, Prausnitz MR, Edelhauser HF. The effect of intraocular pressure on human and rabbit scleral permeability. *Invest Ophthalmol Vis Sci.* 1999 Nov;40(12):3054-8.
- Sabraoui A, Inserra C, Gilles B, Béra JC, Mestas JL. Feedback loop process to control acoustic cavitation. *Ultrason Sonochem.* 2011 Mar;18(2):589-94.
- Saltzman M. *Drug Delivery : Engineering Principles for Drug Therapy.* Oxford University Press, USA. 1 edition (March 15, 2001)
- Sanghvi NT, Hawes RH. High-intensity focused ultrasound. *Gastrointest Endosc Clin N Am.* 1994 Apr;4(2):383-95.
- Schoenwald RD, Deshpande GS, Rethwisch DG, Barfknecht CF. Penetration into the anterior chamber via the conjunctival/scleral pathway. *J Ocul Pharmacol Ther.* 1997 Feb;13(1):41-59.
- Shaw A, Nunn J. The feasibility of an infrared system for real-time visualization and mapping of ultrasound fields. *Phys Med Biol.* 2010 Jun 7;55(11):N321-7.
- Shaw A, Khokhlova V, Bobkova S, Gavrilov L, Hand J. Calibration of HIFU intensity fields measured using an infra-red camera. 2011; *J. Phys. Conf.* 279 conf. 1
- Shaw A, Hodnett M. Calibration and measurement issues for therapeutic ultrasound. *Ultrasonics.* 2008 Aug;48(4):234-52.
- Short BG. Safety evaluation of ocular drug delivery formulations: techniques and practical considerations. *Toxicol Pathol.* 2008 Jan;36(1):49-62.

- Shu-Yi Z. Ultrasonic infrared thermography and its applications in nondestructive evaluation. *Applied acoustics*. 2004; 23 (5).
- Silverman RH, Vogelsang B, Rondeau MJ, Coleman DJ. Therapeutic ultrasound for the treatment of glaucoma. *Am J Ophthalmol* 1991 Mar; 15(111):327-337.
- Simonin JP. On the mechanisms of in vitro and in vivo phonophoresis; *Journal of Controlled Release*. 1995 Jan; 33(1): 125-141
- Somaglino L, Bouchoux G, Mestas JL, Lafon C. Validation of an acoustic cavitation dose with hydroxyl radical production generated by inertial cavitation in pulsed mode: application to in vitro drug release from liposomes. *Ultrason Sonochem*. 2011 Mar;18(2):577-88.
- Starritt HC, Duck FA, Humphrey VF. An experimental investigation of streaming in pulsed diagnostic ultrasound beams. *Ultrasound Med Biol*. 1989;15(4):363-73.
- Stringer H, Parr J. Shrinkage temperature of eye collagen. *Nature*. 1964 Dec 26;204:1307.
- Sundaram J, Mellein BR, Mitragotri S. An experimental and theoretical analysis of ultrasound-induced permeabilization of cell membranes. *Biophys J*. 2003 May;84(5):3087-101.
- Tang H, Wang CC, Blankschtein D, Langer R. An investigation of the role of cavitation in low-frequency ultrasound-mediated transdermal drug transport. *Pharm Res*. 2002 Aug;19(8):1160-9.
- Tachibana K and Tachibana S. The use of ultrasound for drug delivery. *Echocardiography* 2001;18(4):323-328.
- ter Haar G. Basic physics of therapeutic ultrasound. *Physiotherapy*. 1987. 73:110-113.
- ter Haar G. Therapeutic ultrasound. *Eur J Ultrasound*. 1999;9:3-9.

ter Haar G. Therapeutic applications of ultrasound. *Prog Biophys Mol Biol.* 2007 Jan-Apr;93(1-3):111-29.

ter Haar G, Carnochan P. A comparison of ultrasonic irradiation and RF inductive heating for clinical localized hyperthermia applications. *Br J Cancer Suppl.* 1982 Mar; 5:77-81.

Thrimawithana TR, Young S, Bunt CR, Green C, Alany RG, Drug delivery to the posterior segment of the eye *Drug Discovery Today.* 2011 Mar; 16(5-6): 270-277.

Tsok RM. The use of ultrasonics in inflammatory processes of the anterior portion of the eye. *Vestn Oftalmol.* 1969;82(5):28-32.

Tsok RM, Tsok OE. Ultrasonic transmitter for treatment of eye diseases by ultrasound and electrophoresis. *Vestn Oftalmol.* 1971;2:82-3.

Tsok RM, Stovbenko BS, Bilyk ED. Use of phonophoresis in eye diseases in children. *Oftalmol Zh.* 1983;(7):386-8.

Tsok RM, Gereliuk IP, Tsok OB, Kaminskiĭ IuM. The effect of ultrasonic oscillations of different frequencies on radionuclide accumulation in the eye tissues. *Oftalmol Zh.* 1990;(1):46-9.

Tezel, A., Mitragotri, S. Interactions of inertial cavitation bubbles with stratum corneum lipid bilayers during low frequency sonophoresis. *J.Biophys.* 2003; 85: 3502-3512.

Ueda H, Mutoh M, Seki T, Kobayashi D, Morimoto Y. Acoustic cavitation as an enhancing mechanism of low-frequency sonophoresis for transdermal drug delivery. *Biol Pharm Bull.* 2009 May;32(5):916-20.

Umemura S, Kawabata K, Sasaki K. In vitro and in vivo enhancement of sonodynamically active cavitation by second-harmonic superimposition. *J Acoust Soc Am.* 1997 Jan;101(1):569-77.



- Unger EC, Matsunaga TO, McCreery T, Schumann P, Sweitzer R, Quigley R. Therapeutic applications of microbubbles. *Eur J Radiol.* 2002 May;42(2):160-8.
- Unger EC, Porter T, Culp W, Labell R, Matsunaga T, Zutshi R. Therapeutic applications of lipid-coated microbubbles. *Adv Drug Deliv Rev.* 2004 May 7;56(9):1291-314.
- Urtti A, Salminen L. Minimizing systemic absorption of topically administered ophthalmic drugs. *Surv Ophthalmol.* 1993 May-Jun;37(6):435-56.
- Urtti A. Delivery of antiglaucoma drugs: ocular vs systemic absorption. *J Ocul Pharmacol.* 1994 Spring;10(1):349-57.
- Urtti A. Challenges and obstacles of ocular pharmacokinetics and drug delivery. *Adv Drug Deliv Rev.* 2006 Nov 15;58(11):1131-5. Epub 2006 Sep 26.
- Vaka SR, Sammeta SM, Day LB, Murthy SN. Transcorneal iontophoresis for delivery of ciprofloxacin hydrochloride. *Curr Eye Res.* 2008 Aug;33(8):661-7
- Valtot F, Kopel J, Haut J. Treatment of glaucoma with high intensity focused ultrasound. *Int Ophthalmol.* 1989 Jan;13(1-2):167-70.
- Vangsness CT Jr, Mitchell W 3rd, Nimni M, Erlich M, Saadat V, Schmotzer H. Collagen shortening. An experimental approach with heat. *Clin Orthop Relat Res.* 1997 Apr;(337):267-71.
- Voigt M, de Kozak Y, Halhal M, Courtois Y, Behar-Cohen F. Down-regulation of NOSII gene expression by iontophoresis of anti-sense oligonucleotide in endotoxin-induced uveitis. *Biochem Biophys Res Commun.* 2002 Jul 12;295(2):336-41.
- Villeneuve L., L. Alberti, J.P. Steghens, J.M. Lancelin, J.L. Mestas, Assay of hydroxyl radicals generated by focused ultrasound, *Ultrason. Sonochem.* 16 (2009) 339–344.

Vurgese S, Panda-Jonas S, Jonas JB. Scleral thickness in human eyes. *PLoS One*. 2012;7(1):e29692.

Vykhodtseva N, McDannold N, Hynynen K. Progress and problems in the application of focused ultrasound for blood-brain barrier disruption. *Ultrasonics*. 2008 Aug;48(4):279-96.

Wang S, Mahesh SP, Liu J, Geist C, Zderic V. Focused ultrasound facilitated thermo-chemotherapy for targeted retinoblastoma treatment: a modeling study. *Exp Eye Res*. 2012 Jul;100:17-25.

Wang S, Shin IS, Hancock H, Jang BS, Kim HS, Lee SM, Zderic V, Frenkel V, Pastan I, Paik CH, Dreher MR. Pulsed high intensity focused ultrasound increases penetration and therapeutic efficacy of monoclonal antibodies in murine xenograft tumors. *J Control Release*. 2012 Aug 20; 162(1):218-24.

Watson PG, Young RD. Scleral structure, organisation and disease. A review. *Exp Eye Res*. 2004 Mar; 78(3):609-23.

Wen H, Hao J, Li SK. Influence of permeant lipophilicity on permeation across human sclera. *Pharm Res*. 2010 Nov; 27(11):2446-56.

Werner L, Chew J, Mamalis N. Experimental evaluation of ophthalmic devices and solutions using rabbit models. *Vet Ophthalmol*. 2006 Sep-Oct;9(5):281-91.

Wu J, Winkler AJ, O'Neill TP. Effect of acoustic streaming on ultrasonic heating. *Ultrasound Med Biol*. 1994;20:195-201.

Wu Z, Li S, Wang N, Liu W, Liu W. A comparative study of the safety and efficacy effect of 5-fluorouracil or mitomycin C mounted biological delivery membranes in a rabbit model of glaucoma filtration surgery. *Clin Ophthalmol*. 2013; 7:655-62.

Wu J, Nyborg WL. Emerging therapeutic ultrasound. World Scientific Pub Co Inc; 2006 Sep; 1: 8-10.

Xie W, McCahon P, Jakobsen K, Parish C. Evaluation of the ability of digital infrared imaging to detect vascular changes in experimental animal tumours. *International Journal of Cancer*. 2004 Feb; 108 (5): 790–794.

Yamabayashi S, Ohno S, Aguilar RN, Furuya T, Hosoda M, Tsukahara S. Ultrastructural studies of collagen fibers of the cornea and sclera by a quick-freezing and deep-etching method. *Ophthalmic Res*. 1991;23(6):320-9.

Yamashita T, Sonoda S, Suzuki R, Arimura N, Tachibana K, Maruyama K, et al. A novel bubble liposome and ultrasoundmediated gene transfer to ocular surface: RC-1 cells in vitro and conjunctiva in vivo. *Exp Eye Res* 2007; 85:741–748.

Young FR. Cavitation. McGraw-Hill 1989, P 45-371.

Zderic V, Vaezy S, Martin RW, Clark JI. Ocular drug delivery using 20-kHz ultrasound. *Ultrasound Med Biol*. 2002 Jun; 28(6):823-9.

Zderic V, Clark JI, Martin RW, Vaezy S. Ultrasound-enhanced transcorneal drug delivery. *Cornea*. 2004 Nov; 23 (8):804-11.

### ***Articles publiés dans le cadre de la thèse:***

1. Contribution of inertial cavitation in the enhancement of in vitro transscleral drug delivery.  
**Razavi A.**, Clement D., Fowler A., Birer A., Chavrier F., Mestas JL., Romano F., Chapelon JY., Béglé A., Lafon C.  
Ultrasound Med Biol. 2014 Jun;40(6):1216-27.
2. Short- and long-term effects on the ciliary body and the aqueous outflow pathways of high intensity focused ultrasound cyclocoagulation.  
Aptel F., Béglé A., **Razavi A.**, Charrel T., Romano F., Chapelon JY., Lafon C.  
In press UMB 2014.

### ***Communications dans le cadre de la thèse:***

1. 14th International Society for Therapeutic Ultrasound (ISTU), 2014 April. Las Vegas, Nevada, USA.  
Razavi A., Baffie L., Charrel T., Chapuis P., Lafon C.
2. 17e Journée Scientifique de l'EDISS, 2013 Sep. Lyon, France.  
Razavi A., Clement D., Fowler RA., Birer A., Chavrier F., Mestas JL., Romano F., Chapelon JY., Béglé A., Lafon C.
3. 13th ISTU, 2013 May. Shanghai, China.  
Razavi A., Clement D., Fowler RA., Birer A., Chavrier F., Mestas JL., Romano F., Chapelon JY., Béglé A., Lafon C.
4. 16e Journée Scientifique de l'EDISS, 2012 Sep. Lyon, France.  
Razavi A., Clement D., Birer A., Chavrier F., Romano F., Chapelon JY., Béglé A., Lafon C.
5. 12th ISTU, 2012 Jun. Heidelberg, Germany.  
Razavi A., Clement D., Birer A., Chavrier F., Romano F., Chapelon JY., Béglé A., Lafon C.

